University of Stuttgart

Institute for Theoretical Physics III

Master Thesis

Topological edge states in a one-dimensional ladder system

Kai-Simon Guther

Supervised by

Prof. Dr. H.P. Büchler

Secondary corrector

Prof. Dr. M. Daghofer

September 1, 2016

I hereby declare that

- I have authored the submitted thesis single-handed,
- I used only the declared sources and marked all statements adopted either literally or in content from other work as such,
- the submitted thesis has not been part of any previous examination procedure, neither in part nor complete,
- the submitted thesis has not been already published, neither in part nor complete,
- the contents of the digital and the printed versions agree.

Stuttgart, September 1, 2016, Kai-Simon Guther

Abstract

In this thesis, an interacting, particle number conserving model of spinless fermions in a two-leg ladder system is analyzed in the context of topological edge states. As proven in [1], where the model was proposed first, the ground state has a topologically protected degeneracy and features edge states with non-Abelian braiding statistics for a special choice of parameters.

In a first step, the model is treated using bosonization, allowing for a qualitative prediction of the behaviour of the described system depending on the parameters. In this description, the system can be separated into a symmetric and an antisymmetric sector with respect to wire exchange. Then, depending on the parameters, renormalization group arguments can be employed to make statements about the possible occuring phases. In this way, the topological phase is predicted as well as a Luttinger liquid phase and a phase gapped in the antisymmetric sector. For half filling, a charge density wave and a phase with a gap in the symmetric sector can occur. While the assignment of the occuring phases to the appearing parameters can be made qualitatively, a quantitative phase diagram could not be constructed for the initial model this way.

Hence, a numerical study using the density-matrix renormalization group is done. An implementation of the algorithm for this task is written to gain maximal flexibility in the available features. Then, the ground state properties of the model dependent on the parameters are computed and a quantitative phase diagram is generated, which is in good agreement with the expectations from bosonization. The qualitative predictions from bosonization about the behaviour of correlation functions is employed to allow for a comparison of the numerical results to the bosonized theory.

Also, the stability of the topological phase with respect to symmetry breaking is considered and the protection of the ground state degeneracy by both time-reversal invariance and subchain parity conservation is verified and the analytical results obtained in [1] in perturbation theory are confirmed.

Zusammenfassung

Im Rahmen dieser Arbeit wird ein wechselwirkendes, teilchenzahlerhaltendes Modell spinloser Fermionen in einem System zweier gekoppelter Ketten im Zusammenhang mit topologischen Randzuständen untersucht. Wie in [1], wo das Model zuerst vorgeschlagen wurde, gezeigt werden konnte, liegt für eine spezielle Wahl der Parameter eine topologisch geschützte Grundzustandsentartung vor und Randzustände mit nichtabelscher Austauschstatistik treten auf.

In einem ersten Schritt wird das Modell mittels Bosonisierung untersucht, wodurch eine qualitative Vorehrsage des Verhaltens des beschriebenen Systems abhängig von den Parametern ermöglicht wird. Im Rahmen dieser Beschreibung kann das System in einen Sektor symmetrischen und einen antisymmetrischen Sektor bezüglich Vertauschung der Ketten zerlegt werden. Dann können Resultate aus der Renormierungsgruppentheorie angewandt werden, um Aussagen über die auftretenden Phasen zu treffen. Auf diese Weise ist es möglich die topologische Phase sowie das Auftreten einer Luttinger-Flüssigkeit und einer Anregungslücke im antisymmetrischen Sektor vorherzusagen. Im Fall halber Füllung können zudem eine Ladungsdichtewelle und eine Anregungslücke im symmetrischen Sektor auftreten. Zwar können die möglichen Phasen qualitativ den einzelnen Parametern der Theorie zugeordnet werden, es kann aber kein quantitatives Phasendiagram erstellt werden.

Daher wird das System mittels der Dichtematrix-Renormierungsgruppe numerisch untersucht. Zu diesem Zweck wird eine Implementierung des Algorithmus erstellt, um maximale Flexibilität bezüglich der verfügbaren Features zu erhalten. Damit können die Grundzustandseigenschaften des Modells in Abhängigkeit von den Parametern berechnet werden und ein quantitatives Phasendiagram erstellt werden, welches gute Übereinstimmung mit den Erwartungen der Bosonisierung zeigt. Die Vorhersagen der bosonisierten Theorie über das Verhalten von Korrelationsfunktionen können hier verwendet werden, um einen Vergleich mit den numerischen Resultaten zu ermöglichen.

Zudem wird die Stabilität der topologischen Phase bezügliche Symmetriebrechung betrachtet und der Schutz der Grundzustandsentartung sowohl durch Zeitumkehrinvarianz als auch durch Erhaltung der fermionischen Parität der einzelnen Ketten werden geprüft und die störungstheoretischen Ergebnisse aus [1] werden bestätigt.

Contents

Abstract **3**

Zusammenfassung **4**

1 Introduction **7**
1.1 Model Hamiltonian 8

2 Introduction to the applied methods **10**
2.1 The bosonization scheme 10
2.1.1 The free boson 11
2.1.2 Boson-Fermion correspondence 12
2.1.3 Relevant and irrelevant interactions 13
2.2 The DMRG scheme 16
2.2.1 Computation of ground states 18
2.2.2 Symmetries and MPS 24
2.2.3 Computation of excited states 25
2.2.4 Implementation 26

3 Analysis of the ladder system **27**
3.1 Bosonization approach to the ladder system 27
3.1.1 Bosonization of the Hamiltonian in continuum limit 27
3.1.1.1 Intra-Chain interactions 28
3.1.1.2 Inter-Chain pair-hopping 29
3.1.1.3 Inter-Chain density-density interactions 31
3.1.2 Gapped phases 33
3.1.2.1 Topological phase 34
3.1.2.2 Charge density waves 35
3.1.2.3 Charge gap in the symmetric sector 35
3.2 Correlation functions of the bosonized theory 37
3.2.1 Bosonization of correlation functions 37
3.2.2 Correlation functions in the topological phase 38
3.2.2.1 Bosonic correlation functions 38
3.2.2.2 Fermionic correlation functions 39
3.2.3 Probing the gap 40

3.3 Numerical characterization of the topological phase 42
3.4 $J - g$ phase diagram 45
3.4.1 Perturbations around the exact point 45
3.4.2 Strong interactions 49
3.5 Effects of symmetry breaking perturbations 55
3.6 Effects of disorder 58
3.7 Considerations for weak pair-hopping 59

Conclusion **60**

A RG Analysis **61**

B Dynamical basis adaption and subspace expansion **65**

C Construction of the projector for excited state search **68**

D Performance of the DMRG implementation **70**

List of Figures **72**

Acknowledgments **74**

Bibliography **75**

Chapter 1

Introduction

After the concept of topological order [2, 3] was developed following the discovery of the quantum Hall effect [4] and the fractional quantum Hall effect [5] and the connection to non-Abelian anyons was made [6, 7, 8], topological states of matter have become a very active research topic, both in condensed matter physics [9] and in cold atomic gases [10, 11, 12]. The most promising perspective for non-Abelian anyons lies in fault-tolerant quantum computation [13, 14] which is one of the main reasons for the rising interest in topological states of matter.

The main focus in the context of non-Abelian anyons lies on topological p-wave superconductors [15, 16, 17] where the existence of Majorana modes has been derived in one [16] and two dimensions [18, 19] and recent experiments on indium antimonide and iron nanowires showed signatures of zero-energy Majorana modes in one-dimensional proximity-induced topological superconductors [20, 21].

The most prominent model for a topological superconductor is the Kitaev-chain [16] which describes a one-dimensional p-wave superconductor of spinless fermions in mean-field theory. It is described by the Hamiltonian

$$H = \sum_{i=1}^{L-1} \left(-t c_i^\dagger c_{i+1} + \Delta c_i^\dagger c_{i+1}^\dagger \right) + \text{h.c.} - \mu \sum_i c_i^\dagger c_i \,. \tag{1.1}$$

This toy model already exhibits a topological phase with exponentially localized Majorana edge states [16] which realize the braiding statistics of Ising anyons [22] and is an apt model for plenty applications.

In systems like cold atomic gases in optical lattices however, where the mean-field picture might not fully describe the physics, a particle number conserving theory is desirable to analyse the occurence of topological states. Such a theory then has to be an interacting theory, and in contrast to mean-field theories like the Kitaev-chain, there are only few exactly solvable models [1, 23] of interacting theories featuring non-Abelian edge states. On the other hand, cold atomic gases feature unique possibilities for the realization of quasiparticles with non-Abelian statistics and numerous proposals for potential candidates exist [12, 24, 25].

Due to the available tools, most studies of particle number conserving models consider one-dimensional systems. There, the powerful field theoretical method of bosonization

[26, 27] can be applied and a numerical analysis can be performed using the density matrix renormalization group (DMRG)[28, 29]. Numerous models of interacting systems which are described as p-wave superconductors in mean-field theories have been discussed using bosonization [23, 30, 31, 32, 33] with results similar to those presented in this thesis. There are also several studies of those or similar models making use of the density matrix renormalization group [23, 24].

1.1 Model Hamiltonian

The goal of this thesis is to give a detailed analysis of a generalization of the ladder system model which was introduced in [1].

Consider a two-leg ladder lattice with open boundary conditions of spinless fermions with annihilation operators a_i for site i of the upper chain with chain index 1 and b_i for site i of the lower chain with chain index 2. Let n_i^σ be the number of fermions on site i of chain $\sigma \in \{a, b\}$.

$$\begin{aligned} H = \sum_{i=1}^{L-1} \Big[& a_i^\dagger a_{i+1} + a_{i+1}^\dagger a_i + b_i^\dagger b_{i+1} + b_{i+1}^\dagger b_i \\ & + J \left(n_i^a + n_{i+1}^a - 2 n_i^a n_{i+1}^a + n_i^b + n_{i+1}^b - 2 n_i^b n_{i+1}^b \right) \\ & + W \left(a_i^\dagger a_{i+1}^\dagger b_i b_{i+1} + b_i^\dagger b_{i+1}^\dagger a_i a_{i+1} \right) \\ & + g \left(n_i^a n_{i+1}^a \left(1 - n_i^b\right) (1 - n_{i+1}^b) + n_i^b n_{i+1}^b (1 - n_i^a)(1 - n_{i+1}^a) \right) \Big] \, . \end{aligned} \tag{1.2}$$

The special case of $W = J = g = 1$ was analyzed thoroughly in [1], where an exact solution for the low-energy physics was presented, explicitly demonstrating the existence of topologically protected edge states with non-Abelian braiding statistics.

This model is not only particle number conserving, but it also features time-reversal invariance and conservation of the fermionic subchain parity α on each chain. The latter is analogous to the conserved fermionic parity in the Kitaev model and distinguishes the degenerate ground states in the topological phase. As the model is particle number conserving, it is safe to consider only sectors of fixed particle number N, or equivalently fixed filling fraction $\rho = \frac{N}{2L}$ where L is the chain length. While some properties do depend on the filling factor, the existence of topological edge states turns out not to do in principle, except for trivial cases like $N = 0$. For $J = g = W = 1$ it is shown in [1], that the ground state is even degenerate with respect to N. As will be seen in section 3.4, this is a special property of that point and does not survive a variation of paramters.

The Hamiltonian (1.2) also has been analyzed in the absence of density-density interactions, that is, for $J = g = 0$, in [24] using bosonization as well as the numerical tool of density matrix renormalization group. There, the existence of a topological phase was demonstrated for moderate W away from half filling. These results are particularly interesting in the context of [1] as they show that the density-density interactions can contribute to the occurence of Majorana-like edge states. A possible experimental realization using cold atomic gases in an optical lattice with Raman assisted tunneling

without explicitly including density-density interactions was also proposed in [24]. There density-density interactions might naturally appear as perturbations [24].

A similar model was considered in [23], where the existence of topological edge states was demonstrated using bosonization and density matrix renormalization group and by deriving an exact solution for a special choice of parameters.

Chapter 2

Introduction to the applied methods

2.1 The bosonization scheme

The bosonization scheme applied here is the one presented in [34]. Although the bosonization procedure itself can be rigorously applied to any one-dimensional system e.g. via constructive bosonization as presented in [27], it might not be rewarding for arbitrary systems. Certain interacting fermionic theories can however be treated easily in the language of bosonization [26, 35, 36, 37], and this common framework of describing the system as a Luttinger liquid with additional perturbations will be used here. In the following, a short overview of the results from [34] shall be given.

Starting from a theory of free fermions with some filling fixed by the Fermi-wavenumber k_F and corresponding Fermi velocity v, the low-energy limit is considered. Excitations can now be separated into left- and right-moving modes such that the fermionic annihilation operators decompose [34]

$$\psi_i(x) = \psi_{R\sigma}(x)\mathrm{e}^{ik_F x} + \psi_{L\sigma}(x)\mathrm{e}^{-ik_F x}\,, \tag{2.1}$$

here, σ is the index denoting the type of fermion. From now on, the right-moving fermions annihilated by $\psi_{R\sigma}$ and the left-moving fermions corresponding to $\psi_{L\sigma}$ are treated as two distinct types of fermions, with the corresponding anticommutators.

It should be noted that the theory of free fermions is a conformal field theory and the fermionic operators ψ_σ are primary fields [38]. The separation into left-/ right-movers is nothing but the separation into a holomorphic and an antiholomorphic part as it is common in the context of conformal field theories. In particular, the fermionic fields have conformal weights $\left(\frac{1}{2},0\right)$ and $\left(0,\frac{1}{2}\right)$, respectively [38]. In particular, they obey

$$\langle\psi_\sigma^\dagger(x)\psi_\sigma(x')\rangle = \frac{A}{x-x'}\,. \tag{2.2}$$

The constant A is only a normalization constant. If the fields are normalized such that they obey canonical commutation relations, it is $A = \frac{1}{2\pi}$.

2.1.1 The free boson

It turns out [26, 35] that the fermionic operators $\psi_{R\sigma}$, $\psi_{L\sigma}$ can be expressed in terms of free boson fields ϕ_σ. The Hamiltonian density of the free boson is defined as

$$\mathcal{H}_{b,i} = \frac{v}{2}\left((\partial_{vt}\phi_\sigma)^2 + (\partial_x\phi_\sigma)^2\right) . \tag{2.3}$$

And the field operators ϕ_σ are self-adjoint. It is convenient to introduce the dual boson fields θ_σ as

$$\partial_x\theta_\sigma = -\partial_{vt}\phi_\sigma . \tag{2.4}$$

Since $\partial_x\theta_\sigma$ is the canonical momentum operator of ϕ_σ, this implies the commutation relation

$$[\phi_\sigma(x),\, \theta_\sigma(\tilde{x})] = -i\theta_{\mathrm{H}}(x-\tilde{x}) , \tag{2.5}$$

where θ_{H} is the Heaviside step function, not to be confused with the dual boson.

This theory can be solved straightforwardly by Fourier transformation. It can also be treated using the powerful tool of conformal field theory like presented in [34, 38], as the theory is conformally invariant. Contrary to the fermionic theory, the boson fields ϕ_σ are not primary, however [38]. In this content, the introduction of complex coordinates

$$z = -i(x-vt) \tag{2.6}$$
$$\bar{z} = i(x+vt) \tag{2.7}$$

is useful and these shall be used within this section. The correspodning derivatives are

$$\partial \equiv \partial_z = -\frac{i}{2}\left(\partial_{vt} - \partial_x\right) \tag{2.8}$$
$$\bar{\partial} \equiv \partial_{\bar{z}} = -\frac{i}{2}\left(\partial_{vt} + \partial_x\right) . \tag{2.9}$$

A separation of the boson field into left-/right-moving parts φ_σ and $\bar{\varphi}_\sigma$, or in the language of conformal field theory into a holomorphic and antiholomorphic part, is possible [34] such that

$$\bar{\partial}\varphi_\sigma = 0 = \partial\bar{\varphi}_\sigma . \tag{2.10}$$

And the separation is given by

$$\phi_\sigma = \varphi_\sigma + \bar{\varphi}_\sigma \tag{2.11}$$
$$\theta_\sigma = \varphi_\sigma - \bar{\varphi}_\sigma . \tag{2.12}$$

This will become useful both in the bosonization formula as well as in treating density terms. It is common to denote the (x,t)-dependence of these fields as $\phi_\sigma(z,\bar{z})$ to emphasize the possibility to separate the field into a holomorphic and an antiholomorphic part.

The two-point function of ϕ_σ may be calculated in several ways, for example via the mode expansion, by solution of the Poisson equation [34] or using the fact that $\partial\varphi_\sigma$ is a

primary field with conformal weight $(1,0)$ [38]. It is then

$$\langle \varphi_\sigma(z)\varphi_\sigma(w)\rangle = -\frac{1}{4\pi}\ln(z-w) \tag{2.13}$$

$$\langle \bar{\varphi}_\sigma(\bar{z})\bar{\varphi}_\sigma(\bar{w})\rangle = -\frac{1}{4\pi}\ln(\bar{z}-\bar{w}) \tag{2.14}$$

$$\langle \varphi_\sigma(z)\bar{\varphi}_\sigma(\bar{z})\rangle = 0\,. \tag{2.15}$$

Inserting these correlation functions into those of ϕ_σ and θ_σ yields obviously

$$\langle \phi_\sigma(z,\bar{z})\phi_\sigma(w,\bar{w})\rangle = \langle \theta_\sigma(z,\bar{z})\theta_\sigma(w,\bar{w})\rangle = -\frac{1}{2\pi}\ln(|z-w|)\,. \tag{2.16}$$

This equation in it's equal-time form will be the starting point for computing correlation functions in the bosonized theory.

2.1.2 Boson-Fermion correspondence

From conformal field theory, it is known [38] that the vertex operators

$$V_{\alpha i}(z) =: \mathrm{e}^{i\alpha\varphi_\sigma(z)} : \tag{2.17}$$

are primary fields with conformal weight

$$(h,\bar{h}) = (\frac{\alpha^2}{8\pi}, 0)\,, \tag{2.18}$$

and analogously for $\bar{\varphi}_\sigma$.

Recall the Fermionic fields being primary fields with conformal weights $\left(\frac{1}{2},0\right)$ and $\left(0,\frac{1}{2}\right)$, respecitvely. This already allows for the conjecture that these might be expressed as vertex operators with $\alpha = \sqrt{4\pi}$ with some prefactor to ensure the fermionic statistics.

A thorough derivation of the bosonization identity shall not be demonstrated here but can be found e.g. in [27, 34], but the results from these works shall be summarized here.

It turns out that the fermionic operators can indeed be expressed as vertex operators, leading to the famed bosonization identity [27, 34, 39]

$$\psi_{R\sigma} = \frac{\eta_\sigma}{\sqrt{2\pi}} : \mathrm{e}^{-i\sqrt{4\pi}\varphi_\sigma} := \frac{\eta_\sigma}{\sqrt{2\pi}} : \mathrm{e}^{-i\sqrt{\pi}(\phi_\sigma+\theta_\sigma)} : \tag{2.19}$$

$$\psi_{L\sigma} = \frac{\bar{\eta}_\sigma}{\sqrt{2\pi}} : \mathrm{e}^{-i\sqrt{4\pi}\bar{\varphi}_\sigma} := \frac{\bar{\eta}_\sigma}{\sqrt{2\pi}} : \mathrm{e}^{-i\sqrt{\pi}(\phi_\sigma-\theta_\sigma)} : \,. \tag{2.20}$$

There are some additional assumptions concerning boundary conditions [38], but the more important requirement is the compactification of the boson [34] as

$$\phi_\sigma = \phi_\sigma + \sqrt{\pi} \tag{2.21}$$

$$\theta_\sigma = \theta_\sigma + \sqrt{\pi}\,. \tag{2.22}$$

The so-called Klein factors η_σ, $\bar{\eta}_\sigma$ are hermitian operators on an auxiliary space to ensure anticommutation of the fermion operators, therefore they obey [27]

$$\{\eta_\sigma, \eta_{\sigma'}\} = \{\bar{\eta}_\sigma, \bar{\eta}_{\sigma'}\} = 2\delta_{ij} \tag{2.23}$$

$$\{\eta_\sigma, \bar{\eta}_{\sigma'}\} = 0\,. \tag{2.24}$$

However, in the system considered within this thesis, all products of Klein factors in the Hamiltonian can be made diagonal by choice of an appropiate basis in the auxiliary space. In this case, different eigenstates of the Klein factor products decouple and the Klein factors are of no further concern. Also, since all correlation functions considered are of the form $\langle O(x)O^\dagger(x')\rangle$, Klein factors do not appear in the considered correlation functions. Therefore, they are not written explicitly from now on.

Using equations (2.19) and (2.20), the fermionic densities can also be expressed via the boson fields in an elegant way. This can be easily derived using point splitting as demonstrated in [34]. Due to normal ordering, the exponentials do not obey the functional equation of the exponential function but instead the identity

$$:\mathrm{e}^A::\mathrm{e}^B:=:\mathrm{e}^{A+B}:\,\mathrm{e}^{\langle AB\rangle} \tag{2.25}$$

holds [34], for some bosonic fields A, B.

The fermion densities can now be derived using point splitting as presented in [34] (exemplary for $\psi_{R\sigma}$)

$$\begin{aligned}
:\psi^\dagger_{R\sigma}\psi_{R\sigma}: &= \frac{1}{2\pi}\lim_{\epsilon\to 0}\left(:\mathrm{e}^{i\sqrt{4\pi}\varphi_\sigma(z+\epsilon)}::\mathrm{e}^{-i\sqrt{4\pi}\varphi_\sigma(z)}:-\frac{1}{\epsilon}\right)\\
&= \frac{1}{2\pi}\lim_{\epsilon\to 0}\left(\frac{:\mathrm{e}^{i\sqrt{4\pi}(\epsilon\partial\varphi_\sigma(z)+\mathcal{O}(\epsilon^2))}:-1}{\epsilon}\right)\\
&= \frac{i}{\sqrt{\pi}}\partial\varphi_\sigma\,.
\end{aligned} \tag{2.26}$$

And analogously

$$:\psi^\dagger_{L\sigma}\psi_{L\sigma}:=\frac{-i}{\sqrt{\pi}}\bar{\partial}\bar{\varphi}_\sigma\,. \tag{2.27}$$

2.1.3 Relevant and irrelevant interactions

So far only free theories were considered, but of course, the subject of this thesis is not a free theory. It is however possible to study the low energy physics of the full interacting theory in proximity to the free theory by means of bosonization and conformal field theory perturbatively.

While the free theory is conformally invariant and thereby scale invariant, the perturbations are in general not and their coupling constants are therefore subject to renormalization group (RG) flow [40, 41], that is, they depend on the energy scale. Perturbations then can be categorized into three classes: relevant, irrelevant and marginal [42]. The coupling

constants of irrelevant perturbations vanish algebraically under RG flow whereas those of relevant perturbations increase algebraically upon renormalization and those of marginal terms vary logarithmically [34]. Hence, the low energy physics is unaffected by irrelevant terms and they can be neglected.

The behaviour of some operator O under renormalization is connected to its conformal weights $(h, \bar{h})$. For an operator with $h = \bar{h}$, this is especially simple: It is relevant if $\Delta < 2$, irrelevant if $\Delta > 2$ and marginal if $\Delta = 2$ [42], where $\Delta = h + \bar{h}$ is the scaling dimension. From conformal field theory, it is straightforward to determine the scaling dimension [38] as it is

$$\langle O(z,\bar{z}) O^\dagger(w,\bar{w})\rangle_0 = \frac{1}{z^{2h}\bar{z}^{2\bar{h}}}\,, \tag{2.28}$$

where the expectation value is here taken with respect to the free theory. Since the scaling dimension of interactions is computed within the free theory, this approach is perturbative. Also, the classification with respect to Δ cited above only captures the behaviour under RG flow when neglecting higher orders in the RG equations.

A useful and important identity in determining the scaling dimension of perturbations is the neutrality condition [34]

$$\langle : \mathrm{e}^{i\alpha\varphi_\sigma(z)+i\beta\varphi_\sigma(z')} : \rangle \neq 0 \Rightarrow \alpha+\beta = 0\,, \tag{2.29}$$

and analogously for $\bar{\varphi}_\sigma$. Together with equation (2.25) this allows for a straightforward determination of scaling dimensions of operators via the bosonization identities (2.19) and (2.20), reducing the correlation function to a function of the boson correlation functions (2.16).

Density-density interactions however do not need be treated using equations (2.25) and (2.29) but instead can be bosonized directly using the identity (2.26).

An important result is that derivatives of the bosonic fields of order higher than two or any higher power than two in the derivatives of the bosonic fields is irrelevant. This can be readily seen using Wick's theorem, for example for $(\partial\varphi_\sigma)^3$

$$\begin{aligned}
\langle : (\partial\varphi_\sigma(z))^3 :: (\partial\varphi_\sigma(w))^3 : \rangle =& \langle : (\partial\varphi_\sigma(z))^3 (\partial\varphi_\sigma(w))^3 : \rangle \\
&+ 9\langle \partial\underbrace{\varphi_\sigma(z)\partial\varphi_\sigma}(w) : (\partial\varphi_\sigma(z))^2 (\partial\varphi_\sigma(w))^2 : \rangle \\
&+ 18\langle (\partial\underbrace{\varphi_\sigma(z)\partial\varphi_\sigma}(w))^2 : (\partial\varphi_\sigma(z))(\partial\varphi_\sigma(w)) : \rangle \\
&+ 18\langle (\partial\underbrace{\varphi_\sigma(z)\partial\varphi_\sigma}(w))^3 \rangle \\
=& 18\langle (\partial\underbrace{\varphi_\sigma(z)\partial\varphi_\sigma}(w))^3 \rangle \\
=& 18\left(\langle \partial\varphi_\sigma(z)\partial\varphi_\sigma(w)\rangle\right)^3 \\
=& 18\left(\partial_z\partial_w\langle \varphi_\sigma(z)\varphi_\sigma(w)\rangle\right)^3 \\
=& \frac{18}{(4\pi)^3}\frac{1}{(z-w)^6}\,.
\end{aligned} \tag{2.30}$$

Therefore, $(\partial\varphi_\sigma)^3$ has a scaling dimension of $\Delta = 3$.

In general, the scaling dimension of $(\partial\varphi_\sigma)^n$ is $\Delta = n$ since it is

$$\langle : (\partial\varphi_\sigma(z))^n :: (\partial\varphi_\sigma(w))^n : \rangle \propto \left(\partial_z\partial_w\langle \varphi_\sigma(z)\varphi_\sigma(w)\rangle\right)^n\,. \tag{2.31}$$

This further generalizes to products of different boson fields like $(\partial\varphi_\sigma)^2\bar{\partial}\bar{\varphi}_{\sigma'}$. What can be concluded is that any interaction of power three or higher in the fermion densities is irrelevant as its scaling dimension is equal to the power of derivatives of the bose fields.

For simplicity, normal ordering is not explicitly written from now on, although all exponentials are still normal ordered.

2.2 The DMRG scheme

In contrast to the traditional approach to DMRG [28, 29], the contemporary formulation of the DMRG algorithm is as a variational approach using matrix product states (MPS) [43, 44]. While the core algorithm is mathematically equivalent [45], extensions thereof like excited state search are not and it is often much easier or more efficient to formulate those using the matrix product ansatz [46]. The numerical results in this thesis were obtained using the variational MPS algorithm as described in [45, 47, 46]. In the following, a short overview of the method shall be given, beginning with the concept of MPS. This is based on the introduction to MPS in [45].

Consider a many-body system where the single-particle Hilbert space is of finite dimension. In solid-state physics, this is usually realized by a lattice of finite size with L sites, but there are also applications in quantum chemistry (e.g. [48]) where the size of the single-particle Hilbert space is given by the number of orbitals considered. As the system can always be formulated in terms of lattice sites, it is enough to consider just a lattice of L sites. In occupation number representation, the many-body Hilbert space can be decomposed as

$$H_{\text{Full}} = \bigotimes_{i=1}^{L} V_i \,, \tag{2.32}$$

with a d_i-dimensional on-site Hilbert space V_i. The local dimension d_i is given by the physical system and is just the dimension of the many-body Hilbert space on a single site. For bosonic systems however, V_i is not finite dimensional. Since the algorithm can only handle finite d_i, a truncation has to be made in this case and each site has to be assigned a maxmimum particle number. In most applications, d_i is independent of i, the i-dependence is hence omitted although the algorithm does not change if d_i is taken explicitly i-dependent.

Let $\{|\sigma_i\rangle \,|\sigma_i \in \{1, \ldots, d_i\}\}$ be a basis of V_i. Take some state $|\psi\rangle = \sum_{\underline{\sigma}} c_{\underline{\sigma}} \,|\underline{\sigma}\rangle \in H_{\text{Full}}$ where $\underline{\sigma} = (\sigma_1, \ldots, \sigma_L)$ labels one vector of the product basis of H_{Full}. This state can now be brought into MPS form via singular value decomposition applied iteratively to the vector $c_{\underline{\sigma}}$, a demonstration thereof can be found in [45]. That is, there are dL matrices $A^{[i]\,\sigma_i}$ such that

$$|\psi\rangle = \sum_{\underline{\sigma}} A^{[1]\,\sigma_1} A^{[2]\,\sigma_2} \cdots A^{[L]\,\sigma_L} \,|\underline{\sigma}\rangle \ . \tag{2.33}$$

When unambigious, the matrices $A^{[i]\,\sigma_i}$ are henceforth denoted as A^{σ_i} for convenience. The matrix elements are denoted as $A^{\sigma_i}_{a_{i-1}\,a_i}$. In principle, any state $|\psi\rangle \in H_{\text{Full}}$ can be brought into that form. Since the dimension of H_{Full} however is d^L but the number of matrices is only dL, their dimension has to be exponential in L, which is in fact the case [45]. It is common and useful to represent an MPS graphically as e.g. done in [45, 46, 47, 49]. This common notation is depicted in figure 2.1 and 2.3, allowing for an intuitive handling of those states.

The main approximation made in the variational MPS algorithm is now the truncation of the dimension of the matrices A^{σ_i}, such that the variational ansatz is of the form (2.33) where the matrices are of dimension $(D \times D)$ at maximum. In practice, most of the

matrices A^{σ_i} will have size $D \times D$ but not all of them, thus, the virtual bond dimension D_i has to be taken as site-dependent in the implementation. This ansatz effectively limits the entanglement of the state, as the matrices A^{σ_i} are directly connected to the entanglement entropy of the state [50]. Up to this point, no restrictions concerning the spatial dimension of the lattice were made, and in the following, no assumptions of that kind will be made. The reason why the variatonal MPS ansatz works well in one dimension but struggles in higher dimensions lies only in the truncation. The entanglement entropy of ground states of local Hamiltonians obeys area laws [51]. In one spatial dimension, the ansatz is therefore very good for the ground state while in higher dimensions, the area laws imply a rapid growth of entanglement entropy with system size.

Any linear operator O on H_{Full} can also be viewed as a vector in $H^*_{\text{Full}} \otimes H_{\text{Full}}$. In the trivial product basis, it can then also be brought into matrix product form, that is, there are matrices $W^{[i]\,\sigma_i\,\sigma_i'}$ with

$$O = \sum_{\underline{\sigma}\,\underline{\sigma}'} W^{[1]\,\sigma_1\,\sigma_1'} W^{[2]\,\sigma_2\,\sigma_2'} \cdots W^{[L]\,\sigma_L\,\sigma_L'} \left|\underline{\sigma}\right\rangle \left\langle\underline{\sigma}'\right| \,. \tag{2.34}$$

This form is called matrix product operator (MPO) and the matrix elements of $W^{\sigma_i\,\sigma_i'}$ are denoted as $W^{\sigma_i\,\sigma_i'}_{b_{i-1}\,b_i}$. When using MPS, it is necessary to use also the MPO representation of any operator appearing to have an efficient algorithm, in particular of the Hamiltonian. Fortunately, local operators can be brought easily into MPO form, see for example [52]. Analogously to the MPS, a graphical representation of an MPO is common in the form depicted in figure 2.2. While the MPO representation of an operator is in principle also an MPS in a higher dimensional physical space, it is treated separately in the implementation since it appears in another context in the algorithm. For example, its entries are fixed from the beginning and the matrices $W^{[i]}$ are sparse for a typical Hamiltonian whereas the matrices of the MPS are not necessarily sparse. A local Hamiltonian can usually be expressed as an MPO with a comparably low bond dimension of $D_W \sim 5 \ldots 15$. The ladder system Hamiltonian (1.2) can be represented with a bond dimension of $D_W = 12$ which is already quite high.

The ground state search is now reduced to the optimization of a number of parameters scaling as $\mathcal{O}(L)$.

A short notice on boundary conditions shall be made at this point. Similar to the spatial dimension of the system, no explicit assumptions have been made about the boundary conditions implemented in the Hamiltonian. It is, however, much easier to represent the ground state of a Hamiltonian describing a system with open boundaries as an MPS than that of the same Hamiltonian with periodic boundary conditions [45]. The reason for that is that the periodic boundaries act non-locally in a sense and therefore can cause long-range entanglement between the first and the last site [45]. There are workarounds which make handling periodic boundaries possible without largely increasing the bond dimension [53, 54], but these require major modifications from the algorithm for open boundaries.

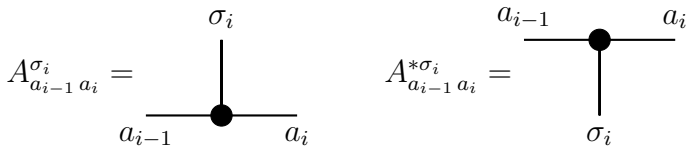

Figure 2.1: Graphical representation of a single matrix of an MPS and the adjoint matrix. The dot corresponds to the site i and each leg to one of the indices. Usually, vertical legs denote physical indices σ_i and horizontal legs virtual bond indices which were introduced in the MPS decomposition. This simple notation allows for an easy formulation of lots of common operations on an MPS and also grants an intuitive access to a numerically efficient formulation of those operations.

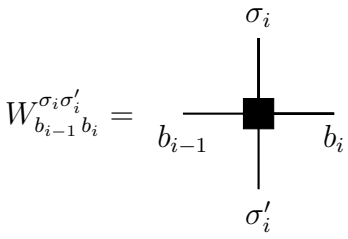

Figure 2.2: Graphical representation of a single matrix of an MPO. The conventions are analogous to the graphical representation of the MPS.

2.2.1 Computation of ground states

In the following section, a short overview of the ground state search using the variational MPS ansatz shall be given, again closely following [45], where a detailed discussion can be found. In principle, the MPS ansatz is just a variational ansatz, that is, the matrices A^{σ_i} are to be varied such that

$$E[\psi] = \frac{\langle \psi \,|\, H \,|\, \psi \rangle}{\langle \psi \,|\, \psi \rangle} \tag{2.35}$$

becomes minimal or equivalently, that $|\psi\rangle$ minimizes $\langle \psi \,|\, H \,|\, \psi \rangle$ under the constraint $\langle \psi \,|\, \psi \rangle = \text{const}$. While the MPS ansatz in principle scales linearly with the system size L, it is also a nonlinear ansatz, which is difficult to handle considering the still high number of free parameters. A useful approach is to vary the tensors $A^{[i]}$, composed of all matrices $A^{[i]\,\sigma_i}$, one after another. In general, the notation $A^{[i]}$ shall be used for these tensors of order three.

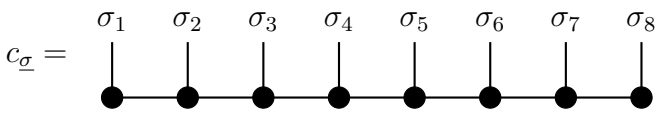

Figure 2.3: Graphical representation of the componentwise equation (2.33) exemplary for $L = 8$. As for the single matrix, each dot represents a site and each leg a matrix index. Connected legs correspond to contractions, i.e. a summation over all virtual bond indices is executed. Since the vertical legs correspond to physical indices, they are unconnected.

$\langle\psi\,|\,O\,|\,\phi\rangle =$

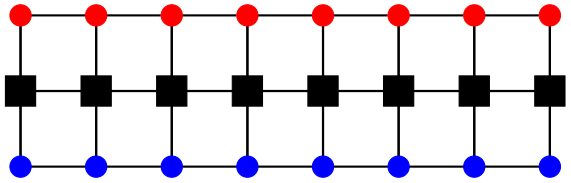

Figure 2.4: Graphical representation of a matrix element of some operator O. Here, the squares denote the matrices of the MPO representation of O, the blue dots the matrices of the MPS representation of $|\phi\rangle$ and the red dots the matrices of the MPS representation of $\langle\psi|$. Clearly, the matrix element is obtained by complete summation over all indices.

$T^{[i-1]}_{a_{i-1}\,b_{i-1}\,a'_{i-1}} =$

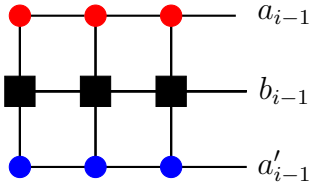

$\longrightarrow\ T^{[i]}_{a_i\,b_i\,a'_i} =$

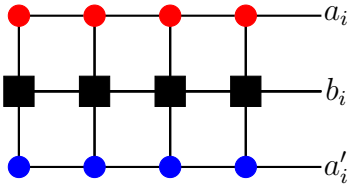

Figure 2.5: Graphical representation of one iteration in building T for the matrix element $\langle\psi\,|\,O\,|\,\phi\rangle$ of some operator O. Again, the squares are the matrices of the MPO representation of O, the blue dots denote the MPS form of $|\phi\rangle$ and the red dots that of $\langle\psi|$. The iteration simply consists of adding the matrices of a new site to the contraction, advancing T by one site. In this representation, the connection to the matrix elements is especially clear. In numerical practice, it is much more efficient to add the new tensors one by one, such that intermediate steps are performed.

Therefore, it is required to find tensors $A^{[i]}$ such that

$$\frac{\partial}{\partial A^{*\,\sigma_i}_{a_{i-1}\,a_i}} \left(\langle\psi\,|\,H\,|\,\psi\rangle - \lambda\,\langle\psi\,|\,\psi\rangle\right) = 0 \tag{2.36}$$

for all $A^{*\,\sigma_i}_{a_{i-1}\,a_i}$ for fixed i. Here, λ is a Lagrangian multiplier to enforce the constraint of constant norm.

To do so efficiently, one of the major strenghts of the MPS framework can be employed: Highly efficient caching of intermediate results and partial contractions of tensors. This can be demonstrated when considering the calculation of a matrix element $\langle\psi|O|\phi\rangle$ of some operator O. Let A^{σ_i} be the MPS representation of $|\psi\rangle$ and B^{σ_i} that of $|\phi\rangle$ as well as $W^{\sigma_i\,\sigma'_i}$ the MPO representation of O. In principle, the computation of the matrix element is straightforward as the matrix elements of O and the vector coefficients of $|\psi\rangle$, $|\phi\rangle$ in the product basis can be obtained using the MPO/MPS representations. Then, the matrix element is just obtained by total contraction of all tensors $W^{[i]}$, $A^{[i]}$ and $B^{[i]}$ as

$$\langle\psi\,|\,O\,|\,\phi\rangle = \sum A^{*\,\sigma_1}_{a_0\,a_1} W^{\sigma_1\,\sigma'_1}_{b_0\,b_1} B^{\sigma'_1}_{a'_0\,a'_1} \cdots A^{*\,\sigma_L}_{a_{L-1}\,a_L} W^{\sigma_L\,\sigma'_L}_{b_{L-1}\,b_L} B^{\sigma'_L}_{a'_{L-1}\,a'_L}\,, \tag{2.37}$$

where the summation goes over all appearing indices. Graphically, this can be written as elegantly as in figure 2.4.

To obtain this expression in an efficient way, it is highly useful to compute the necessary

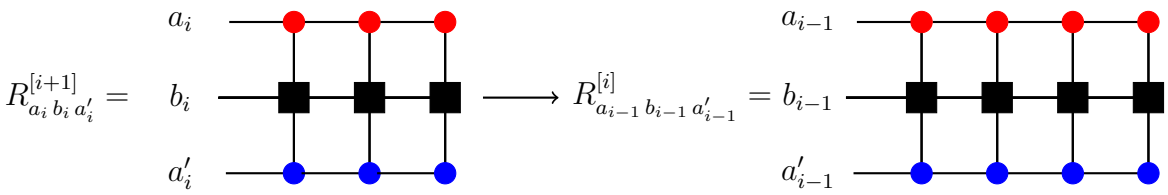

Figure 2.6: Graphical representation of one iteration in the iterative computation of matrix elements when starting from the right end of the chain. The tensors $R^{[i]}$ are build analogously to $T^{[i]}$ by contracting the previous tensor $R^{[i+1]}$ with the matrices of one site. Again, the complete summation is not carried out explicitly but the matrices are added one after another.

tensor contractions iteratively for one site after another. Therefore, define

$$\begin{aligned} T^{[0]}_{0,0,0} &= 1 \\ T^{[i]}_{a_i,b_i,a'_i} &= \sum_{\sigma_i, a_{i-1}} A^{*\,\sigma_i}_{a_{i-1},\, a_i} \left[\sum_{\sigma'_i\, b_{i-1}} W^{\sigma_i\, \sigma'_i}_{b_{i-1}\, b_i} \left(\sum_{a'_{i-1}} T^{[i-1]}_{a_{i-1}\, b_{i-1}\, a'_{i-1}} A^{\sigma'_i}_{a'_{i-1}\, a'_i} \right) \right] . \end{aligned} \tag{2.38}$$

Then, $T^{[i]}$ is the contraction of the appearing tensors up to site i and one iteration in building T corresponds to adding one to the contraction. This can be represented intuitively using the graphical representation for MPS and MPO as depicted in figure 2.5. The iteration procedure in (2.38) was written such that each sum corresponds to adding one tensor to the contraction. This is also precisely the order of summation that is used in the algorithm since it allows for optimal caching of intermediate results. It may readily be checked that the final iteration $T^{[L]}$ contains contractions over all indices and is therefore nothing but $\langle\psi|\, O\, |\phi\rangle$. This already allows for efficient computation of matrix elements of general opertors, for example to obtain correlation functions. But for the variational ground state search, the expectation value of the Hamiltonian, or its derivative respectively, has to be computed anew quite often. It is therefore desirable to cache as much intermediate results as possible.

Therefore, tensors $R^{[i]}$ may be defined iteratively by starting at the right end of the lattice and iterating towards $i = 0$ analogously to the procedure in building T, see figure 2.6.

As the ordering of contraction does not matter, the expectation value can, for any value of $0 < i < L + 1$ be rewritten as

$$\langle\psi|\, O\, |\phi\rangle = \sum_{a_i\, b_i\, a'_i} R^{[i+1]}_{a_i\, b_i\, a'_i} \left[\sum_{\sigma_i\, a_{i-1}} A^{*\,\sigma_i}_{a_{i-1}\, a_i} \left[\sum_{\sigma'_i\, b_{i-1}} W^{\sigma_i\, \sigma'_i}_{b_{i-1}\, b_i} \left(\sum_{a'_{i-1}} B^{\sigma_i}_{a'_{i-1}\, a'_i} T^{[i-1]}_{a_{i-1}\, b_{i-1}\, a'_{i-1}} \right) \right] \right] . \tag{2.39}$$

Again, the bracketing is set to indicate the optimal ordering of contractings. Here, the contractions are iteratively computed from the left from site 1 to site $i-1$ and from the right from site L to site $i+1$ and then combined at site i. This will just be formulation used for evaluating the expectation value of the Hamiltonian in the optimization scheme. A huge advantage is that the computation of $\langle\psi|\, O\, |\phi\rangle$ now only explicitly uses the matrices

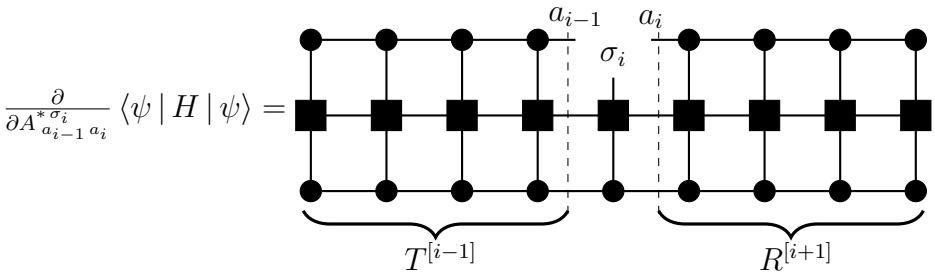

Figure 2.7: Graphical representation of equation (2.40) using the notations introduced in figures 2.1 and 2.2. In this notation, it is clear that the derivative of $\langle\psi \,|\, H \,|\, \psi\rangle$ with respect to $A^{*[i]}$ is of the same form as $A^{[i]}$. Also, the necessary contractions for performing the operation can be read off easily.

on site i, whereas the contribution from other sites is contained only in T and R. That is, when only varying the matrices of one site, recalculating the expectation value of the Hamiltonian is cheap.

When varying one tensor $A^{[i]}$ after another, the formulation (2.39) of $\langle\psi \,|\, H \,|\, \psi\rangle$ is particularly useful as it is quadratic in all matrix elements and the first derivative in (2.36) becomes an ordinary matrix-vector product. Let $W^{\sigma_i\,\sigma_i'}$ be the MPO matrices of the Hamiltonian and A^{σ_i} the MPS representation of some state $|\psi\rangle$, it is then

$$\frac{\partial}{\partial A^{*\,\sigma_i}_{a_{i-1}\,a_i}} \langle\psi \,|\, H \,|\, \psi\rangle = \sum_{a_i'\,b_i} R^{[i+1]}_{a_i\,b_i\,a_i'} \left[\sum_{\sigma_i'\,b_{i-1}} W^{\sigma_i\,\sigma_i'}_{b_{i-1}\,b_i} \left(\sum_{a_{i-1}'} T^{[i-1]}_{a_{i-1}\,b_{i-1}\,a_{i-1}'} A^{\sigma_i'}_{a_{i-1}'\,a_i'} \right) \right] \equiv H^{[i]}_{\text{eff}} A^{[i]} \,, \tag{2.40}$$

here, $R^{[i]}$ and $T^{[i]}$ are the partial contractions for the Hamiltonian with the state $|\psi\rangle$ and are defined as in (2.38). In general, it is more efficient to directly execute the contractions as this can be done in $\mathcal{O}(D^3)$ operations while constructing the matrix $H^{[i]}_{\text{eff}}$ corresponding to the matrix-vector product (2.40) requires $\mathcal{O}(D^4)$ operations. The outer and inner contractions are usually the dominant steps and scale as $\mathcal{O}(dD_W D^3)$.

As T and R are build iteratively, intermediate results $T^{[i]}/R^{[i]}$ for all sites to the left-/right from i are available such that it is not necessary to compute T and R anew from scratch when looking at a different i.

These properties make a 'sweeping' variation of the matrices attractive, where the matrices at site 1 are optimized first such that energy becomes minimal, then those on site 2 and so on, changing direction of the sweep when hitting the end of the chain. These sweeps can then be repeated until convergence is reached.

For the variation of the matrices, one further component is required, which is the normalization of the state. The scalar product of two states and therefore the norm of a state may be computed in a similar fashion as the matrix element of some operator in equation (2.39), by inserting the identity operator and implicitly evaluating the contractions involving it. This yields the expression depicted in figure 2.8. In contrast to the evaluation of matrix elements, the scalar product has not to be calculated explicitly for normalization, instead the norm can be obtained in an elegant way by keeping the MPS

$\langle\psi\,|\,\phi\rangle =$ 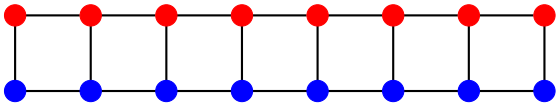

Figure 2.8: Scalar product of two MPS $|\psi\rangle$ and $|\phi\rangle$ whose matrices are denoted as blue and red dots respectively, using the graphical notation from figure 2.1. This directly follows from equation (2.39) and can be evaluated efficiently using a similar approach as in the evaluation of matrix elements.

in a so called mixed-canonical shape such that

$$\frac{\partial}{\partial A^{*\,\sigma_i}_{a_{i-1}\,a_i}} \langle\psi\,|\,\psi\rangle = A^{\sigma_i}_{a_{i-1}\,a_i}\,. \tag{2.41}$$

Therefore, a gauge degree of freedom in the matrices A^{σ_i} is used to reshape them after each step, such that one of the following holds

$$\sum_{\sigma_i} (A^{\sigma_i})^\dagger\, A^{\sigma_i} = \mathrm{id} \qquad \text{(left-normalization)} \tag{2.42}$$

$$\sum_{\sigma_i} A^{\sigma_i}\, (A^{\sigma_i})^\dagger = \mathrm{id} \qquad \text{(right-normalization)}\,. \tag{2.43}$$

A MPS is called left/right-canonical if all matrices are left/right-normalized and mixed-canonical if all matrices A^{σ_j} for are left-normalized for $j < i$ and right-normalized for $j > i$ for some i which is called orthogonality center. Normalization can be obtained via thin QR/RQ-decomposition [55] where the rectangular matrix R is multiplied into the matrices of the next site, destroying their normalization. Since the normalization of the orthogonality center in a mixed-canonical state is of no importance, this does not cause any problems however.

The normalization scheme is applied via operations on the matrices obtained by concatenating the A^{σ_i}, these are

$$A^{[i]}_l = \begin{pmatrix} A^{[i]\,1} \\ \vdots \\ A^{[i]\,d} \end{pmatrix} \tag{2.44}$$

$$A^{[i]}_r = \begin{pmatrix} A^{[i]\,1} & \cdots & A^{[i]\,d} \end{pmatrix}\,, \tag{2.45}$$

with matrix elements $A_{(a_{i-1}\,\sigma_i)\,a_i}$ and $A_{a_{i-1}\,(\sigma_i\,a_i)}$, respectively. For a detailed discussion including the usage of symmetries, see appendix B.

The normalization can be written in the graphical notation as in figure 2.9, revealing that the optimal form of the MPS for the variation of $A^{[i]}$ is in fact the mixed-canoncial form with orthogonality center i as this implies

$$\langle\psi\,|\,\psi\rangle = \sum_{\sigma_i\,a_{i-1}\,a_i} A^{*\,\sigma_i}_{a_{i-1}\,a_i} A^{\sigma_i}_{a_{i-1}\,a_i}\,. \tag{2.46}$$

The variational problem (2.36) is now reduced to the eigenvalue problem

$$H^{[i]}_{\mathrm{eff}} A^{[i]} = \lambda A^{[i]}\,, \tag{2.47}$$

(left-normalization) (right-normalization)

Figure 2.9: Graphical notation for the left/right-normalization of matrices. Since the first/last matrices of an MPS have row/column dimension of one, the summation over the left/right index can also be omitted there, such that this form can be inserted into figure 2.8, yielding equation (2.46).

which is of dimension dD^2. As only the solution with lowest energy is of interest, the eigenvalue problem can be solved iteratively, making the problem numerically treatable.

The ground state search algorithm may now be formulated as follows:

1. Pick an initial state ψ and get the right-canonical form of ψ. Then calculate $R^{[i]}$ of the Hamiltonian for all $i < L$.

2. Perform the right-sweep: For $0 < i < L$ starting with $i = 1$:
   a) Solve the eigenvalue problem (2.36) iteratively for the lowest eigenvalue, using the matrix-vector mutliplication (2.40) and the normalization (2.46) implied by the mixed-canonical form.
   b) Bring the matrices A^{σ_i} into left-normalized form by applying a QR-decomposition.
   c) Compute $T^{[i]}$ from $T^{[i-1]}$ and the new matrices A^{σ_i}.
   d) Go to the next site $i \to i + 1$.

3. Perform the left-sweep: For $1 < i < L + 1$ starting with $i = L$:
   a) Solve the eigenvalue problem (2.36) iteratively for the lowest eigenvalue.
   b) Bring the matrices A^{σ_i} into right-normalized form by applying a RQ-decomposition.
   c) Compute $R^{[i]}$ from $R^{[i+1]}$ and the new matrices A^{σ_i}.
   d) Go to the next site $i \to i - 1$.

4. Repeat steps 2 and 3 until either convergence is reached or a maximum number of sweeps has been executed.

Convergence is defined via the variance of energy, the search is said to be converged if $(\Delta E)^2$ drops below some threshold. The variance can here be obtained using the procedure of computing expectation values described above. Strictly spoken, since the variance vanishes for any eigenstate of the Hamiltonian, this does not guarantee the obtained state to be the ground state. Since the ansatz is usually better for the ground state than for excited states and the minimization aims at the lowest lying state, this does not pose a serious problem in practice [46].

In addition, there is also the problem of converging into local minima, which occurs mainly, but not exclusively [47], when including symmetries. Numerous schemes have been developed to evade this issue, see also section 2.2.2 and appendix B.

2.2.2 Symmetries and MPS

A remarkable speedup can be achieved when additional global symmetries of the Hamiltonian are utilized [49]. A useful interpretation in this context is that of the matrices A^{σ_i} being the coefficients of a decomposition of the form [47]

$$|\psi\rangle = \sum_{a_{i-1}\,\sigma_i\,a_i} A^{\sigma_i}_{a_{i-1}\,a_i}\, |a_{i-1}\rangle_l \otimes |\sigma_i\rangle \otimes |a_i\rangle_r \ , \tag{2.48}$$

where the basis states $|a_i\rangle_{l/r}$ are defined recursively via

$$\begin{aligned} |a_1\rangle_l &= \sum_{\sigma_1} A^{\sigma_1}_{1\,a_1}\, |\sigma_1\rangle \\ |a_i\rangle_l &= \sum_{\sigma_i\,a_{i-1}} A^{\sigma_i}_{a_{i-1}\,a_i}\, |a_{i-1}\rangle_l \otimes |\sigma_i\rangle \quad (i>1) \end{aligned} \tag{2.49}$$

$$\begin{aligned} |a_L\rangle_r &= \sum_{\sigma_L} A^{\sigma_L}_{a_L\,1}\, |\sigma_L\rangle \\ |a_i\rangle_r &= \sum_{\sigma_i\,a_{i+1}} A^{\sigma_{i+1}}_{a_i\,a_{i+1}}\, |\sigma_{i+1}\rangle \otimes |a_{i+1}\rangle_r \quad (i<L)\,. \end{aligned} \tag{2.50}$$

In particular, it is $|a_0\rangle_r = |a_L\rangle_l = |\psi\rangle$.

If i is the orthogonality center, the decomposition (2.48) can be made a Schmidt-decomposition via singular value decomposition of $A^{[i]}_l$, that is, the left and right basis states are orthonormal. This proves to be useful for obtaining the entanglement spectrum [56].

Since only abelian symmetries are utilized here, only these are implemented and shall briefly be discussed here. The usage of abelian symmetries is then realized via introducing quantum numbers for the states $|a_i\rangle_{l/r}$ to fix the quantum number of $|\psi\rangle$, meaning that $|\psi\rangle$ is then fixed in one symmetry sector [45, 52]. For demonstration, $U(1)$ is assumed as a symmetry group, describing for example a conserved particle number. In the model (1.2), there is both conserved particle number and conserved subchain parity, thus, the symmetry group utilized in the calculations will be $U(1) \otimes \mathbb{Z}_2$.

As discussed in [45, 52, 57], this can be achieved by attributing the concatenated matrices $A^{[i]}_{l/r}$ a block structure. Therefore, all states $|a_i\rangle_{l/r}$ are labeled with some quantum number $q_i(a_i)$. The quantum number N of $|\psi\rangle$ is then just $q_i(a_L)$. If this is to be consistent, the label $q_i(a_i)_r$ of $|a_i\rangle_r$ has to be fixed by the label $q_i(a_i)_l$ of $|a_i\rangle_l$ as $q_i(a_i)_r = N - q_i(a_i)_l$. Therefore, the index r/l is dropped and $q_i(a_i)$ henceforth refers always to $q_i(a_i)_l$. Formally, define also $q_i(a_0) = 0$. The physical indices σ_i have their quantum numbers $q(\sigma_i)$ fixed by construction of the product space as they correspond to states in the local Hilbert spaces. As with the local Hilbert space dimension d, the quantum numbers of σ_i can in principle depend on the site i, but it is assumed here for convenience that they do not as this does

not influence the procedure described here. Together with (2.49) and (2.50) this already fixes the block structure. It is then given simply by [45]

$$A^{\sigma_i}_{a_{i-1}\,a_i} \neq 0 \Rightarrow q_{i-1}(a_{i-1}) + q(\sigma_i) = q_i(a_i)\,. \tag{2.51}$$

To generalize this to other abelian symmetry groups like $U(1) \otimes \mathbb{Z}_2$, the addition of quantum numbers just has to be replaced by the corresponding group operation.

There are two subtleties appearing here that shall briefly be mentioned and are discussed in detail in appendix B. The first one is of a more technical nature and has to be taken care of in the implementation but does not affect the algorithm. The point is that the constraint (2.51) is sufficient for $|\psi\rangle$ to have a fixed quantum number N but not necessary. Therefore, it is possible for operations like normalization that conserve the total quantum number to destroy the block structure with potentially fatal results. Thus, one has to make sure that all operations conserve the block structure.

The second one is more of an obstacle to the algorithm and concerns the choice of the functions q_i. It turns out that the constraint put on the state $|\psi\rangle$ by the described procedure is stronger than just fixing the quantum number of $|\psi\rangle$ [45, 47]. It is readily seen that not only the quantum number of $|\psi\rangle$ is uniquely determined by (2.51) but also that of the left/right basis for any Schmidt decomposition. Unfortunately, it is impossible for the algorithm described in section 2.2.1 to dynamically adapt the labeling functions q_i. Therefore, in the likely case that the initial choice of q_i does not fit the variationally optimal state, it can not be found by the algorithm presented in section 2.2.1 [45].

There are several approaches that circumvent this obstacle, including the two-site DMRG [28], the density matrix perturbation [58] and the center wavefunction formalism [52]. In the implementation used here, the strictly-single-site algorithm DMRG3S presented in [47] based on subspace expansion is used due to both its simplicity and the low required numerical effort.

2.2.3 Computation of excited states

In order to calculate energy gaps or to consider the ground state degeneracy in the absence of the $\mathbb{Z}_2$ symmetry, it is required to compute not only the ground state of a given Hamiltonian but also other eigenstates. In practice and due to limited computational resources, this is usually limited to a few low-energy states. Also, while the area law of entanglement entropy guarantees that the MPS ansatz is a good approximation for the ground state, I am unaware of an analogous result for excited states, these may or may not be able to be expressed as an MPS with numerically treatable bond dimension. Here, the approach presented in [46] is employed. The basic idea behind this excited state search scheme is to limit the variation of the state $|\psi\rangle$ to the space orthogonal to all previously obtained states $|\phi_k\rangle$.

In principle, in addition to $\langle\psi\,|\,\psi\rangle = 1$, the constraint $\langle\psi\,|\,\phi_k\rangle = 0$ is now imposed. The local eigenvalue problem can then be reformulated [46] as

$$P^{[i]\dagger} H^{[i]}_{\text{eff}} P^{[i]} A^{[i]} = \lambda A^{[i]}\,, \tag{2.52}$$

with the projector $P^{[i]}$ onto the space orthogonal to all $|\phi_k\rangle$. It is self-adjoint, the hermitian conjugation can therefore be omitted. The construction and application of the projection operator is done using the scheme presented in [46], a short description thereof can be found in appendix C.

2.2.4 Implementation

The DMRG3S algorithm is implemented using C++11 and making use of the BLAS [59], LAPACK [60] and Arpack [61] libraries. The BLAS and LAPACK routines and their C interface from Intel MKL [62] are therefore used, as well as the Arpack++ interface for Arpack [63]. The implementation contains functions for variationally obtaining ground and excited state for a given Hamiltonian in MPO representation and for computing the expectation value of obserables for the resulting states. Correlation functions can be obtained in an efficient way without computing the full expectation value at each site anew. The entanglement spectrum can also be obtained as described below.

Unfortunately, efforts to also implement the iDMRG algorithm did not succeed to include the symmetries, in particular the $\mathbb{Z}_2$ symmetry, in a meaningful way.

The source code is freely available, please contact guther@itp3.uni-stuttgart.de for access.

The evaluation of the results and the generation of the corresponding plots is done using Python 2.7.6 and the matplotlib library [64].

Chapter 3

Analysis of the ladder system

3.1 Bosonization approach to the ladder system

Apart from the numerical treatment, bosonization is employed to analyze the Hamiltonian (1.2) perturbatively. This will yield a qualitative insight into the behaviour of correlation functions and allow for a prediction of possible occuring phases. In the thermodynamic limit, the potential term $\sum J\left(n_i^a + n_{i+1}^a + n_i^b + n_{i+1}^b\right)$ is just a filling dependent constant and it is therefore omitted in the bosonization analysis. In the numerical analysis it has to be included however.

Since bosonization is a field theoretical method, the continuum limit $a \to 0$ while $k_F a = \text{const.}$ is considered, where a is the lattice spacing.

3.1.1 Bosonization of the Hamiltonian in continuum limit

Here, start from the on-chain kinetic part of the Hamiltonian (1.2) which is a theory of free fermions. In bosonized form, this reads as shown e.g. in [39]

$$H_0 = \frac{1}{2} \sum_{\sigma=a,2} \int \mathrm{d}x \, (\partial_x \theta_\sigma)^2 + (\partial_x \phi_\sigma)^2 \,, \tag{3.1}$$

up to some constant prefactor which is the Fermi velocity v. The coupling constants are then expressed in units of v. Here, σ is again the wire index. It is convenient for the treatment of this system to express the boson fields in terms of the symmetric and the antisymmetric combinations analogously to [32] which are defined as

$$\phi_\pm = \frac{1}{\sqrt{2}}(\phi_a \pm \phi_b) \tag{3.2}$$

$$\theta_\pm = \frac{1}{\sqrt{2}}(\theta_a \pm \theta_b) \,. \tag{3.3}$$

The new fields are also periodic with $\phi_\pm = \phi_\pm + \sqrt{\pi}$ and $\theta_\pm = \theta_\pm + \sqrt{\pi}$. It may be readily checked that the free theory does not change form under this transformation, it

reads now

$$H_0 = \frac{1}{2} \sum_{\eta=+,-} \int \mathrm{d}x \, (\partial_x \theta_\eta)^2 + (\partial_x \phi_\eta)^2 \, . \tag{3.4}$$

3.1.1.1 Intra-Chain interactions

To end up with the model (1.2), three interaction terms have to be added. The first one is a local on-chain interaction of the form

$$H_1 = -2J \sum_i n_i^a n_{i+1}^a + n_i^b n_{i+1}^b \, , \tag{3.5}$$

which has frequently been discussed using bosonization [27, 34, 65] in the framework of the Luttinger liquid theory. This standard procedure will also be applied here. The continuum limit is now taken using the procedure described in [38] by defining

$$\psi_a(ia) = \frac{a_i}{\sqrt{a}} \tag{3.6}$$

$$\psi_b(ia) = \frac{b_i}{\sqrt{a}} \, , \tag{3.7}$$

with $a_i \, (b_i)$ being the fermionic annihilation operator on site i of wire $a(b)$. Beware that non-subscript a is the lattice spacing, which is only not completely unambigious at this point. Left-/right-movers are then introduced using equation (2.1)

$$\psi_\sigma(x) = \mathrm{e}^{ik_F x} \psi_{R\sigma}(x) + \mathrm{e}^{-ik_F x} \psi_{L\sigma}(x) \, , \tag{3.8}$$

where $\psi_{R\sigma}$ is the right-moving field and $\psi_{L\sigma}$ the left-moving field on wire σ.

Using the bosonization identities (2.19), (2.19), the fermionic fields are now in terms of $\phi_\pm$ and $\theta_\pm$ expressed as

$$\psi_{\alpha\sigma} = \frac{\eta_{\alpha\sigma}}{\sqrt{2\pi}} \exp\left[i \sqrt{\frac{\pi}{2}} \left(\theta_+ + s_\sigma \theta_- + s_\alpha \phi_+ + s_\alpha s_\sigma \phi_- \right) \right] \, , \tag{3.9}$$

where again σ is the wire index and α the left-/right-mover index. The x-dependence of the fields is not explicitly noted, but all fields are taken at the same position. Here, the sign prefactors

$$s_R = 1 \tag{3.10}$$

$$s_L = -1 \tag{3.11}$$

$$s_a = 1 \tag{3.12}$$

$$s_b = -1 \tag{3.13}$$

were defined. From now on, this definition holds for the rest of this thesis.

Taking the continuum limit for the perturbation (3.5) for $k_F a \neq \frac{\pi}{2}$ gives

$$H_{1,c} = -J \sum_{\sigma=a,2} \int \mathrm{d}x \, (\psi_{R\sigma}^\dagger \psi_{R\sigma})^2 + (\psi_{L\sigma}^\dagger \psi_{L\sigma})^2 + 4 \sin^2(k_F a) \psi_{R\sigma}^\dagger \psi_{R\sigma} \psi_{L\sigma}^\dagger \psi_{L\sigma} \, . \tag{3.14}$$

The umklapp terms $\psi^\dagger_{R\sigma}\psi_{L\sigma}\psi^\dagger_{R\sigma}\psi_{L\sigma}$ etc. vanish upon integration away from half filling. Bosonization is straightforward using the bosonization of density terms (2.26), leading to

$$\begin{aligned} H_{1,c} =& \frac{J}{4\pi}\sum_\sigma \int \mathrm{d}x\, \frac{1}{4}\left(\partial_x(\phi_\sigma+\theta_\sigma)\right)^2 + \frac{1}{4}\left(\partial_x(\phi_\sigma-\theta_\sigma)\right)^2 + \sin^2(k_F a)\partial_x(\phi_\sigma-\theta_\sigma)\partial_x(\phi_\sigma+\theta_\sigma) \\ =& \frac{J}{4\pi}\sum_\sigma \int \mathrm{d}x\, \left(\frac{1}{2}+\sin^2(k_F a)\right)\left(\partial_x\phi_\sigma\right)^2 + \left(\frac{1}{2}-\sin^2(k_F a)\right)\left(\partial_x\theta_\sigma\right)^2 \end{aligned} \tag{3.15}$$

Again, the transformation towards $\theta_\pm$ and $\phi_\pm$ can be applied and the resulting Hamiltonian density can be absorbed into H_0 via introduction of two constants

$$K = \sqrt{\frac{1+\frac{J}{4\pi}(1+2\sin^2(k_F a))}{1+\frac{J}{4\pi}(1-2\sin^2(k_F a))}} \tag{3.16}$$

$$\nu = 2\sqrt{1+\frac{2J}{4\pi}+\frac{J^2}{16\pi^2}(1-4\sin^4(k_F a))}\,. \tag{3.17}$$

The Luttinger parameter K leads to a rescaling of the fields $\theta_\pm$ and $\phi_\pm$ while the velocity ν is just a global prefactor [34]. In principle, K and ν do not have to be the same for the $\pm$-sectors, but the sector index $K_\pm$ will not be denoted explicitly if it is clear which Luttinger paramter is meant.

The Hamiltonian density including the perturbation is now

$$\mathcal{H}_{0+1,c} = \sum_{\eta=\pm}\frac{\nu}{2}\left[K(\partial_x\theta_\eta)^2 + \frac{1}{K}(\partial_x\phi_\eta)^2\right], \tag{3.18}$$

The rescaled fields $\tilde{\phi}_\pm = \sqrt{K}\phi_\pm$ and $\tilde{\theta}_\pm = \frac{1}{\sqrt{K}}\theta_\pm$ are introduced, which are dual to each other, as demonstrated in [34]. From now on, only the rescaled fields are considered, and thereby they are denoted just as θ and ϕ. In terms of the rescaled fields, $H_{0+1,c}$ has now the same form as the free theory $H_{0,c}$. In particular, the rescaled fields in $H_{0+1,c}$ have the same correlation fucntions as the bare fields in $H_{0,c}$, that is

$$\langle\theta_\pm(x)\theta_\pm(0)\rangle = \langle\phi_\pm(x)\phi_\pm(0)\rangle = -\frac{1}{2\pi}\log(|x|) \tag{3.19}$$

$$\langle\theta_\pm(x)\phi_\pm(0)\rangle = -\langle\phi_\pm(x)\theta_\pm(0)\rangle = \frac{i}{2}\mathrm{sgn}(x) + \frac{i}{2} \tag{3.20}$$

Also, the compactification is rescaled to $\phi_\pm = \phi_\pm + \sqrt{\frac{\pi}{K}}$ and analogously $\theta_\pm = \theta_\pm + \sqrt{\pi K}$.

3.1.1.2 Inter-Chain pair-hopping

The second perturbation considered is a pair-hopping with the discrete form

$$H_2 = W\sum_i a_i^\dagger a_{i+1}^\dagger b_i b_{i+1} + \text{h.c.}\,. \tag{3.21}$$

Such interactions have previously been considered using bosonization in the context of topological order e.g. in [32, 24] with similar results. See in particular [32] for a detailed discussion including refermionization and the connection to topological edge states.

Inserting expressions (3.6), (3.7) and (2.1) and taking the continuum limit yields

$$\begin{aligned}
H_{2,c} =& W \int \mathrm{d}x \left(\mathrm{e}^{-ik_F x}\psi^\dagger_{Ra} + \mathrm{e}^{ik_F x}\psi^\dagger_{La}\right)\left(\mathrm{e}^{-ik_F(x+a)}\psi^\dagger_{Ra} + \mathrm{e}^{ik_F(x+a)}\psi^\dagger_{La}\right) \\
&\times \left(\mathrm{e}^{ik_F x}\psi_{Rb} + \mathrm{e}^{-ik_F x}\psi_{Lb}\right)\left(\mathrm{e}^{ik_F(x+a)}\psi_{Rb} + \mathrm{e}^{-ik_F(x+a)}\psi_{Lb}\right) + \mathrm{h.c.} \\
=& W \int \mathrm{d}x \left[2\psi^\dagger_{Ra}\psi^\dagger_{La}\psi_{Lb}\psi_{Rb} + \mathrm{e}^{-2ik_F a}\psi^\dagger_{Ra}\psi^\dagger_{La}\psi_{Rb}\psi_{Lb} + \mathrm{e}^{2ik_F a}\psi^\dagger_{La}\psi^\dagger_{Ra}\psi_{Lb}\psi_{Rb}\right. \\
&\left. + \left(\psi^\dagger_{Ra}\psi_{Rb}\right)^2 + \left(\psi^\dagger_{La}\psi_{Lb}\right)^2\right] + \mathrm{h.c.} \\
=& W \int \mathrm{d}x \left[2(1-\cos(2k_F a))\psi^\dagger_{Ra}\psi^\dagger_{La}\psi_{Lb}\psi_{Rb} + \left(\psi^\dagger_{Ra}\psi_{Rb}\right)^2 + \left(\psi^\dagger_{La}\psi_{Lb}\right)^2\right] + \mathrm{h.c.}
\end{aligned} \tag{3.22}$$

The term $\psi^\dagger_{Ra}\psi^\dagger_{La}\psi_{Lb}\psi_{Rb}$ may be rewritten using the bosonization identity 3.9 as

$$\begin{aligned}
\psi^\dagger_{Ra}\psi^\dagger_{La}\psi_{Lb}\psi_{Rb} \propto& \frac{1}{(2\pi)^2}\exp\left[-i\sqrt{\frac{\pi}{2}}\left(\frac{1}{\sqrt{K}}(2s_a - 2s_b)\theta_- + \sqrt{K}(s_A + s_B - s_A - s_B)\phi_+\right.\right. \\
&\left.\left. + \sqrt{K}(s_a s_A + s_a s_B - s_b s_B - s_b s_A)\phi_-\right)\right] \\
=& \frac{1}{(2\pi)^2}\exp\left(-i\sqrt{\frac{8\pi}{K}}\theta_-\right) .
\end{aligned} \tag{3.23}$$

And the quadratic term can be rewritten analogously using

$$\psi^\dagger_{\alpha 1}\psi_{\alpha 2} \propto \frac{1}{2\pi}\exp\left[i\sqrt{2\pi}\left(\frac{1}{\sqrt{K}}\theta_- + s_\alpha\sqrt{K}\phi_-\right)\right] . \tag{3.24}$$

Then, it is simply

$$\left(\psi^\dagger_{Ra}\psi_{Rb}\right)^2 + \mathrm{h.c.} \propto \cos\left(\sqrt{8\pi}\left(\frac{1}{\sqrt{K}}\theta_- + \sqrt{K}\phi_-\right)\right) , \tag{3.25}$$

and analogously for $\left(\psi^\dagger_{La}\psi_{Lb}\right)^2$.

Let q_i be the prefactors of the resulting terms, then the Hamiltonian density of $H_{2,c}$ can be written as

$$\begin{aligned}
\mathcal{H}_{2,c} =& q_1 \cos\left(\sqrt{\frac{8\pi}{K}}\theta_-\right) + q_2 \cos\left(\sqrt{8\pi}\left(\frac{1}{\sqrt{K}}\theta_- + \sqrt{K}\phi_-\right)\right) \\
&+ q_3 \cos\left(\sqrt{8\pi}\left(\frac{1}{\sqrt{K}}\theta_- - \sqrt{K}\phi_-\right)\right) .
\end{aligned} \tag{3.26}$$

The latter two terms turn out to be always irrelevant, the resulting Hamiltonian without these is then in fact the well known sine-Gordon model [42, 56] which has already been studied in the context of topological order [32] and is known for the Kosterlitz-Thouless transition [66, 67]. In [32] it has been shown that the resulting Hamiltonian can be refermionized to the continuum limit of the Kitaev chain in a special case and can therefore describe the topological phase with the corresponding ground state degeneracy [30, 32].

Before further discussing this result, the last term shall be considered, that is, the inter-chain density-density interaction.

3.1.1.3 Inter-Chain density-density interactions

To end up with the analyzed model an additional perturbation has to be taken into account. This is, on the microscopic level, an inter-chain density-density interaction of the form

$$H_3 = g \sum_i n_i^a n_{i+1}^a (1 - n_i^b)(1 - n_{i+1}^b) + (1 \leftrightarrow 2)\,. \tag{3.27}$$

This decomposes into two-, three- and four-particle interactions. The respective terms are defined as

$$H_3 = g \sum_i A_i + B_i + C_i \tag{3.28}$$

$$A_i = n_i^a n_{i+1}^a + n_i^b n_{i+1}^b \tag{3.29}$$

$$B_i = 2 n_i^a n_{i+1}^a n_i^b n_{i+1}^b \tag{3.30}$$

$$C_i = -n_i^a n_{i+1}^a n_i^b - n_i^a n_{i+1}^a n_{i+1}^b - n_i^b n_{i+1}^b n_i^a - n_i^b n_{i+1}^b n_{i+1}^a\,. \tag{3.31}$$

The two-particle term A_i is proportional to H_1 as described above.

Consider now the four-particle term B_σ. The prefactor of 2 comes from the symmetrization of H_3 with respect to wire exchange. In contrast to the two-particle term, the oscillating terms of $n_{\sigma,i} n_{\sigma,i+1}$ do contribute here. The full lowest order continuum limit U_σ for $n_{\sigma,i} n_{\sigma,i+1}$ reads (all fields are taken at position x, an x-dependency is not explicitly expressed):

$$\begin{aligned}
U_\sigma =& \left(\mathrm{e}^{-ik_F x}\psi_{R\sigma}^\dagger + \mathrm{e}^{ik_F x}\psi_{L\sigma}^\dagger\right)\left(\mathrm{e}^{ik_F x}\psi_{R\sigma} + \mathrm{e}^{-ik_F x}\psi_{L\sigma}\right) \\
&\times \left(\mathrm{e}^{-ik_F(x+a)}\psi_{R\sigma}^\dagger + \mathrm{e}^{ik_F(x+a)}\psi_{L\sigma}^\dagger\right)\left(\mathrm{e}^{ik_F(x+a)}\psi_{R\sigma} + \mathrm{e}^{-ik_F(x+a)}\psi_{L\sigma}\right) \\
=& \left(\psi_{R\sigma}^\dagger\psi_{R\sigma} + \psi_{L\sigma}^\dagger\psi_{L\sigma} + \mathrm{e}^{-2ik_F x}\psi_{R\sigma}^\dagger\psi_{L\sigma} + \mathrm{e}^{2ik_F x}\psi_{L\sigma}^\dagger\psi_{R\sigma}\right) \\
&\times \left(\psi_{R\sigma}^\dagger\psi_{R\sigma} + \psi_{L\sigma}^\dagger\psi_{L\sigma} + \mathrm{e}^{-2ik_F(x+a)}\psi_{R\sigma}^\dagger\psi_{L\sigma} + \mathrm{e}^{2ik_F(x+a)}\psi_{L\sigma}^\dagger\psi_{R\sigma}\right) \\
=& (\psi_{R\sigma}^\dagger\psi_{R\sigma}^\dagger)^2 + (\psi_{L\sigma}^\dagger\psi_{L\sigma}^\dagger)^2 + 4\sin^2(k_F a)\psi_{R\sigma}^\dagger\psi_{R\sigma}\psi_{L\sigma}^\dagger\psi_{L\sigma} \\
&+ \mathrm{e}^{4ik_F x + 2ik_F a}\psi_{L\sigma}^\dagger\psi_{R\sigma}\psi_{L\sigma}^\dagger\psi_{R\sigma} + \mathrm{e}^{-4ik_F x - 2ik_F a}\psi_{R\sigma}^\dagger\psi_{L\sigma}\psi_{R\sigma}^\dagger\psi_{L\sigma} \\
&+ \mathrm{e}^{2ik_F x}\psi_{L\sigma}^\dagger\psi_{R\sigma}\left(\psi_{R\sigma}^\dagger\psi_{R\sigma} + \psi_{L\sigma}^\dagger\psi_{L\sigma}\right)(1 + \mathrm{e}^{2ik_F a}) \\
&+ \mathrm{e}^{-2ik_F x}\psi_{R\sigma}^\dagger\psi_{L\sigma}\left(\psi_{R\sigma}^\dagger\psi_{R\sigma} + \psi_{L\sigma}^\dagger\psi_{L\sigma}\right)(1 + \mathrm{e}^{-2ik_F a}) \\
=& (\psi_{R\sigma}^\dagger\psi_{R\sigma}^\dagger)^2 + (\psi_{L\sigma}^\dagger\psi_{L\sigma}^\dagger)^2 + 4\sin^2(k_F a)\psi_{R\sigma}^\dagger\psi_{R\sigma}\psi_{L\sigma}^\dagger\psi_{L\sigma} \\
&+ \mathrm{e}^{2ik_F x}\psi_{L\sigma}^\dagger\psi_{R\sigma}(1 + \mathrm{e}^{2ik_F a}) + \mathrm{e}^{-2ik_F x}\psi_{R\sigma}^\dagger\psi_{L\sigma}(1 + \mathrm{e}^{-2ik_F a}) \\
&+ \mathrm{e}^{4ik_F x + 2ik_F a}\psi_{L\sigma}^\dagger\psi_{R\sigma}\psi_{L\sigma}^\dagger\psi_{R\sigma} + \mathrm{e}^{-4ik_F x - 2ik_F a}\psi_{R\sigma}^\dagger\psi_{L\sigma}\psi_{R\sigma}^\dagger\psi_{L\sigma} \\
=& V_\sigma + M_\sigma + F_\sigma\,,
\end{aligned} \tag{3.32}$$

Note that the two-particle term from H_1 is just $U_a + U_b$, but the oscillating terms drop out during integration away from half filling, leaving precisely the Hamiltonian density of $H_{1,c}$. In the last step, the anticommutation relations were employed to get rid of the

density term in M. Here, it is defined

$$V_\sigma = (\psi^\dagger_{R\sigma}\psi^\dagger_{R\sigma})^2 + (\psi^\dagger_{L\sigma}\psi^\dagger_{L\sigma})^2 + 4\sin^2(k_F a)\psi^\dagger_{R\sigma}\psi_{R\sigma}\psi^\dagger_{L\sigma}\psi_{L\sigma} \tag{3.33}$$

$$M_\sigma = \mathrm{e}^{2ik_F x}\psi^\dagger_{L\sigma}\psi_{R\sigma}(1+\mathrm{e}^{2ik_F a}) + \text{h.c.} \tag{3.34}$$

$$F_\sigma = \mathrm{e}^{4ik_F x + 2ik_F a}\left(\psi^\dagger_{L\sigma}\psi_{R\sigma}\right)^2 + \text{h.c.} \tag{3.35}$$

Also note that any term mixing V, M and F contains an oscillating prefactor and thus does not contribute unless $4k_F a = 2\pi$ which is the case at half filling. In the following, any oscillating term is neglected as it drops out during integration save for special cases, see also section 3.1.2. Therefore, it is

$$B_{\text{cont}} = V_a V_b + M_a M_b + F_a F_b\,. \tag{3.36}$$

From equation (3.33) one can readily see that $V_a V_b$ consists only of density terms and these always appear with power of four. However, in bosonized form, density terms are of the form $\partial_x(\theta \pm \phi)$ and therefore, $V_a V_b$ only contains derivatives of the boson fields in powers of four. Such terms are irrelevant in the RG sense independent of any other parameter as has been shown in section 2.1.3. Thus, $V_a V_b$ is always irrelevant with a scaling dimension of $\Delta = 4$. The second term on the other hand reads

$$M_a M_b = 2(1+\cos(2k_F a))\psi^\dagger_{La}\psi_{Ra}\psi^\dagger_{Rb}\psi_{Lb} + \text{h.c.}\,. \tag{3.37}$$

Now, the density terms dropped out and therefore, the term is not per se irrelevant. The bosonized form of $M_a M_b$ is now

$$\begin{aligned} M_a M_b &\propto 2(1+\cos(2k_F a))\left(\exp\left(2i\sqrt{2\pi K}\phi_-\right) + \exp\left(-2i\sqrt{2\pi K}\phi_-\right)\right) \\ &= 4(1+\cos(k_F a))\cos(\sqrt{8\pi K}\phi_-)\,. \end{aligned} \tag{3.38}$$

Here, equation (3.62) was used in the form

$$\psi^\dagger_{Ra}\psi_{La} = \text{const.}\ \times\ \exp\left(-i\sqrt{2\pi K}(\phi_+ + \phi_-)\right) \tag{3.39}$$

$$\psi^\dagger_{Lb}\psi_{Rb} = \text{const.}\ \times\ \exp\left(i\sqrt{2\pi K}(\phi_+ - \phi_-)\right)\,. \tag{3.40}$$

The third term $F_a F_b$ simply gives, neglecting oscillating terms, the square of $M_a M_b$ without the density-dependent prefactor. This is

$$F_a F_b = \left(\psi^\dagger_{La}\psi_{Ra}\right)^2\left(\psi^\dagger_{Rb}\psi_{Lb}\right)^2 \propto \cos\left(\sqrt{32\pi K}\phi_-\right)\,, \tag{3.41}$$

again using equation (3.62). Like $M_a M_b$, this term is also potentially relevant. Analogously to the procedure in section 3.1.2, the scaling dimension may be computed yielding $\Delta = 8K$ as scaling dimension for $F_a F_b$.

This can also be understood qualitatively using the naive argument that the continuum limit of $n^a_i n^a_{i+1}$ should be of the same form as that of $(n^a_i)^2$. Since the density is idempotent, this is just the same as n^a_i, explaining why the four particle-interaction has a continuum limit similar to that of the Hubbard interaction $n^a_i n^b_i$. When taking into account the

three-particle contribution however, it will become clear that the term $M_a M_b$ drops out in the final form of H_3 and thus will not be of further concern.

To see that, consider the continuum limit of the three-particle interactions in H_3. It will now be shown that these only differ from $M_a M_b$ in irrelevant terms. Since they appear in H_3 with the opposite sign, the potentially relevant contribution of $M_a M_b$ will drop out of H_3. The three particle contribution is of the form

$$C_i = -n_i^a n_{i+1}^a n_i^b - n_{1,j} n_{i+1}^a n_{i+1}^b + (1 \leftrightarrow 2)\,. \tag{3.42}$$

The continuum limit of the first term reads, while omitting oscillating terms that drop out in integration

$$\begin{aligned} n_i^a n_{i+1}^a n_i^b \to & U_a \left(\mathrm{e}^{-ik_F x}\psi_{Rb}^\dagger + \mathrm{e}^{ik_F x}\psi_{Lb}^\dagger\right)\left(\mathrm{e}^{ik_F x}\psi_{Rb} + \mathrm{e}^{-ik_F x}\psi_{Lb}\right) \\ = & \left((\psi_{Ra}^\dagger\psi_{Ra})^2 + (\psi_{La}^\dagger\psi_{La})^2 + 4\sin^2(k_F a)\psi_{Ra}^\dagger\psi_{Ra}\psi_{La}^\dagger\psi_{La}\right)\left(\psi_{Rb}^\dagger\psi_{Rb} + \psi_{Lb}^\dagger\psi_{Lb}\right) \\ & + \psi_{La}^\dagger\psi_{Ra}\psi_{Rb}^\dagger\psi_{Lb}(1+\mathrm{e}^{2ik_F a}) + \psi_{Ra}^\dagger\psi_{La}\psi_{Lb}^\dagger\psi_{Rb}(1+\mathrm{e}^{-2ik_F a})\,. \end{aligned} \tag{3.43}$$

The density terms are of third order and therefore have scaling dimension $\Delta = 3$ and are irrelevant. Again, the oscillating terms drop in integration. The possibly relevant terms are therefore the same as for the four-particle term. The second term appearing in C_i is essentially of the same form, save for an additional $\mathrm{e}^{ik_F a}$:

$$\begin{aligned} n_i^a n_{i+1}^a n_{i+1}^b \to & U_a \left(\mathrm{e}^{-ik_F x}\psi_{Rb}^\dagger + \mathrm{e}^{ik_F x}\psi_{Lb}^\dagger\right)\left(\mathrm{e}^{ik_F (x+a)}\psi_{Rb} + \mathrm{e}^{-ik_F (x+a)}\psi_{Lb}\right) \\ = & \left(\psi_{Ra}^\dagger\psi_{Ra})^2 + (\psi_{La}^\dagger\psi_{La})^2 + 4\sin^2(k_F a)\psi_{Ra}^\dagger\psi_{Ra}\psi_{La}^\dagger\psi_{La}\right)\left(\psi_{Rb}^\dagger\psi_{Rb} + \psi_{Lb}^\dagger\psi_{Lb}\right) \\ & + \psi_{La}^\dagger\psi_{Ra}\psi_{Rb}^\dagger\psi_{Lb}(1+\mathrm{e}^{-2ik_F a}) + \psi_{Ra}^\dagger\psi_{La}\psi_{Lb}^\dagger\psi_{Rb}(1+\mathrm{e}^{2ik_F a})\,. \end{aligned} \tag{3.44}$$

Thus, the only possibly relevant term in C_i is

$$-2\left(\psi_{La}^\dagger\psi_{Ra}\psi_{Rb}^\dagger\psi_{Lb} + \psi_{Ra}^\dagger\psi_{La}\psi_{Lb}^\dagger\psi_{Rb}\right)2(1+\cos(2k_F a)) + \text{h.c.} = -2M_a M_b \tag{3.45}$$

Again, the factor of 2 comes from symmetrization with respect to wire exchange.

This cancels precisely the term $M_a M_b$ from the four particle contribution.

At half filling, an additional contribution of the form $\cos(\sqrt{32\pi K}\phi_+)$ arises, as terms with oscillating prefactors remain. This is discussed in section 3.1.2.

3.1.2 Gapped phases

Perturbations can in principle open a gap in the gapless free theory. In the bosonized theory, the opening of a gap can, in the low-energy limit, be described by one of the fields $\phi_\pm$, $\theta_\pm$ becoming massive [42, 56]. This also leads to exponential decay of the fermionic correlation functions [68] as will be seen in section 3.2.1.

It should be kept in mind, that for the whole theory to become gapped, there has to be a gap in both sectors. Hence, the topological phase is still gapless even though the field θ_- becomes massive as is demonstrated below.

All possible gaps in certain sectors discussed so far except for the charge gap in the antisymmetric sector have been confirmed using DMRG.

3.1.2.1 Topological phase

The hamiltonian density including all perturbations away from half filling can be written in terms of the rescaled fields as

$$\begin{aligned}\mathcal{H} = &\sum_{\eta=\pm} \frac{\nu}{2}\left[(\partial_x\theta_\eta)^2 + (\partial_x\phi_\eta)^2\right] + q_1\cos\left(\sqrt{\frac{8\pi}{K}}\theta_-\right)\\ &+ q_2\cos\left(\sqrt{8\pi}\left(\frac{1}{\sqrt{K}}\theta_- + \sqrt{K}\phi_-\right)\right) + q_3\cos\left(\sqrt{8\pi}\left(\frac{1}{\sqrt{K}}\theta_- - \sqrt{K}\phi_-\right)\right)\\ &+ q_4\cos\left(\sqrt{32\pi K}\phi_-\right)\,,\end{aligned} \tag{3.46}$$

with coupling constants q_i. To determine whether the terms is relevant or not, the scaling dimension has to be computed. This is done accordingly to [42]. Consider first the $\cos\left(\sqrt{\frac{8\pi}{K}}\theta_-\right)$-term, which turns out to be responsible for the topological phase and characterizes the sine-Gordon model [56] with well-known RG equations [67]. Here, the simple argumentation from section 2.1.3 according to [42] shall be employed. A more detailed discussion can be found in [32, 34, 67]. According to the neutrality condition (2.29) together with (2.25), it is

$$\langle \mathrm{e}^{i\sqrt{\frac{8\pi}{K}}\theta_-(x)}\mathrm{e}^{i\sqrt{\frac{8\pi}{K}}\theta_-(0)}\rangle = 0\,. \tag{3.47}$$

And therefore

$$\left\langle \cos\left(\sqrt{\frac{8\pi}{K}}\theta_-(x)\right)\cos\left(\sqrt{\frac{8\pi}{K}}\theta_-(0)\right)\right\rangle \propto \left\langle \mathrm{e}^{i\sqrt{\frac{8\pi}{K}}\theta_-(x)}\mathrm{e}^{-i\sqrt{\frac{8\pi}{K}}\theta_-(0)}\right\rangle\,. \tag{3.48}$$

According to equation (2.25), it is then

$$\left\langle \cos\left(\sqrt{\frac{8\pi}{K}}\theta_-(x)\right)\cos\left(\sqrt{\frac{8\pi}{K}}\theta_-(0)\right)\right\rangle \propto \mathrm{e}^{\frac{8\pi}{K}\langle\theta_-(x)\theta_-(0)\rangle}\,. \tag{3.49}$$

Since the expectation value is taken with respect to the unperturbed groundstate, the correlation functions (2.16) can be inserted, yielding

$$\left\langle \cos\left(\sqrt{\frac{8\pi}{K}}\theta_-(x)\right)\cos\left(\sqrt{\frac{8\pi}{K}}\theta_-(0)\right)\right\rangle \propto |x|^{-\frac{4}{K}}\,. \tag{3.50}$$

The scaling dimension is therefore $\Delta = \frac{2}{K}$ and the term is thus relevant for $K > 1$.

Analogously the scaling dimensions of the other terms from (3.46) can be computed. The two terms with coupling constant $q_{2,3}$ have scaling dimension $\Delta = 2\left(K + \frac{1}{K}\right)$ and are therefore always irrelevant. The last term has a scaling dimension of $\Delta = 8K$ and therefore is relevant only for $K < \frac{1}{4}$. In particular, it is irrelevant in the topological phase. Unfortunately, it is not possible to see this effect in the numerical results as there are no accurate results in the corresponding parameter region away from half filling whereas at half filling, there is a charge density wave anyway.

The corresponding Lagrangian density taking into account only the $\cos\left(\sqrt{\frac{8\pi}{K}}\theta_-\right)$-term is then

$$\mathcal{L} = \underbrace{\frac{1}{2}\left[\frac{1}{\nu}(\partial_t\theta_+)^2 - \nu(\partial_x\theta_+)^2\right]}_{\mathcal{L}_+} + \underbrace{\frac{1}{2}\left[\frac{1}{\nu}(\partial_t\theta_-)^2 - \nu(\partial_x\theta_-)^2\right] - q\cos\left(\sqrt{\frac{8\pi}{K}}\theta_-\right)}_{\mathcal{L}_-} . \tag{3.51}$$

In [32], a detailed analysis of this and similar bosonized theories was made and it was shown that this effective theory can be refermionized to the continuum limit of the Kitaev chain [16] in a special case, and that this is a description of a topological phase in general. See also [24] where the bosonized theory was derived for this model in absence of density-density interactions leading to the same description of the topological phase.

For $q > 0$, that is, for $W > 0$, the cosine potential has two minima within the compactification interval of θ_-, these are $\theta_- = \pm\sqrt{\frac{\pi K}{4}}$. If the term is relevant, this leads to a ground state degeneracy, and an effective low-energy treatment can be made by expanding the cosine around the respective minima, leading to a massive Klein-Gordon Hamiltonian in θ.

3.1.2.2 Charge density waves

At half filling, Umklapp scattering processes both from H_1 and H_3 now contribute to the Hamiltonian [34] and are now capable of pinning $\phi_+ - \phi_-$ and $\phi_+ + \phi_-$, leading to a commensurate charge density wave on both wires. This implies that the fields ϕ_+ and ϕ_- are pinned themselves, which can be checked using the correlations described in section 3.2.3.

The form of the Umklapp term may be read off from equation (3.32) as

$$\left(\psi^\dagger_{R\sigma}\psi_{L\sigma}\right)^2 + \text{h.c.} \propto \cos\left(\sqrt{8\pi K}(\phi_+ + s_\sigma\phi_-)\right) . \tag{3.52}$$

The scaling dimension can be obtained from the correlator

$$\begin{aligned}\langle \mathrm{e}^{i\sqrt{32\pi}\left(\sqrt{K_+}\phi_+(x)+s_\sigma\sqrt{K_-}\phi_-(x)\right)}\mathrm{e}^{-i\sqrt{32\pi K}(\phi_+(x)-s_\sigma\phi_-(x))}\rangle \\ \propto \mathrm{e}^{32\pi(K_+\langle\phi_+(x)\phi_+(0)\rangle+K_-\langle\phi_-(x)\phi_-(0)\rangle)} \propto |x|^{-32K} ,\end{aligned} \tag{3.53}$$

using the free-field correlator:

$$\langle\phi_-(x)\phi_-(0)\rangle = -\frac{1}{2\pi}\ln(|x|) \tag{3.54}$$

Therefore, the scaling dimension is $\Delta = 2(K_+ + K_-)$ and this term is relevant for $(K_- + K_+) < 1$, neglecting couplings in the RG flow.

3.1.2.3 Charge gap in the symmetric sector

In addition to the Umklapp process, the density-density interaction H_3 also gives rise to an additional contribution at half filling. To obtain the form of this term, recall the continuum limit of H_3 from section 3.1.1.3.

The oscillating terms for which the prefactor becomes 1 at half filling are then either on-chain Umklapp terms as discussed in section 3.1.2.2 or inter-chain Umklapp interactions of the form

$$\left(\psi_{La}^{\dagger}\psi_{Ra}\right)^2\left(\psi_{Lb}^{\dagger}\psi_{Rb}\right)^2 + \text{h.c.} \propto \cos(\sqrt{32\pi K}\phi_+)\,. \tag{3.55}$$

All other potential candidates have a prefactor of $(1+\mathrm{e}^{2ik_F a})$ which is 0 at half filling.

It may be readily checked that the scaling dimension of this term is $\Delta = 8K$ and it is therefore relevant for $K < \frac{1}{4}$, making the ϕ_+-field massive.

In principle, there can also be a gap in the antisymmetric sector as demonstrated in section 3.1.1.3 with the same properties. Such a phase could not be found in the numerical results however, most likely due to the fact that there are no results of sufficient accuracy away from half filling and the antisymmetric charge field is pinned in the corresponding parameter regions at half filling anyway due to the occurence of a charge density wave.

3.2 Correlation functions of the bosonized theory

3.2.1 Bosonization of correlation functions

Autocorrelation functions of fermionic operators or products thereof can be treated using equation (2.25). Using this, a product of fermionic operators can first be expressed in terms of the boson fields

$$\psi_{\alpha\sigma}\psi_{\beta\sigma'} = \frac{1}{2\pi}\mathrm{e}^{-i\sqrt{\frac{\pi}{2}}\tau_{\alpha\sigma}}\mathrm{e}^{-i\sqrt{\frac{\pi}{2}}\tau_{\beta\sigma'}} = \frac{1}{2\pi}\mathrm{e}^{-i\sqrt{\frac{2}{\pi}}(\tau_{\alpha\sigma}+\tau_{\beta\sigma'})}\mathrm{e}^{-\sqrt{\frac{\pi}{2}}\langle\tau_{\alpha\sigma}\tau_{\beta\sigma'}\rangle}\,, \tag{3.56}$$

where it is

$$\tau_{\alpha\sigma} = \frac{1}{\sqrt{K}}(\theta_+ + s_\sigma\theta_-) + s_\alpha\sqrt{K}(\phi_+ + s_\sigma\phi_-) = \begin{cases}\varphi_\sigma & \text{if } \alpha = A\\ \bar{\varphi_\sigma} & \text{if } \alpha = B\end{cases}. \tag{3.57}$$

Since the boson fields were rescaled but the fields appearing in (3.9) are the bare ones, the factors of $\sqrt{K}$ have to be added here. Physically, this corresponds to a mixing between left- and right-moving fermions [34].

Equation (3.56) generalizes to the statement that any product of the fermion fields O can be expressed in bosonized form as $O \propto \mathrm{e}^{\tau_O}$ where τ_O is some linear combination of the bosonic fields. One should however keep in mind that this is a rough simplification and there are some subtle details to be aware of.

The neutrality condition (2.29) now implies

$$\langle O(x)O^\dagger(x')\rangle \propto \mathrm{e}^{\langle\tau_0(x)\tau_0^\dagger(x')\rangle}\,. \tag{3.58}$$

This expectation value can now be computed using the known correlation functions of $\theta_\pm$ and $\phi_\pm$. Since these only depend on $x - x'$, it is safe to set $x' = 0$ for convenience. Of interest are mainly correlation functions of operators O of first and second order in the left- and right-moving fermions. The fermionic operators for the left- and right-movers are rewritten in terms of the rescaled fields $\theta_\pm$ and $\phi_\pm$, omitting constant prefactors:

$$\psi_{\alpha\sigma} \propto \exp\left[i\sqrt{\frac{\pi}{2}}\left(\frac{1}{\sqrt{K}}\theta_+ + s_\sigma\frac{1}{\sqrt{K}}\theta_- + \sqrt{K}s_\alpha\phi_+ + \sqrt{K}s_\alpha s_\sigma\phi_-\right)\right] \tag{3.59}$$

$$\psi^\dagger_{\alpha\sigma}\psi_{\beta\sigma'} \propto \exp\left[-i\sqrt{\frac{\pi}{2}}\left(\frac{s_\sigma - s_{\sigma'}}{\sqrt{K}}\theta_- + \sqrt{K}(s_\alpha - s_\beta)\phi_+ + \sqrt{K}(s_\alpha s_\sigma - s_\beta s_{\sigma'})\phi_-\right)\right] \tag{3.60}$$

$$\psi^\dagger_{\alpha\sigma}\psi^\dagger_{\beta\sigma'} \propto \exp\left[-i\sqrt{\frac{\pi}{2}}\left(\frac{2}{\sqrt{K}}\theta_+ + \frac{s_\sigma + s_{\sigma'}}{\sqrt{K}}\theta_- + \sqrt{K}(s_\alpha + s_\beta)\phi_+ + \sqrt{K}(s_\alpha s_\sigma + s_\beta s_{\sigma'})\phi_-\right)\right], \tag{3.61}$$

with $s_a = s_R = 1$ and $s_b = s_L = -1$. As discussed before, the correlations of fermionic field operators can be reduced to functions of the bosonic Green's function discussed in

section 2.1.1.

$$\langle\psi^\dagger_{\alpha\sigma}(x)\psi_{\beta\sigma'}(0)\rangle \propto \delta_{\alpha\beta}\delta_{ij}\exp\left[\frac{\pi}{2}\left(\frac{1}{K}\langle\theta_+(x)\theta_+(0)\rangle + \frac{1}{K}\langle\theta_-(x)\theta_-(x)\rangle + K\langle\phi_-(x)\phi_-(0)\rangle\right.\right.$$
$$+ K\langle\phi_+(x)\phi_+(0)\rangle + \langle\theta_+(x)\phi_+(0)\rangle + \langle\phi_+(x)\theta_+(0)\rangle$$
$$\left.\left. + \langle\theta_-(x)\phi_-(0)\rangle + \langle\phi_-(x)\theta_-(0)\rangle\right)\right] \tag{3.62}$$

$$\langle\psi^\dagger_{\alpha\sigma}(x)\psi_{\beta\sigma'}(x)\psi^\dagger_{\beta\sigma'}(0)\psi_{\alpha\sigma}(0)\rangle \propto \exp\left(\frac{\pi}{2}\left[\frac{(s_\sigma - s_{\sigma'})^2}{K}\langle\theta_-(x)\theta_-(0)\rangle + (s_\sigma - s_{\sigma'})(s_\sigma s_\alpha - s_{\sigma'}s_\beta)\right.\right.$$
$$\times(\langle\phi_-(x)\theta_-(0)\rangle + \langle\theta_-(x)\phi_-(0)\rangle) + K(s_\alpha - s_\beta)^2\langle\phi_+(x)\phi_+(0)\rangle$$
$$\left.\left. + K(s_\sigma s_\alpha - s_{\sigma'}s_\beta)^2\langle\phi_-(x)\phi_-(0)\rangle\right]\right) \tag{3.63}$$

$$\langle\psi^\dagger_{\alpha\sigma}(x)\psi^\dagger_{\beta\sigma'}(x)\psi_{\beta\sigma'}(0)\psi_{\alpha\sigma}(0)\rangle \propto \exp\left(\frac{\pi}{2}\left[\frac{(s_\sigma + s_{\sigma'})^2}{K}\langle\theta_-(x)\theta_-(0)\rangle + (s_\sigma + s_{\sigma'})(s_\sigma s_\alpha + s_{\sigma'}s_\beta)\right.\right.$$
$$\times(\langle\phi_-(x)\theta_-(0)\rangle + \langle\theta_-(x)\phi_-(0)\rangle) + K(s_\alpha + s_\beta)^2\langle\phi_+(x)\phi_+(0)\rangle$$
$$\left.\left. + K(s_\sigma s_\alpha + s_{\sigma'}s_\beta)^2\langle\phi_-(x)\phi_-(0)\rangle + \frac{4}{K}\langle\theta_+(x)\theta_+(0)\rangle\right]\right). \tag{3.64}$$

From the numerical results of DMRG, only correlation functions of the fermionic operators a_σ and b_σ can be obtained, whose behaviour in thermodynamic limit mirrors that of ψ_a and ψ_b. That is, for an O of first or second order, only the functions

$$\langle\psi^\dagger_\sigma(x)\psi_{\sigma'}(0)\rangle = 2\langle\psi^\dagger_{Ra}(x)\psi_{Ra}(0)\rangle \tag{3.65}$$

$$\langle\psi^\dagger_\sigma(x)\psi_{\sigma'}(x)\psi^\dagger_{\sigma'}(0)\psi_\sigma(0)\rangle = \langle\psi^\dagger_{Ai}(x)\psi_{Aj}(x)\psi^\dagger_{Aj}(0)\psi_{Ai}(0)\rangle + \langle\psi^\dagger_{Bi}(x)\psi_{Bj}(x)\psi^\dagger_{Bj}(0)\psi_{Bi}(0)\rangle$$
$$+ \mathrm{e}^{-2ik_Fx}\langle\psi^\dagger_{Ai}(x)\psi_{Bj}(x)\psi^\dagger_{Bj}(0)\psi_{Ai}(0)\rangle$$
$$+ \mathrm{e}^{2ik_Fx}\langle\psi^\dagger_{Bi}(x)\psi_{Aj}(x)\psi^\dagger_{Aj}(0)\psi_{Bi}(0)\rangle \tag{3.66}$$

$$\langle\psi^\dagger_\sigma(x)\psi^\dagger_{\sigma'}(x)\psi_{\sigma'}(0)\psi_\sigma(0)\rangle = \langle\psi^\dagger_{Ai}(x)\psi^\dagger_{Aj}(x)\psi_{Aj}(0)\psi_{Ai}(0)\rangle + \langle\psi^\dagger_{Bi}(x)\psi^\dagger_{Bj}(x)\psi_{Bj}(0)\psi_{Bi}(0)\rangle$$
$$+ \mathrm{e}^{-2ik_Fx}\langle\psi^\dagger_{Ai}(x)\psi^\dagger_{Bj}(x)\psi_{Bj}(0)\psi_{Ai}(0)\rangle$$
$$+ \mathrm{e}^{2ik_Fx}\langle\psi^\dagger_{Bi}(x)\psi^\dagger_{Aj}(x)\psi_{Aj}(0)\psi_{Bi}(0)\rangle \tag{3.67}$$

are of interest.

These formulas now allow for a qualitative prediction of fermionic correlation functions for different phases and therefore yield qualitative criteria for identification of phases characterized by one of the fields $\phi_\pm$, $\theta_\pm$ becoming massive.

3.2.2 Correlation functions in the topological phase

3.2.2.1 Bosonic correlation functions

To obtain the correlation functions of the boson fields in the topological phase, consider again the Lagrangian (3.51).

From $\mathcal{L}_+$ the Green's function of θ_+,and thereby ϕ_+ via duality, can be obtained. Since $\mathcal{L}_+$ is the Lagrangian of a Luttinger liquid, they are both given by

$$G_+(x, t = 0) = -\frac{1}{2\pi} \log(|x|) \,. \tag{3.68}$$

In momentum space it is $G_+(k, w) = \frac{1}{\frac{\omega^2}{\nu} - \nu k^2}$, respectively [69].

Taking into account the periodicity of $\theta_\pm$ in the form $\theta_\pm = \theta_\pm + \sqrt{\pi K}$ reduces the possible minima of the potential resulting from the pair-hopping. Therefore the pair-hopping term is minimal for $\theta = \pm\sqrt{\frac{K\pi}{8}}$ for $q > 0$ and $\theta = 0$, $\sqrt{\frac{K\pi}{2}}$ for $q < 0$, respectively. Semiclassically, the field θ_- can be viewed as pinned to a minimum of the cosine potential. The cosine is expanded around a minimum θ_0 and leads to a mass term in the Lagrangian of the form

$$\mathcal{L}_- = \frac{1}{2}\left[\frac{1}{\nu}(\partial_t \theta_-)^2 - \nu(\partial_x \theta_-)^2\right] - \frac{m^2}{2}(\theta_- - \theta_0)^2 \,, \tag{3.69}$$

with mass $m^2 = |q|\frac{8\pi}{K}$.

Therefore, the Green's function of θ_- is

$$G_{\theta_-}(k,\, \omega) = \frac{1}{\frac{\omega^2}{\nu} - \nu k^2 - m^2} \,. \tag{3.70}$$

Using the duality $\partial_x \phi = -\Pi_\theta = -\frac{1}{\nu}\partial_t \theta$, the Green's function for ϕ is obtained as

$$G_{\phi_-} = \frac{\omega^2}{\nu^2 k^2} \frac{1}{\frac{\omega^2}{\nu} - \nu k^2 - m^2} \,. \tag{3.71}$$

Although θ_- and ϕ_- are not uncorrelated, the correlation $\langle \theta_-(x)\phi_-(0)\rangle$ is still fixed by the duality between θ and ϕ [34].

To explicitly compute the correlation function $\langle \phi_-(x)\phi_-(0)\rangle$, apply the duality on the known function G_{θ_-} without Fourier transforming the derivatives ∂_x^2, yielding

$$\partial_x^2 \langle \phi_-(x)\phi_-(0)\rangle = -\frac{i}{\nu^2} \int \mathrm{d}^\omega \frac{\omega^2}{\frac{\omega^2}{\nu} - \nu k^2 - m^2} = -\frac{m}{\pi|x|} K_1(m|x|) \,, \tag{3.72}$$

with the Bessel function K_1 [69]. As the Bessel function decays exponentially asymptotically for $x \to \infty$, the correlation function $\langle \phi_-(x)\phi_-(0)\rangle$ behaves asymptotically linear.

3.2.2.2 Fermionic correlation functions

The expressions for fermionic correlation functions from section 3.2.1 can now be used to make qualitative statements about the two-point functions in the topological phase.

In [1] the effect of a symmetry breaking term of the form $\mathrm{e}^{i\gamma} a_i^\dagger b_i$ + h.c. were also considered with the result that, in first order perturbation theory, the symmetry breaking term cannot lift the ground state degeneracy if time-reversal symmetry is not broken simultaneously, that is, only for $\gamma \neq 0$.

To embed this result in the framework presented here, consider the continuum version of such a symmetry breaking term

$$h_\gamma = \mathrm{e}^{i\gamma}\psi_a^\dagger\psi_b + \mathrm{e}^{-i\gamma}\psi_b^\dagger\psi_a\,. \tag{3.73}$$

To classify the effect of h_γ, consider the correlation function $\langle h_\gamma(x)h_\gamma(0)\rangle$. Therefore, in addition to those functions listed in section 3.2.1, the following function makes an appearance.

$$\langle\psi_{\alpha\sigma}^\dagger(x)\psi_{\beta\sigma'}(x)\psi_{\beta\sigma}^\dagger(0)\psi_{\alpha j}(0)\rangle = \text{const.}\times\exp\left(\frac{\pi}{2}\left[-\frac{4}{K}\langle\theta_-(x)\theta_-(0)\rangle + 4K\langle\phi_+(x)\phi_+(0)\rangle\right]\right), \tag{3.74}$$

for $\alpha\neq\beta$ and $i\neq j$.

Using this, it can be determined

$$\begin{aligned}
&\left\langle\left(\mathrm{e}^{i\gamma}\psi_a^\dagger(x)\psi_b(x) + \mathrm{e}^{-i\gamma}\psi_b^\dagger(x)\psi_a(x)\right)\left(\mathrm{e}^{i\gamma}\psi_a^\dagger(0)\psi_b(0) + \mathrm{e}^{-i\gamma}\psi_b^\dagger(0)\psi_a(0)\right)\right\rangle\\
=&\langle\psi_a^\dagger(x)\psi_b(x)\psi_b^\dagger(0)\psi_a(0)\rangle + \langle\psi_b^\dagger(x)\psi_a(x)\psi_a^\dagger(0)\psi_b(0)\rangle\\
&+\mathrm{e}^{2\gamma}\langle\psi_a^\dagger(x)\psi_b(x)\psi_a^\dagger(0)\psi_b(0)\rangle + \mathrm{e}^{-2\gamma}\langle\psi_b^\dagger(x)\psi_a(x)\psi_b^\dagger(0)\psi_a(0)\rangle\\
=&2\Big(\langle\psi_{Ra}^\dagger(x)\psi_{Rb}(x)\psi_{Rb}^\dagger(0)\psi_{Ra}(0)\rangle + \langle\psi_{La}^\dagger(x)\psi_{Lb}(x)\psi_{Lb}^\dagger(0)\psi_{La}(0)\rangle\\
&+\mathrm{e}^{2ik_Fx}\langle\psi_{La}^\dagger(x)\psi_{Rb}(x)\psi_{Rb}^\dagger(0)\psi_{La}(0)\rangle + \mathrm{e}^{-2ik_Fx}\langle\psi_{Ra}^\dagger(x)\psi_{Lb}(x)\psi_{Lb}^\dagger(0)\psi_{Ra}(0)\rangle\Big)\\
&+\mathrm{e}^{2\gamma}2\cos(2k_Fx)\langle\psi_{Ra}^\dagger(x)\psi_{Lb}(x)\psi_{Lb}^\dagger(0)\psi_{Ra}(0)\rangle + \mathrm{e}^{-2\gamma}2\cos(2k_Fx)\langle\psi_{Rb}^\dagger(x)\psi_{La}(x)\psi_{La}^\dagger(0)\psi_{Rb}\rangle\\
=&2\langle\psi_{Ra}^\dagger(x)\psi_{Rb}(x)\psi_{Rb}^\dagger(x)\psi_{Ra}(0)\rangle + 2\langle\psi_{La}^\dagger(x)\psi_{Lb}(x)\psi_{Lb}^\dagger(0)\psi_{La}(0)\rangle\\
&+C\cos(2k_Fx)\left(\mathrm{e}^{\frac{2\pi}{K}\langle\theta_-(x)\theta_-(0)\rangle} + \mathrm{e}^{-\frac{2\pi}{K}\langle\theta_-(x)\theta_-(0)\rangle}\cos(2\gamma)\right)x^{-K},
\end{aligned} \tag{3.75}$$

for some $C\in\mathbb{C}$. Note that the terms of the form $\langle\psi_{Ra}^\dagger(x)\psi_{Rb}(x)\psi_{Ra}^\dagger(0)\psi_{Rb}(0)\rangle$ vanish exponentially and are not listed. Therefore, this autocorrelation decays algebraically except for $\gamma=\gamma_0$ with

$$\cos(2\gamma_0) = -\mathrm{e}^{\frac{4\pi}{K}\langle\theta_-(x)\theta_-(0)\rangle}\,, \tag{3.76}$$

which gives (asymptotical) exponential decay. Due to

$$\langle\theta_-(x)\theta_-(0)\rangle\to 0\,, \tag{3.77}$$

on large distances, it is $\gamma_0=0$. In particular, γ_0 does not depend on the expansion point θ_0.

3.2.3 Probing the gap

In section 3.2.1 the form of various correlation functions was calculated, including the on-chain two-point correlation function

$$\begin{aligned}
\langle\psi_\sigma^\dagger(x)\psi_\sigma(0)\rangle = \text{const.}\ &\times\delta_{\alpha\beta}\delta_{ij}\exp\Big[\frac{\pi}{2}\Big(\frac{1}{K}\langle\theta_+(x)\theta_+(0)\rangle + \frac{1}{K}\langle\theta_-(x)\theta_-(x)\rangle + K\langle\phi_-(x)\phi_-(0)\rangle\\
&+\ K\langle\phi_+(x)\phi_+(0)\rangle + \langle\theta_+(x)\phi_+(0)\rangle + \langle\phi_+(x)\theta_+(0)\rangle\\
&+\ \langle\theta_-(x)\phi_-(0)\rangle + \langle\phi_-(x)\theta_-(0)\rangle\Big)\Big]
\end{aligned} \tag{3.78}$$

and the 'spin-flip' correlation

$$\begin{aligned}\langle\psi_a^\dagger(x)\psi_b(x)\psi_b^\dagger(0)\psi_a(0)\rangle = \text{const.}\ \times \exp\left(\frac{\pi}{2}\left[\frac{4}{K}\langle\theta_-(x)\theta_-(0)\rangle + 4\left(\langle\phi_-(x)\theta_-(0)\rangle\right.\right.\right.\\ \left.\left.\left. +\ \langle\theta_-(x)\phi_-(0)\rangle\right) + 4K\langle\phi_-(x)\phi_-(0)\rangle\right]\right)\\ + \text{const.}\ \times\ \cos(2k_Fx)\exp\left(\frac{\pi}{2}\left[\frac{4}{K}\langle\theta_-(x)\theta_-(0)\rangle + 4K\langle\phi_+(x)\phi_+(0)\rangle\right]\right)\end{aligned} \tag{3.79}$$

as well as the pair-correlation

$$\begin{aligned}\langle\psi_a^\dagger(x)\psi_b^\dagger(x)\psi_b(0)\psi_a(0)\rangle = \text{const.}\ \times \exp\left(\frac{\pi}{2}\left[\frac{4}{K}\langle\theta_+(x)\theta_+(0)\rangle + 4K\langle\phi_+(x)\phi_+(0)\rangle\right]\right)\\ + \text{const.}\ \times \cos(2k_Fx)\exp\left(\frac{\pi}{2}\left[\frac{4}{K}\langle\theta_+(x)\theta_+(0)\rangle + 4K\langle\phi_-(x)\phi_-(0)\rangle\right]\right)\end{aligned} \tag{3.80}$$

Assuming that not both, θ_- and θ_+ are pinned, it can be read of that the 'spin-flip' correlation decays asymptotically exponentially if and only if $\langle\theta_-(x)\theta_-(0)\rangle$ is asymptotically linear in x, that is, if the ϕ_--field is pinned. Since there is no contribution in the model that could somehow pin θ_+, the assumption is safe.

The pair-correlation on the other hand decays asymptotically exponentially if and only if the θ_+ autocorellator is asymptotically linear, and therefore if and only if the ϕ_+-field is pinned, see also section 3.4.2 for numerical results.

Thus, these correlation functions are suited for determining the existence of a mass gap of the charge fields $\phi_\pm$. The on-chain two-point correlation function on the other hand will decay asymptotically exponentially as soon as any field has an asymptotically linear autocorrelator and therefore if any sector is gapped and can thus be used as a consistency check.

In the topological phase, both pair-correlations decays algebraically due to the $\langle\phi_+(x)\phi_+(0)\rangle$ contribution which occurs in both in a term that does not shrink exponentially.

3.3 Numerical characterization of the topological phase

The first step after testing the implementation of the DMRG3S algorithm with the Heisenberg- and Hubbard model is to verify its applicability to the analyzed ladder system (1.2) with open boundary conditions. The numerical analysis is always applied to the system with open boundaries as edge states are only occuring in such systems for obvious reasons. Also, it is much harder for DMRG to handle periodic boundary conditions than open ones due to the long-range entanglement from the first to the last site in systems with periodic boundary conditions. Still, the same phases are expected for the open system than in thermodynamic limit studied using bosonization.

Therefore, the first point in parameter space considered is $J = g = W = 1$ which is henceforth called the exact point, since there, analytical results are available [1]. Fortunately, the exact ground state can be represented by an MPS with bond dimension of $D = \min(2N, 2(L-N))$ where N is the particle number [70]. Therefore, precise results can be obtained there and, since the MPS form of the exact ground state is known [70], the overlap of the normalized variationally obtained state with the exact ground state can be determined. For chain lengths of $L = 100$ at half filling, the deviation of the overlap from one is of order 10^{-9}, showing that the exact ground state is found with high precision. This upper bound for the bond dimension is no coincidence but precisely that bond dimension that is required to have each possible quantum number at one bond i assigned to exactly one left basis state $|a_i\rangle_l$ at this bond, and is therefore the minimal bond dimension required to represent an equal weight superposition of all states in a given symmetry sector.

It was shown analytically [1] that the ground state at the exact point for a given particle number is twofold degenerate and can be characterized by the fermionic parity on one chain. The ground states are then equal weight superpositions of all states with the given particle number and a fixed subchain parity α. To be precise, it is only an equal weight superposition in the fermion ordering gauge used in [1]. Since DMRG is formulated in terms of a product basis, the fermionic ordering is taken as

$$|\underline{\sigma}\rangle = (a_1^\dagger)^{n_1^a(\sigma_1)}(b_1^\dagger)^{n_1^b(\sigma_1)}(a_2^\dagger)^{n_2^a(\sigma_2)}\cdots(a_L^\dagger)^{n_L^a(\sigma_L)}(b_L^\dagger)^{n_L^b(\sigma_L)}|0\rangle\ . \tag{3.81}$$

The four-dimensional site basis is chosen as an eigenbasis of the commuting subspace particle number operators $\hat{n}_i^a$ and $\hat{n}_i^b$ and the labels σ_i are given by

$$n_i^a(\sigma_i) = \delta_{\sigma_i,2} + \delta_{\sigma_i,4} \quad n_i^b(\sigma_i) = \delta_{\sigma_i,3} + \delta_{\sigma_i,4} \tag{3.82}$$

for $\sigma_i \in \{1, \ldots, 4\}$.

Hence, the coefficients of the exact ground state in this product basis differ from that of the equal weight superposition in a fermi sign due to reordering. Starting from the equal weight superposition in the gauge from [1], each operator $a_i^\dagger$ now gets a prefactor $(-1)^{\alpha_i}$ where α_i is the subchain parity of chain 2 from sites 1 to i. Fortunately, there is an easy way to implement this sign into the MPS when the $\mathbb{Z}_2$ symmetry is used. Then,

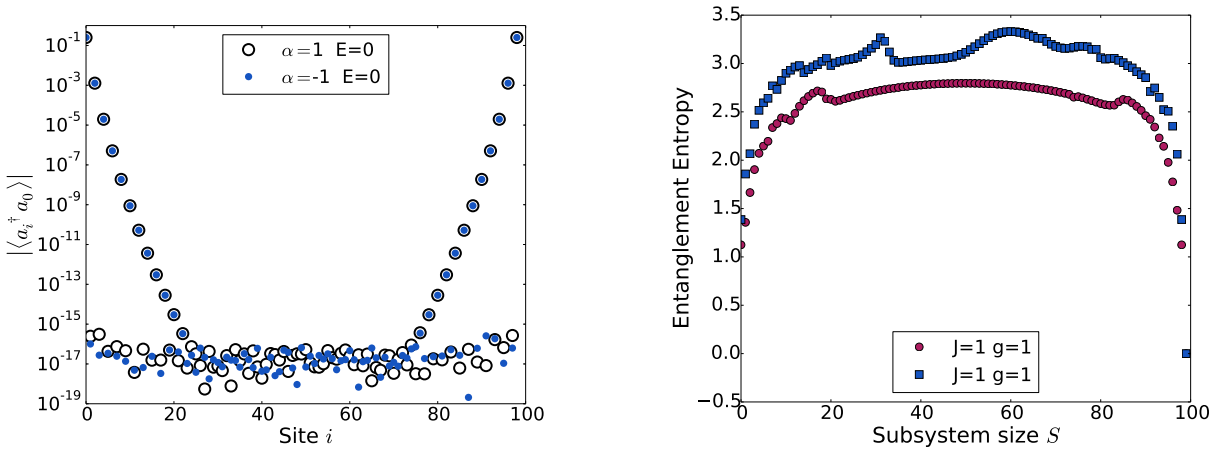

(a) (b)

Figure 3.1: (a) Two-point correlation function at the exact point for $L = 100$ at half filling. The exponential decay and the revival at the other end of the chain are clearly visible. Also the degeneracy of the ground state with respect to the subchain parity is reproduced. (b) Entanglement entropy over the size of the subsystem that is considered at the exact point for $L = 100$. The entanglement entropy is clearly not constant, indicating that the system is gapless.

each entry $A^{\sigma_i}_{a_{i-1}\,a_i}$ simply obtains a prefactor $q_{i\alpha}(a_{i-1})^{n_i^a(\sigma_i)}$, where $q_{i\alpha}(a_{i-1}) \in \{1, -1\}$ is the subchain parity quantum number of the state $|a_i\rangle_l$ as introduced in section 2.2.2.

Since the exact ground state is only known at this special point, in general, another measure for convergence has to be applied. A common choice which is also used here is the variance of energy $(\Delta E)^2 = \left\langle (H - \langle H \rangle)^2 \right\rangle$ which is an indicator of how close to an eigenstate the numerical result is. The energy scale is given by the parameters J, g and W as well as the system size.

There are several signatures of a topological edge-state that can be probed here, cf. the discussion of the analytical results in [1]. This allows for checking the applicability of the numerical method to the system and will demonstrate that the implementation of the DMRG3S algorithm is capable of identifying a topological edge state.

Therefore, the on-chain two-point correlation function $\langle a_i^\dagger a_j \rangle$ is considered, which features an exponential decay and a revival at the edge, indicating the existence of an edge state. An exemplary numerical result for the exact point $J = g = W = 1$ for the two-point function can be seen in figure 3.1a.

The ground state is degenerate with respect to the subchain parity α [1], which is correctly calculated numerically both by targeting the sectors $\alpha = \pm 1$ independently and by computing both the ground state and the first excited state without fixing the $\mathbb{Z}_2$-symmetry.

Then, the entanglement spectrum and thereby also the entanglement entropy is computed. Since the entangelement spectrum for a given bipartition of the system is given by the coefficients of a Schmidt decomposition of the ground state. It can be extracted from the MPS straightforward [50], as the matrices A^{σ_i} basically contain the coefficients of a Schmidt decomposition, as discussed in section 2.2.2. The entanglement spectrum

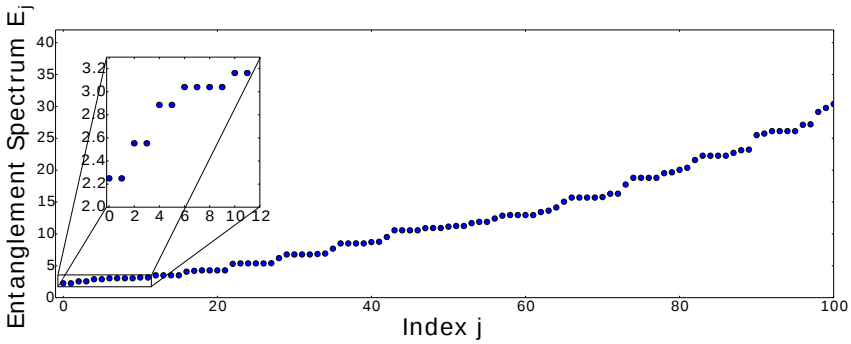

Figure 3.2: Entanglement spectrum for a bipartition at site $i = 45$ for a system of length $L = 100$ at half filling in the $\alpha = -1$ sector. The degeneracy of the lower lying values is emphasized. Since the coefficients of the Schmidt decomposition depend exponentially on the entanglement spectrum, the higher values are highly insignificant and can be neglected.

$\xi_{i,j}$ for a bipartition at site i is then given by the singular values $\lambda_{i,j}$ of $A_l^{[i]}$ [50] as

$$\xi_{i,j} = -2\log(\lambda_{i,j})\,, \tag{3.83}$$

presumed that the left- and right basis states are orthonormal, which is equivalent to the site i being the orthogonality center. Only in this case, the decomposition at site i is also a Schmidt decomposition. The choice of picking $A_l^{[i]}$ over $A_r^{[i]}$ is arbitrary and corresponds to counting site i to the left subsystem.

The twofold degeneracy in the entanglement spectrum [1] can then also be obtained from the numerical data as depicted in figure 3.2. This degeneracy is in general an indicator for a topological state [71].

Also, in contrast to the correlation function, the numerical results for the entanglement entropy are surprisingly far away from the analytical result, which is most likely due to the exponential dependency on of the entanglement spectrum on the singular values of $A^{[i]}$.

Another important consitency check is the energy of low lying excited states at the exact point, in particular the energy of the first excited state since this is obtained rather easily. The analytical solution from [1] predicts the low energy states having energies of

$$E_n = 4\sin^2\left(\frac{\pi n}{2L}\right)\,, \tag{3.84}$$

where $0 \leq n < L$. In particular, the energy of the first excited state is $E_1 = 4\sin^2(\frac{\pi}{2L})$ with $E_1 = \mathcal{O}\left(\frac{1}{L^2}\right)$ for $L \to \infty$. The numerical results show excellent agreement for $L \lesssim 50$ and are still reasonably close for longer chains. This means, the excited state search algorithm used is in principle capable of calculating gaps for the ladder system using moderate bond dimensions of $D \sim 350$.

3.4 $J - g$ phase diagram

3.4.1 Perturbations around the exact point

In [1], the prediction was made that certain perturbations at the exact point will lead to a phase separation whereas the edge state is stable for other perturbations. In this sense, the exact point is a critical point, as it marks a phase boundary. Although bosonization fails to describe this transition, the numerical results obtained with DMRG3S verify the occurence of a transition towards a phase separated state at the exact point. Here, the coupling constants J of the on-chain interaction and g of the inter-chain density-density interaction are varied while the pair-hopping is left constant. This allows for an interpolation between the models studied in [1] and [24]. Variations of the parameter W between 0.9 and 1.1 do not show any effect on the behaviour around the exact point. In section 3.7, the phase diagram for small pair hopping is adressed.

The numerical results show two possible outcomes for small perturbations in J and g around $J = g = 1$. Either the topological phase is retained, which is mainly the case for $J < 1$, or the system enters phase separation, which is mainly the case for $J > 1$. In principle however both, a stronger attractive interaction on-chain and a stronger repulsive interaction between the chains can both lead to phase separation. As can be seen in figure 3.3 however, the on-chain interaction is dominant in determining whether phase separation occurs or not. In this parameter regime, other phases do not occur, see section 3.4.2 for a discussion of further phases.

As can be seen exemplary in figure 3.4a, the edge state and the ground state degeneracy with respec to the subchain parity are preserved for weaker interactions, and the edge state is still exponentially localized. The exponential decay of the greens function, the algebraic decay of the pair correlations as depicted in 3.4b match the predictions from bosonization and indicate a pinning of the θ_--field as discussed in section 3.2.1. The correlation function $\left\langle a_i^\dagger b_i^\dagger b_j b_j \right\rangle$ is a ladder analogon to the on-chain two-point function and also features a revival at the edge in the topological phase. This can also serve as an indicator for edge state and can help to identify those in the numerical results.

Like at the exact point, the ground state is degenerate with respect to the subchain parity. The degeneracy with respect to the particle number is lifted however. Still, for each particle number, except for extreme cases in which $\sin(k_F a) = 0$, there is a ground state degeneracy and a revival of the Green's function at the end of the ladder. Also, the entanglement spectrum still has degeneracies, although it is no longer completely degenerate. It can be concluded that the topological phase extends from the exact point towards weaker interactions. See also figure 3.6b for a comparison of entanglement entropies. The entanglement entropy also does not change form, as shown in figure 3.6a, indicating that the system is still gapless, see also figure 3.7. The phase separation on the other hand is close to a product state, having one dominant value in the entanglement spectrum and vanishing entanglement entropy, save for boundary effects.

Note that the exact point in principle differs from what is identified as the topological phase in the sense that it is not captured by the description using bosonization from section 3.1.2. This manifests in some minor differences, but most properties of the exact

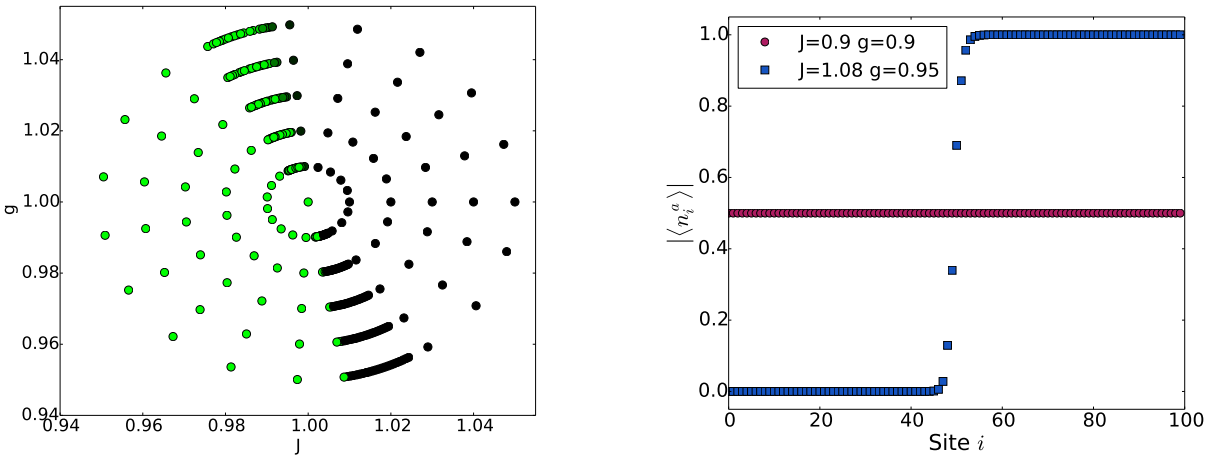

(a) (b)

Figure 3.3: (a) Phase diagram around the exact point, where the topological phase (green) and the phase separation (black) are marked. (b) Local particle number expectation value in the topological phase (red) and in the phase separation (purple) close to the exact point. The results are both for a system of size $L = 100$ at half filling and lower subchain parity $\alpha = -1$.

point are retained. Whereas the p-wave superconducting correlation $\left\langle a_i^\dagger a_{i+1}^\dagger a_j a_{j+1} \right\rangle$ is constant at the exact point, it shows weak decay inside the topological regime. Also, the pair correlations $\left\langle a_i^\dagger b_i^\dagger a_j b_j \right\rangle$ and $\left\langle a_i^\dagger b_i b_j^\dagger a_j \right\rangle$ show algebraic behaviour inside the topological phase in constrast to the exponential behaviour at the exact point, see also figure 3.5 for exemplary results. As mentioned above, the behaviour in the topological phase away from half filling matches the expectations from bosonization. This description is not valid at the exact point, however, and the exact point poses a special case in this aspect.

Since the ground state in the topological phase close to the exact point is expected to be similar to the equal weight superposition which is the ground state at the exact point, it seems to be a good initial state for ground state calculations close to the exact point. In practice, this leads to a very fast convergence within the topological phase. The phase separated state is very close to a product state, as can be seen in figure 3.6b, and is therefore easily represented as an MPS, such that this phase can easily be handled numerically anyway.

Recall the bosonized Hamiltonian from section 3.1 for the topological phase at low energies. There the system is separated into two sectors of which one is described by a massless Klein-Gordon field whereas the other sector is described by a massive Klein-Gordon field. In the end, this implies an excitation spectrum in the low-energy sector which is linear in the momentum. Since momentum is quantized as $k = \frac{\pi}{L} n$, $n \in \{0, \ldots, L\}$, the energy gap in a finite system is proportional to $\frac{1}{L}$, in contrast to the exact point where the gap scales as $\frac{1}{L^2}$. The numerical results do show a scaling close to $\frac{1}{L}$ as shown in figure 3.7. This might be an indicator for the results from the bosonization approach still being valid for strong pair-hopping. The numerical results for the topological phase shwon here are insensitive to the filling fraction, save for some special cases like $N = 0$. The parameter regime in which this phase occurs is filling dependent, however.

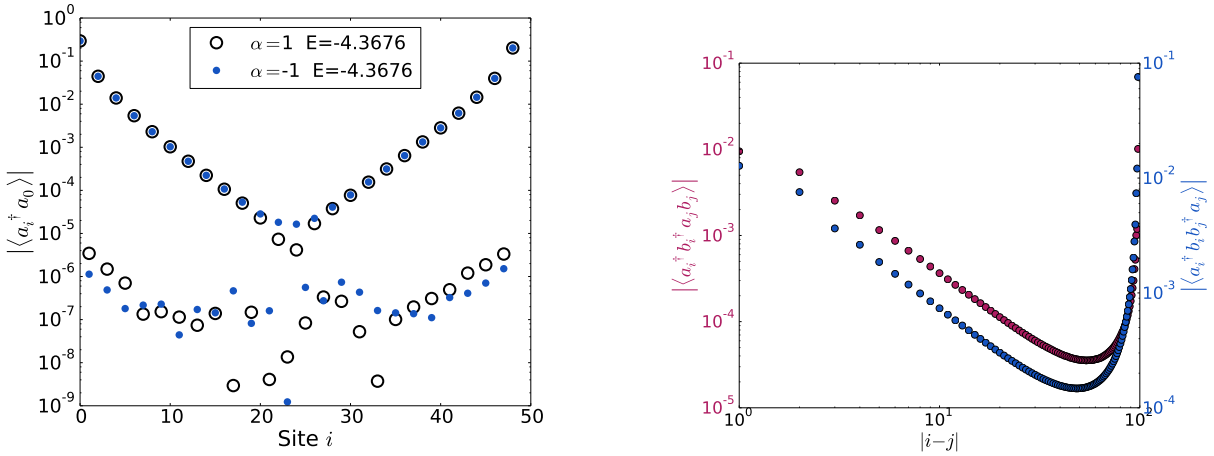

(a) (b)

Figure 3.4: (a) Two point greens function for $J = 0.91$, $g = 1.04$ and $W = 1$ for a ladder of length $L = 50$ with particle number $N = 35$ for both subchain parities. Both the exponential localization at both edges and the degeneracy are still present. (b) Pair correlations for $J = 0.9$, $g = 0.9$ and $W = 1$. Since the algebraic behaviour of the pair correlations is better visible for lager systems, these are for a ladder of length $L = 100$ at half filling. Due to the edge state, they both feature a revival at the other end of the ladder which is characteristic for the topological phase.

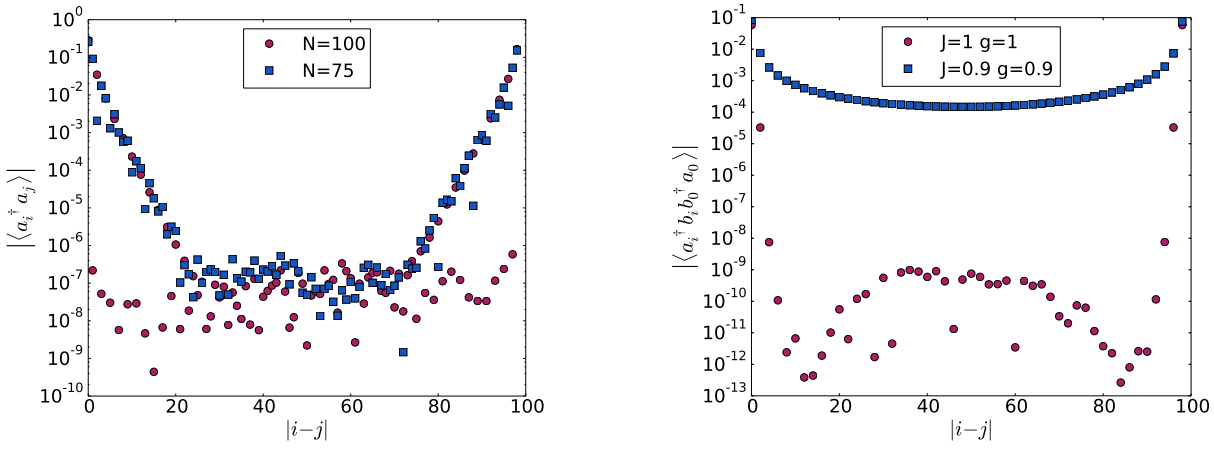

(a) (b)

Figure 3.5: (a) Independence of the edge state from the filling fraction. These results are for $J = g = 0.9$, $W = 1$ and a system of size $L = 100$ and subchain parity $\alpha = -1$. (b) Pair correlation at the exact point and in the topological phase away from it for $L = 100$, $\alpha = 1$ and $N = 80$, see also figure 3.4b. The exponential behaviour at the exact point indicates that this point is not captured with the bosonization approach.

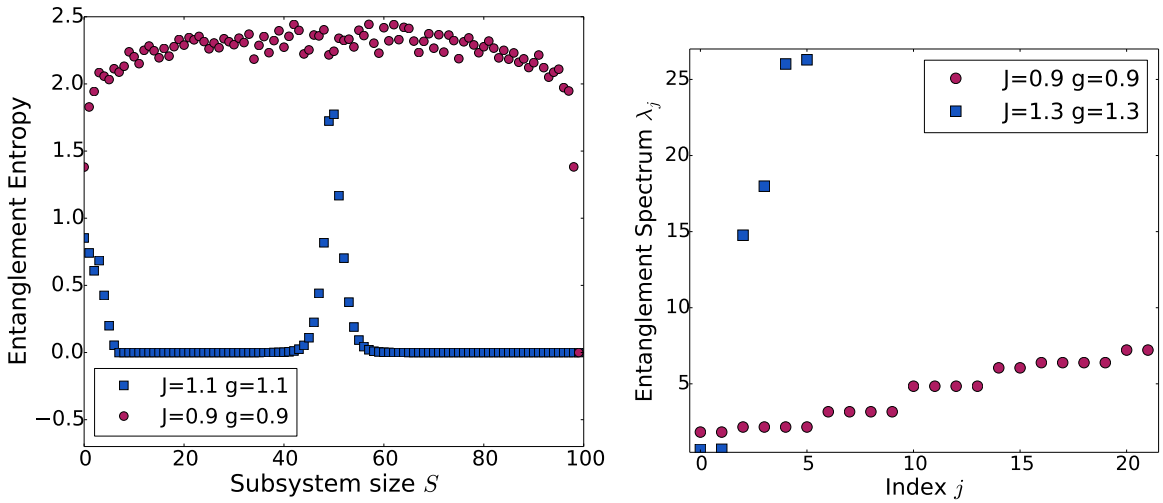

(a) (b)

Figure 3.6: (a) Entanglement entropy in the phase separaion (blue) and topological phase (red) for a system of size $L = 100$ at half filling and lower subchain pariy $L = 100$. While the entanglement entropy for $J = g = 0.9$ resembles that of the exact point, it vanishes in the phase separaion. The peaks in the middle of the chain and at the boundary are numerical artifacts here due to the gradual drop of particle density, see also figure 3.3b. (b) Entanglement spectrum in the phase separation (blue) and topological phase (red) for a system of size $L = 100$ at half filling and lower subchain parity $\alpha = -1$ for $W = 1$. The entanglement spectrum is taken for a bipartition of the system at site $i = 40$. The rapid growth of the entanglement spectrum for the phase separated state indicates that the state is close to a product state.

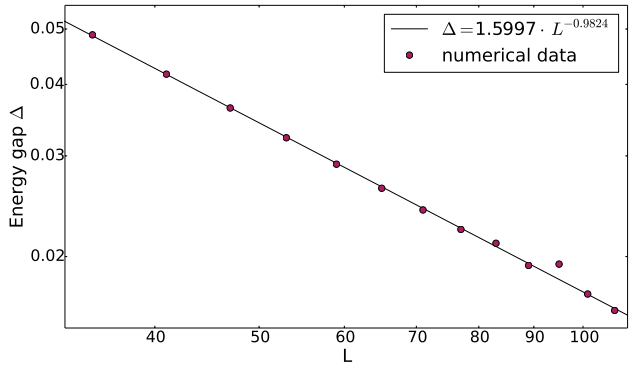

Figure 3.7: Scaling of the excitation gap over system size for $J = g = 0.9$ and $\alpha = -1$ at half filling with algebraic fit. Cleary, the gap vanishes algebraically and the fit reveals a behaviour close to the $\frac{1}{L}$-scaling found in bosonization. The results are obtained using bond dimension $D = 300$.

3.4.2 Strong interactions

Apart from the case of strong, repulsive interactions which lead to phase separation, the bosonization is capable of qualitative predictions of occuring phases as discussed in section 3.1. The low energy excitation spectrum at the exact point is quadratic [1] and it can therefore only be described within bosonization by a divergence of the Luttinger parameter K which corresponds to a theory of free bosons [34].

Recall the possible phases discussed in section 3.1, stating the appearance of a charge density wave due to Umklapp processes for small Luttinger parameters.

As discussed in section 3.2.3, the charge density wave is characterized by the charge fields becoming massive, thus the pair correlations $\left\langle a_i^\dagger b_i b_j^\dagger a_j \right\rangle$ and $\left\langle a_i^\dagger b_i^\dagger b_j a_j \right\rangle$ decay exponentially as can be seen exemplary in figure 3.10b. Apart from that, there is the obvious density oscillation as depicted exemplary in figure 3.10a. There, and also in the pair correlation, it is clearly visible that the charge density wave only exists at half filling. There are multiple realizations of the charge density wave depending on the subchain parities, particle number and system size. Due to the strong intra-chain repulsion in this regime, a half filling of each chain is always favored. For odd particle numbers, this leads to the sectors being degenerate, while for even particle numbers, the ground state is always in the sector allowing for a symmetric distribution of particles and is fourfold degenerate with the four realizations being those in figures 3.11 and 3.12 and their spatially inverted counterparts.

If the charge fields for both wires become massive, the theory will be fully gapped, which matches the numerical results shown in figure 3.9. The additional ground state degeneracy for even particle number and $\alpha = -1$ limits the system sizes which can be considered in this sector, due to the drastic increase of computational cost for computing higher excited states. Note that this drastic increase is not inherent to the excited state search but is mainly due to the unavailability of a well suited initial state, the lack of optimizations of the projector application in the used implementation and the high bond dimension required for higher excited states in larger systems. The entanglement entropy in the charge density wave is indeed constant, up to boundary effect, indicating a gapped phase, see also figure 3.15a.

Away from half filling, the charge density wave vanishes continuously, but numerical treatment of the system in this parameter regime becomes increasingly difficult, such that a clear statement can not be made from numerical data.

Apart from the charge density wave for strong repulsion on the chains, at half filling there is a phase of homogenous density with exponentially decaying correlations. As discussed in section 3.1, this can be understood within the framework of bosonization by one of the boson fields becoming massive, leading to an exponential decay of the on-chain two point function. As shown in section 3.2.3, the pair correlations $\left\langle a_i^\dagger b_i b_j^\dagger a_j \right\rangle$ and $\left\langle a_i^\dagger b_i^\dagger b_j a_j \right\rangle$ are able to probe for a charge gap. As shown exemplary in figure 3.8b, the correlation function $\left\langle a_i^\dagger b_i^\dagger b_j a_j \right\rangle$ decays exponentially whereas $\left\langle a_i^\dagger b_i b_j^\dagger a_j \right\rangle$ does not, indicating that the field ϕ_+ is pinned here. In contrast to the charge density wave appearing for strong on-chain repulsion, the density is homogeneous on both wires. Away from half filling, the correlations decay algebraically, the gap in the symmetric sector vanishes.

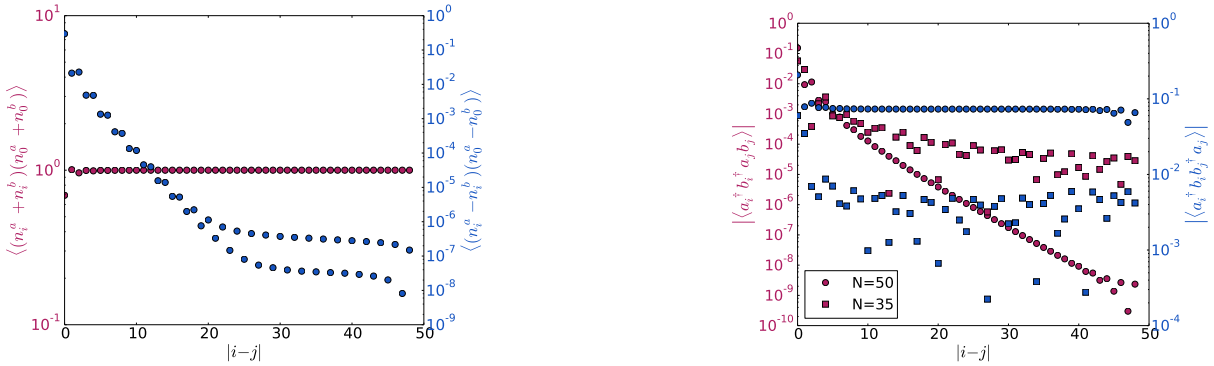

(a) (b)

Figure 3.8: (a) Density correlations for $J = -0.5$, $g = -1$ and $W = 1$ on a chain of length $L = 50$ in the $\alpha = -1$ sector. There is a homogenous density on both chains in this parameter regime. (b) Pair correlations for the same parameters. The saturation for $N = 35$ is due to boundary effects at the end of the chain, as it is observed similarly for the free theory.

The numerical sampling of the phase diagram 3.13 then shows the occuring phases for half filling depending on the density-density interaction strengths. It is not surprising that a strong attractive inter-chain density-density interaction favors a phase separation between the two chains, such that all particles gather on one chain, as the emergence of a charge density wave for strong repulsive on-chain interaction is also quite intuitive. In the same manner, one expects a phase separation on the chains for strong attractive on-chain interaction. A strong repulsive inter-chain interaction however does supress the pair-hopping, such that the system can be well describable as a Luttinger liquid.

For other fillings, the bond dimension required for accurate results is much larger, such that a sampling of the full phase diagram can reveal only the phase separated regions and the topological phase as shown in figure 3.14a. Apart from the regions of phase separation or topological phase, obtaining accurate results is too costly for generating data of the extent shown in figure 3.13. The reference data for $N \neq L$ shown in figure 3.10a and 3.8b for example is obtained with variance of energy of $(\Delta E)^2 = 3.27 \cdot 10^{-3}$ and $(\Delta E)^2 = 3.16 \cdot 10^{-4}$ respectively, which is much worse than the accuracy of the same calculations at half filling, for which it is $(\Delta E)^2 = 1.89 \cdot 10^{-8}$ and $(\Delta E)^2 = 2.24 \cdot 10^{-8}$ respectively for the same bond dimension.

It should be noted that the topological phase occurs at half filling only for $J \neq 0$ or $g \neq 0$, which has already been demonstrated in [24] where the model in absence of inter-chain density-density interactions and intra-chain interactions has been studied in detail. This shows that the density-density interactions can in fact establish topological order. The topological phase also features long-range p-wave superconducting correlations, as can be seen exemplary in figure 3.15b, which confirms the interpretation of the model as a microscopic theory.

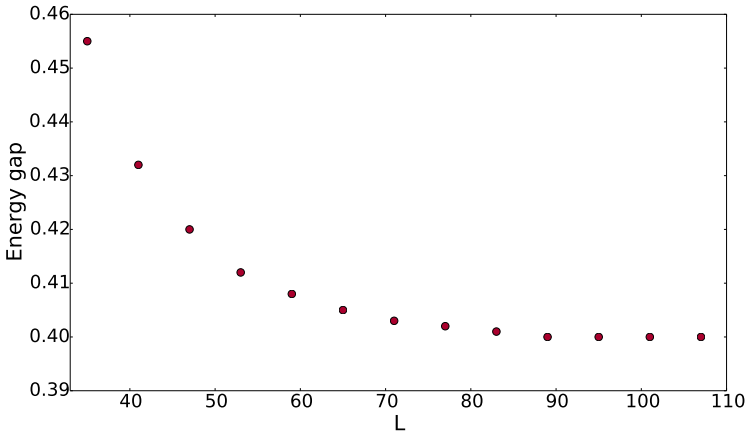

Figure 3.9: Scaling of the energy difference between the first excited state and the ground states over the system size L for $J = g = -2$ and $W = 1$ in the $\alpha = -1$ sector at half filling. The energy gap becomes constant at a value of $E_1 - E_0 = 0.4$, indicating that the system is gapped in thermodynamic limit. Results are obtained using bond dimension $D = 350$.

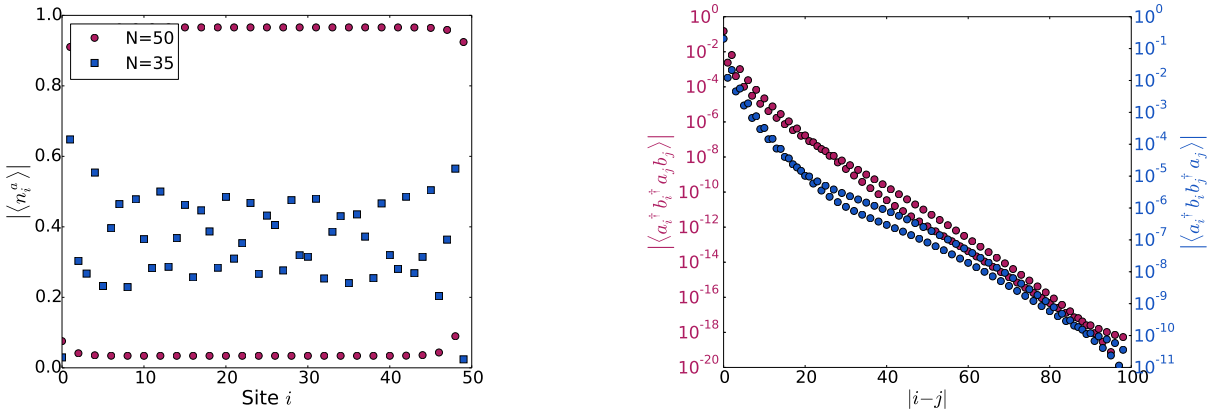

(a) (b)

Figure 3.10: (a) Local particle number expectation value for $J = -4$, $g = -4$, $W = 1$ and chain length $L = 50$ in the $\alpha = 1$ sector. While the results for $N = 50$ clearly show the occurence of a charge density wave, it is nearly absent for $N = 35$, where the oscillations in particle number are most likely numerical artifacts as the accuracy is also much lower than for $N = 50$. (b) Exponential decay of pair correlations for the same parameters, indicating a pinning of the $\phi_\pm$ fields and therefore a gap in the energy spectrum. The system size is $L = 100$ at half filling.

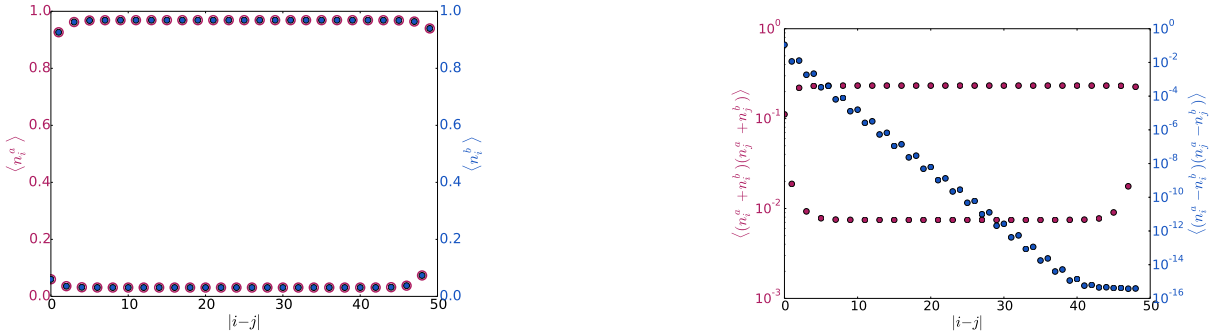

(a) (b)

Figure 3.11: Symmetric realization of a charge density wave on a chain of length $L = 50$ at half filling in the $\alpha = -1$ sector for $J = -4$, $g = 4$ and $W = 1$. For even particle number, like in this example, this and the spatially inverted counterpart are two of the four ground states. For odd particle number, there is no symmetric realization of the charge density wave. (a) Local density on both chains, clearly showing the symmetry. (b) Symmetric and antisymmetric density-density correlations, showing long-range correlations only for the symmetric part. This correlation function can hence easily distinguish between the different realizations of the charge density wave.

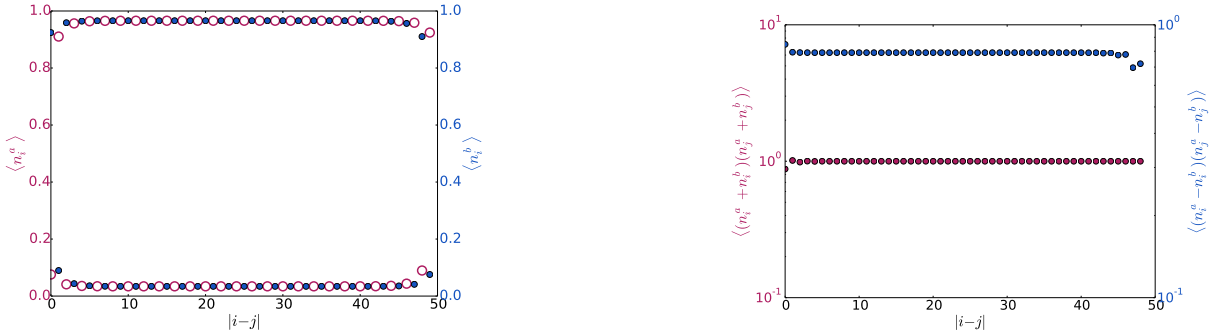

(a) (b)

Figure 3.12: Antisymmetric realization of a charge density wave on a chain of length $L = 50$ at half filling in the $\alpha = -1$ sector for $J = -4$, $g = -4$ and $W = 1$. For even particle number, like in this example, this and the spatially inverted counterpart are two of the four ground states. An analogous version also poses the ground state for odd particle number, with one realization existing in both the $\alpha = 1$ and the $\alpha = -1$ sectors. (a) Local density on both chains, clearly showing the asymmetry. (b) Symmetric and antisymmetric density-density correlations, showing long-range correlations for both parts.

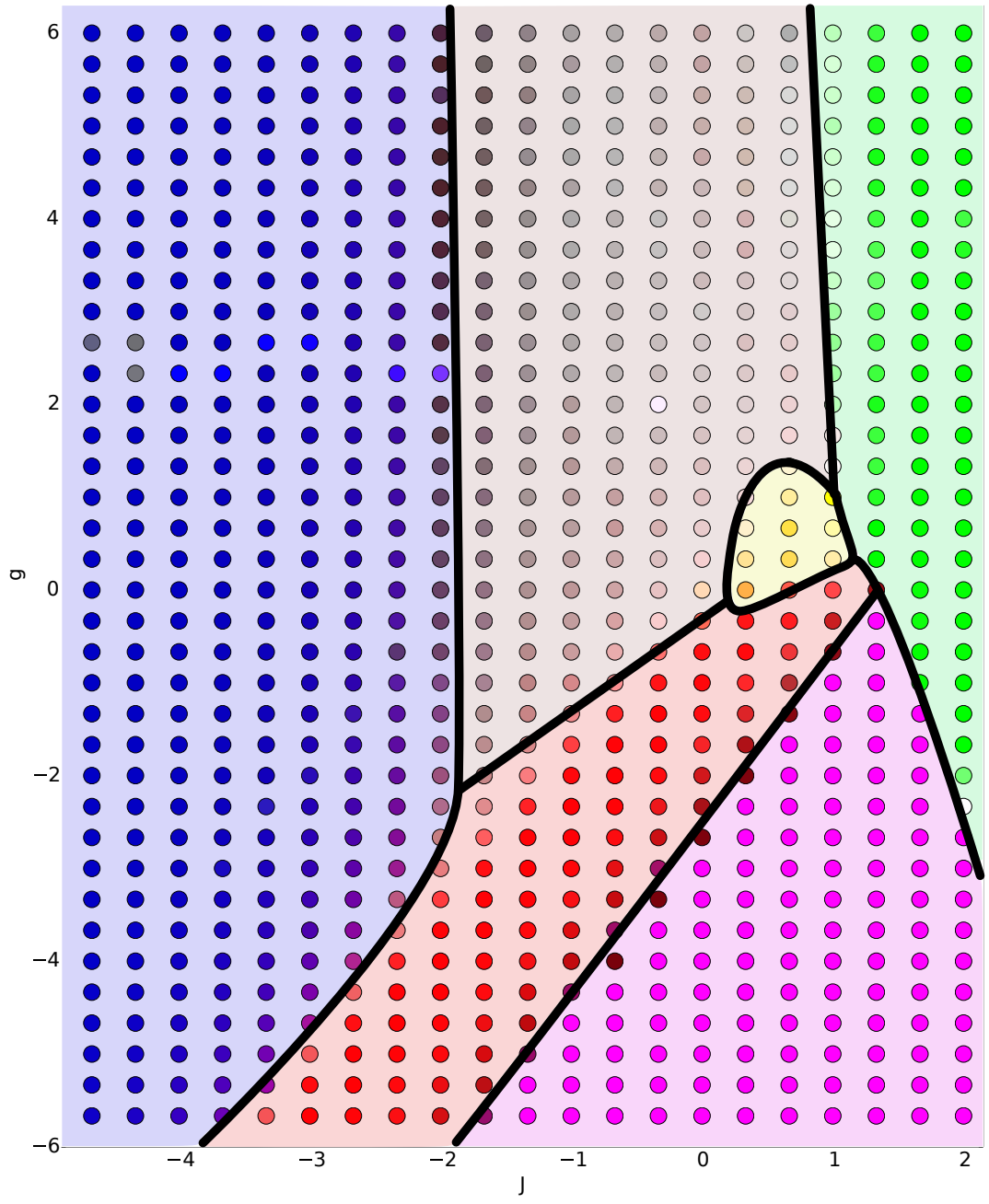

Figure 3.13: $J - g$ phase diagram obtained using DMRG for a system of size $L = 50$ at half filling. The dots correspond to the numerical data, while the demarkation of the phases is approximate and derived from the numerical data. The phases encoded are the charge density wave (blue), the topological phase (yellow), a phase separation along the ladder (green), a phase separation between the two subchains (pink), a gap in the symmetric sector (red) and a gapless Luttinger liquid (grey). The algorithm to determine the color code takes into account the revival of the on-chain two point function, the degeneracy with respect to subchain parity, the decay of the on-chain two point function, the density fluctuations both on each chain and between the chains and the entanglement entropy. The approximate phase boundaries are marked in black. The saturation encodes the variance of energy, since it varies over orders of magnitude between different parameter regimes, this is done on a logarithmic scale. Results are obtained using bond dimension $D = 300$.

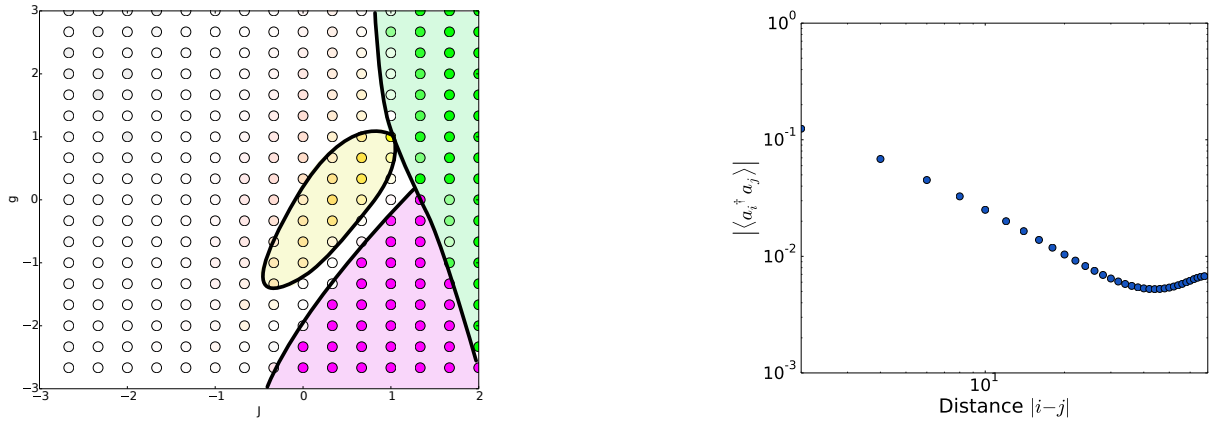

(a) (b)

Figure 3.14: (a) Numerical sampling of the $J-g$ phase diagram obtained using DMRG for a system of size $L = 50$ for $N = 35$ particles. The color code is the same as in figure 3.13. The phase separated regions (green, pink) and the topological phase (yellow) remain, but no statement can be met for the other phases from this data. Remarkably, the topological phase is of much greater extend than at half filling. White dots represent unconverged calculations where the variance of energy is $(\Delta E)^2 \gtrapprox 0.03$. Higher accuracy calculations for single points show that both the charge density wave and the gap in the symmetric sector vanish, see figures 3.10a and 3.8b. (b) Algebraic decay of the on-chain two-point function for $W = 1$, $J = -1$ and $g = 4$ and $L = 70$ at half filling. The saturation is due to boundary effects. The algebraic behaviour indicates a gapless phase that can be described as a Luttinger liquid, see also section 3.2.1.

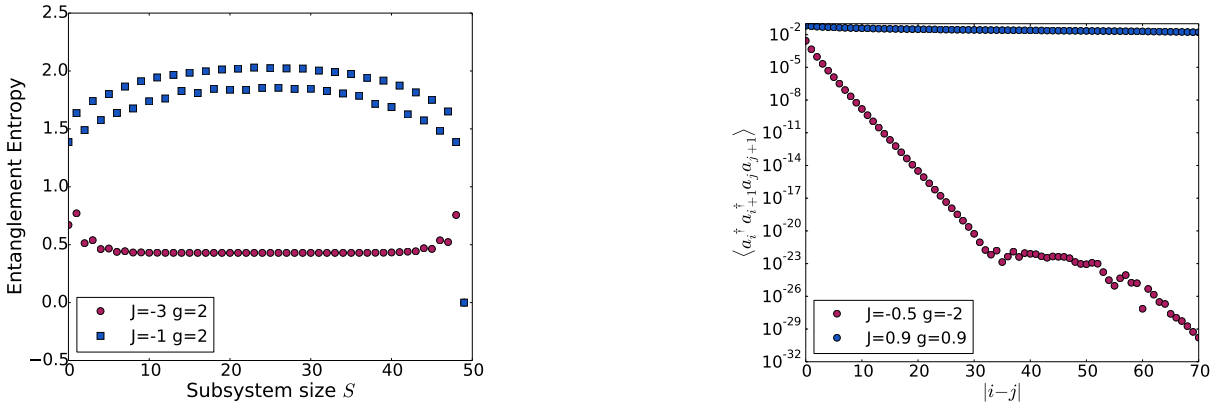

(a) (b)

Figure 3.15: (a) Entanglement entropy in the charge density wave (red), indicating the existence of a gap and Luttinger liquid phase (blue), which appears to be gapless. These data were obtained for a chain of length $L = 50$ at half filling and $\alpha = 1$. (b) p-wave superconducting correlations in the topological phase (blue) and the gap in the symmetric sector (red) obtained for chain of length $L = 100$ with $\alpha = 1$ at half filling. The depicted behaviour of the latter for large $|i-j|$ is not meaningful as the values are way below accuracy. The exponential behaviour however agrees with the occurance of a gap in the symmetric sector.

3.5 Effects of symmetry breaking perturbations

In the topological phase, the degeneracy of the ground state and the entanglement spectrum should be protected against local perturbations. This has been analyzed for $g = J = 0$ in [24], where the effect of a symmetry breaking term was also considered, and robustness against symmetry breaking was shown for a global, time-reversal invariant single-particle hopping. In [1] it was demonstrated for the exact point, that within first order perturbation theory, a local perturbation breaking the $\mathbb{Z}_2$-symmetry can lift the degeneracy if and only if it also breaks time reversal invariance and has support at the end of the ladder where the edge states on the two chains are not spatially separated. In section 3.2.2.2, it was demonstrated that such a single particle inter-chain hopping of the form $\mathrm{e}^{i\gamma}a_j^\dagger b_j + \text{h.c.}$ can only distinguish the two ground states for $\gamma \neq 0$ that is, if the single particle hopping breaks time-reversal invariance. In the numerical calculations, the amplitude of a global single particle inter-chain hopping is taken as site dependant with a random local amplitude $t_i = r_i t_0$ where t_0 is a global parameter adjusting the overall strength and $r_i \in [0.9, 1.1]$ is an evenly distributed random variable. The single particle hopping can be seen as a kind of disorder. Then, the disorder breaks time-reversal invariance if and only if $t_0 \notin \mathbb{R}$. The local single particle hopping has just an amplitude of $t_i = \delta_{i,p} t_0$ where p is the position of the perturbation.

As is illustrated in figures 3.16a to 3.18b, the prediction from [1] holds in the topological phase such that a single particle inter-chain hopping can only lift ground state degeneracy and destroy the edge state if it also breaks time-reversal invariance.

Also, the perturbative arguments presented in [1] indicated that even when both sub-chain parity conservation and time-reveral invariance are broken, the splitting of ground state energy decays with the distance of the support of the perturbation from the end of the chain as depicted in figure 3.19. The decay can not be safely classified, however. A non-exponential decay might be explained by contributions from higher orders of perturbation theory in the context of the arguments from [1]. As can be seen in figures 3.17b, 3.18b and 3.19, the inter-chain single-particle hopping indeed only has an effect if it has support at the end of the chain and can hence connect the edge states. The agreement with the perturbative arguments is remarkable, as the theory is gapless and the second order perturbation theory therefore can be expected to contribute significantly to the impact of the symmetry breaking.

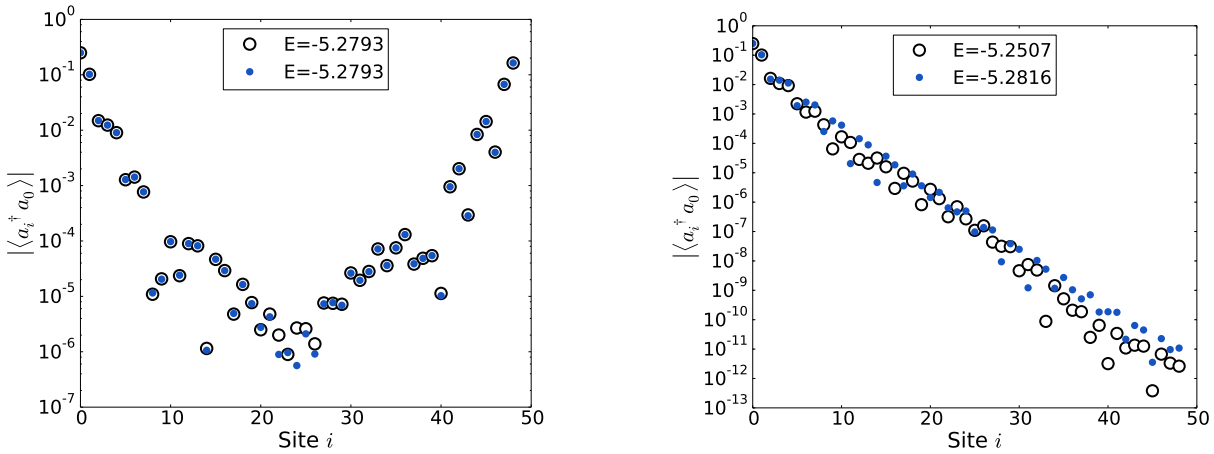

(a) (b)

Figure 3.16: On-chain two-point function for the ground state and the first excited state in presence of a global symmetry breaking term (a) with $t_0 = 0.05$ and (b) with $t_0 = 0.05i$. Clearly, the perturbation can only destroy the edge state and lift the ground state degeneracy if time-reversal symmetry is broken. The parameters used here are $W = 1$, $J = g = 0.9$ for a system of length $L = 50$ with particle number $N = 35$, the results are averaged over 15 sets of disorder.

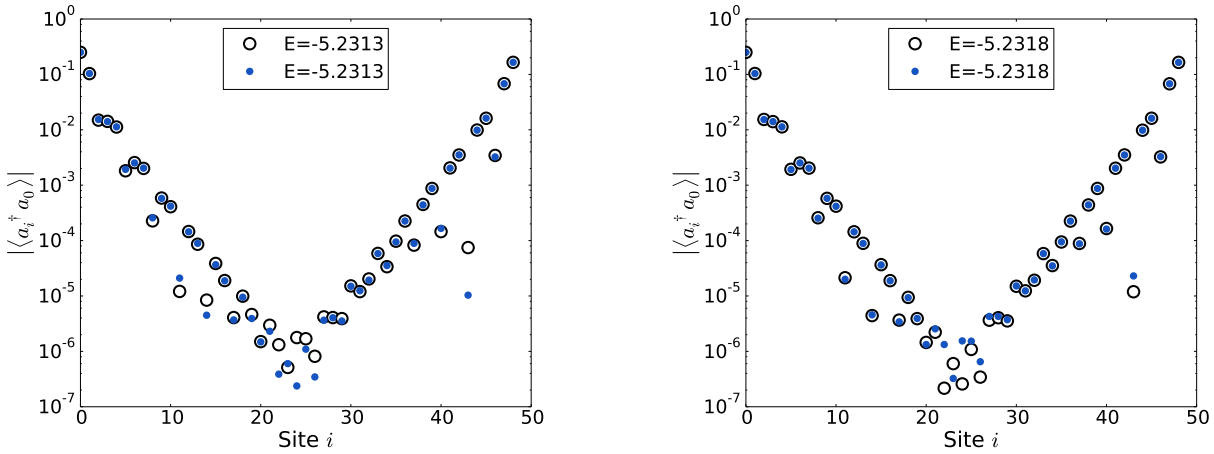

(a) (b)

Figure 3.17: On-chain two-point function for the ground state and the first excited state in presence of a local symmetry breaking term in the bulk (a) with $t_0 = 0.05$ and therefore without violation of time-reversal invariance and (b) with $t_0 = 0.05i$ and therefore also violation of time-reversal invariance. In the bulk, the local perturbation cannot lift the ground state degeneracy. The parameters used here are $W = 1$, $J = g = 0.9$ for a system of length $L = 50$ with particle number $N = 35$.

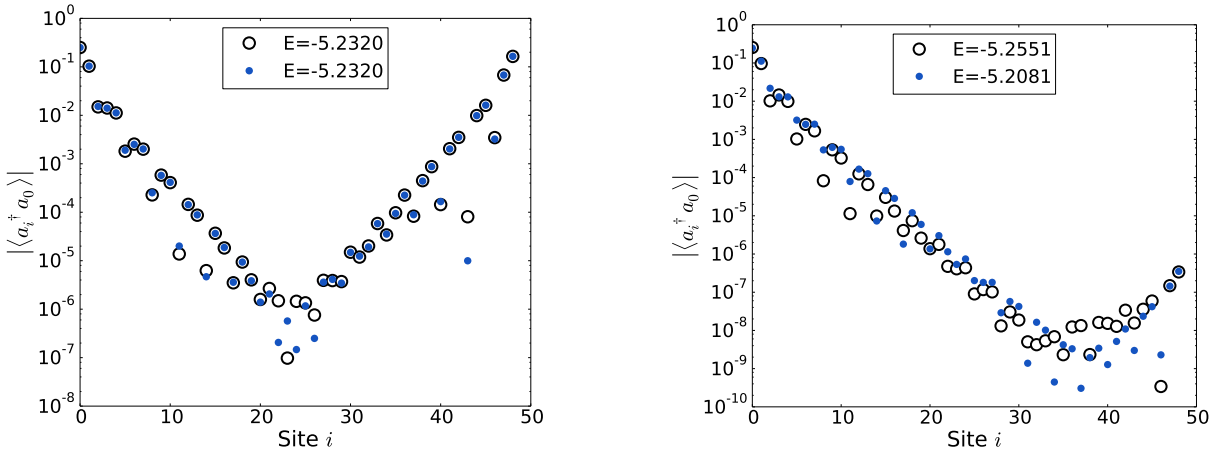

(a) (b)

Figure 3.18: On-chain two-point function for the ground state and the first excited state in presence of a local symmetry breaking term at the edge (a) with $t_0 = 0.05$ and therefore without violation of time-reversal invariance and (b) with $t_0 = 0.05i$ and therefore also violation of time-reversal invariance. As for the global single-particle hopping the breaking of time-reversal invariance is required for the symmetry breaking term to affect the edge states. The parameters used here are $W = 1$, $J = g = 0.9$ for a system of length $L = 50$ with particle number $N = 35$.

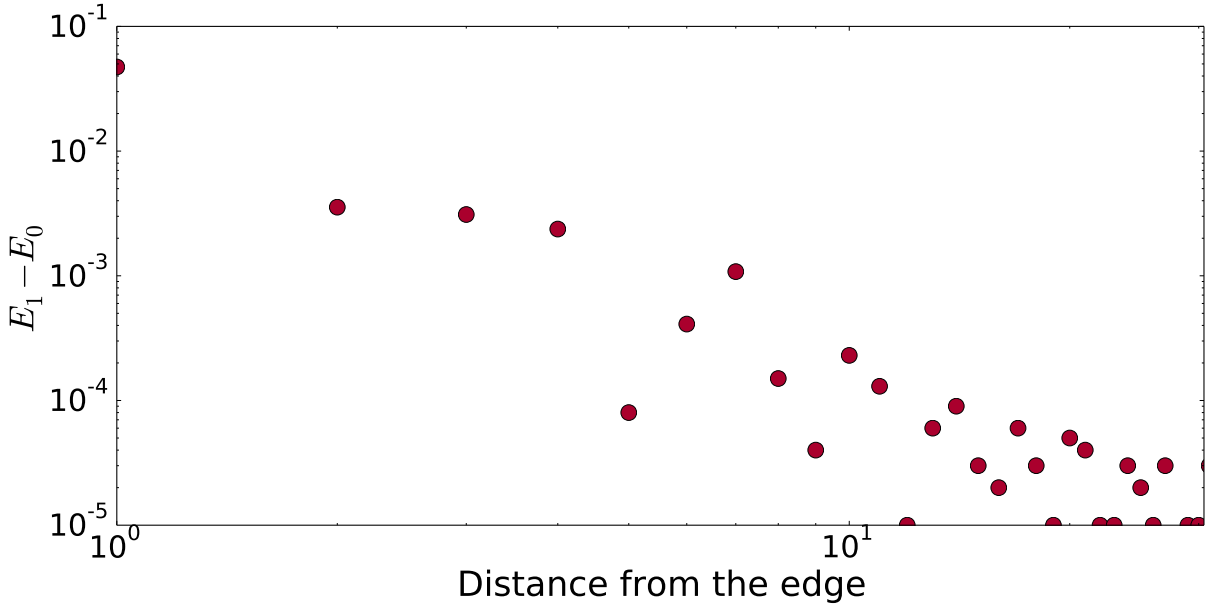

Figure 3.19: Splitting of ground state energies due to a local time-reversal breaking single-particle hopping only at a single site. This is in the topological phase for $W = 1$ and $J = g = 0.9$ where the ground state in absence of symmetry breaking is degenerate. The decay of the energy splitting when moving the single-particle hopping away from the end of the chain is clearly visible, as predicted in [1] for the exact point. For all points, a chain of length $L = 61$ with $N = 43$ particles is considered and the ground state and the first excited state are computed.

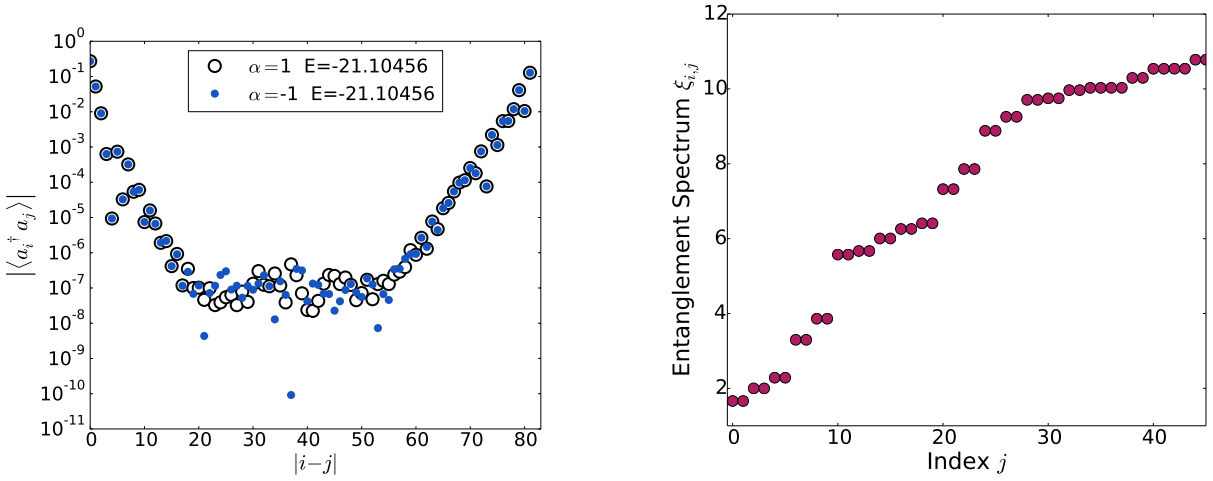

(a) (b)

Figure 3.20: Effects of disorder on the ground state properties of the topological phase. (a) Edge state and ground state degeneracy of the ladder system at $J = g = 0.8$ and $W = 1.1$ for a system of length $L = 83$ with $N = 74$ with a disorder of strengh $\delta = 0.15$. There is no notable effect of the disorder. (b) Entanglement spectrum of the system for a bipartition at $i = 36$ with system size $L = 86$ and $N = 77$ and $\alpha = -1$ with a disorder strengh $\delta = 0.15$. The degeneracy of the entanglement spectrum is also retained, strongly indicating the presence of topological order.

3.6 Effects of disorder

Stability against disorder is one of the key properties of topological order [72], and previously it was demonstrated that it is stable under local symmetry breaking perturbations. For a symmetry conserving disorder, the ground state degeneracy should clearly be conserved, or the splitting should be exponentially small in the system size at least.

This is probed using an equally distributed local variation in the parameters J, g and W by taking them to be site-dependent as $J_i = J(1 + \delta r_i)$ where $r_i \in [-1, 1]$ is an equally distributed random variable and δ is the strength of the disorder. For small δ, a stability of the topological order is expected. This stability is found in the numerical results even for rather strong disorder of $\delta = 0.15$ independently from the exact choice of parameters within the topological phase. For sufficiently large system sizes of $L > 30$, no splitting of the ground state degeneracy or the degeneracy of the entanglement spectrum can be found within numerical accuracy given by $(\Delta E)^2 \approx 10^{-6}$ for bond dimension $D = 350$, as exemplary depicted in figure 3.20.

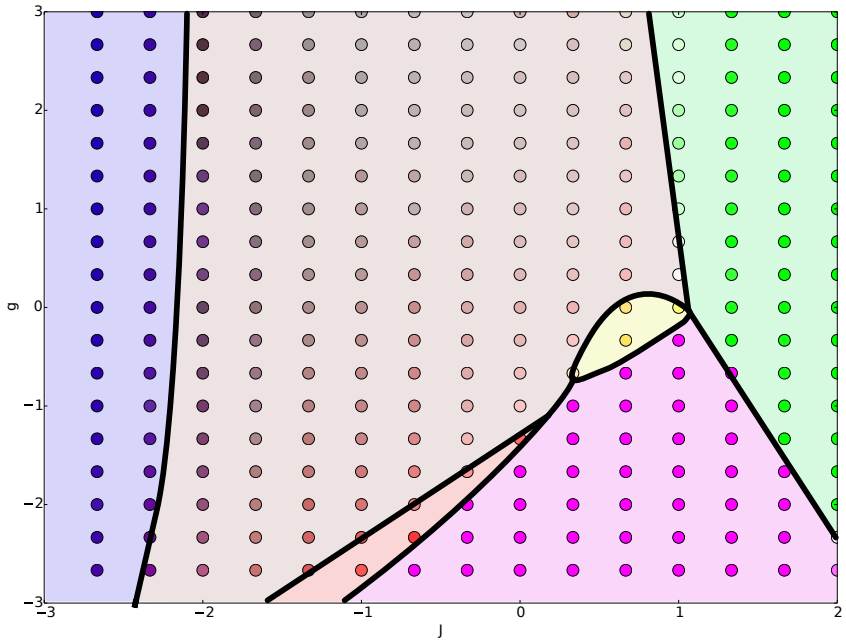

Figure 3.21: $J-g$ phase diagram for $W = 0.1$ for a ladder of length $L = 50$ at half filling. While the pair-hopping obviously has some influence, in particular on the transitions from the topological phase, the qualitative structure of the phase diagram remains unaffected by a drastic decrease in W. This indicates that the considerations for $W = 1$ are also valid for weak pair-hopping.

3.7 Considerations for weak pair-hopping

Up to this point, most of the numerical results were for pair-hopping strength $W = 1$, where the topological phase is good visible. The bosonization approach however starts from a free theory, and the topological phase can hence be expected to exist also for weak pair-hopping. A detailed analysis of the system without on-chain interactions and inter-chain density-density interactions, that is, for $J = g = 0$, based on both low-energy considerations employing bosonization and a numerical analysis using DMRG has been presented in [24]. A main result of [24] is that there is a topological phase away from half filling as long as $|W| \gtrsim$, while a too large value of $|W|$ will lead to a phase separation. This already justifies considering $W = 1$ for small coupling constants J, g. As demonstrated in figure 3.21, the occuring phases in the $J-g$ phase diagram do not change qualitatively when decreasing W, except that in the limit $W \to 0$, the topological phase will disappear. At this point, it is interesting that a pair-hopping of this strengh alone is not able to establish a topological edge state, but in combination with density-density interactions, it can. Also, the gap in the symmetric sector is much less prominent than for larger W but it still exists for strongly attractive inter-chain interactions. It can be concluded that the existence of the topological phase is very robuts against variation of the pair-hopping strengh, but the density-density interactions are crucial therefore.

Conclusion

An analytical and numerical analysis of a number conserving, interacting model of spinless fermions in a one-dimensional ladder system was performed in this thesis. There, the focus was put on the occurence of topological edge states as this is the initial motivation of the model and the existence of non-Abelian edge states has previously been proven for a special case in [1].

By means of bosonization, a qualitative analysis of the model is possible, which revealed the possibility of a symmetry protected ground state degeneracy. The impact of the different interactions assumed in the model was then characterized and it was shown that there are no other relevant terms in the predicted topological phase.

A major part then concerned the numerical treatment of the model using the DMRG algorithm in its formulation as a variational ansatz using a matrix product state. Here, the stability of the special case from [1] was considered and stability against certain perturbations as well as a possible phase separation was confirmed.

From the numerical data, a rich phase diagram could be constructed, showing good agreement with the expectations from the bosonization. Therefore, the entanglement entropy, the particle density, the on-chain two point function and various interchain correlation functions were employed, where the latter have been picked to be easily comparable to the predictions from the bosonized theory. Besides the topological phase and a phase separation on the single chains, a phase separation between the chains, driven by density-density interactions, is possible, as well as a Luttinger liquid phase featuring algebraic correlations and in special cases also a commensurate charge density wave and a gapless phase with exponentially decaying pair correlations.

The impact of symmetry breaking perturbations on the system has been analyzed by numerical means and the symmetry protection of the edge state and the ground state degeneracy in the topological phase have been demonstrated.

In the context of symmetry breaking, the numerical study of wire networks might be particularly interesting as there, the stability of the edge states versus any local perturbation could be shown.

Appendix A

RG Analysis

To study the behaviour of Perturbations under RG flow [40, 41] real-space RG is used as employed in [34], which is here introduced for a lattice since the initial RG step discretizes the theory. In particular, integrals over discrete variables are to be understood with respect to the counting measure. In the following, a short summary of the procedure and results from [34] shall be given, closely following the steps from [34].

Space-time coordinates are denoted as $\mathbf{x} = (\nu\tau, x)$ in this section where τ is the Wick rotated time. Therefore, consider the action corresponding to the Hamiltonian 2.3 in terms of the bare fields

$$S_0 = \int \mathrm{d}^2x \, \frac{1}{2} \left[\frac{1}{\nu^2} (\partial_\tau \theta)^2 + (\partial_x \theta)^2 \right] . \tag{A.1}$$

The RG step is defined as follows. The real space is divided into plaquettes of size $L \times L$, with L given in units of lattice spacing, which are denoted by plaquette coordinates $\hat{\mathbf{x}}$. Then, for each real-space point $\mathbf{x}$ there exists a unique $\hat{\mathbf{x}} \in (L\mathbb{Z})^2$ and $\mathbf{y} \in [0,\, L]^2$ such that $\mathbf{x} = \hat{\mathbf{x}} + \mathbf{y}$. The transition to the block-spin variable $\hat{\mathbf{x}}$ is done by averaging over the plaquettes

$$\hat{\theta}(\hat{\mathbf{x}}) = \frac{1}{L^2} \int_{[0,L]^2} \mathrm{d}^2y \; \theta(\hat{\mathbf{x}} + \mathbf{y}) \, . \tag{A.2}$$

The original field θ is expressed in terms of $\hat{\theta}$ via the decomposition $\theta = \hat{\theta} + \Delta\theta$. The action S_0 separates with respect to $\hat{\theta}$ and $\Delta\theta$. Now, consider a perturbation $S = S_0 + S_{\mathrm{int}}$ with $S_{\mathrm{int}} = \sum_i g_i \int \mathrm{d}^2x \, A_i$ where A_i has scaling dimension Δ_i and is expressed via the operators θ and its derivatives. To obtain the rescaled action, consider the expansion of the integrand of the partition function

$$\begin{aligned} \mathrm{e}^{-S} =& \mathrm{e}^{-S_0[\hat{\theta}]} \Big[1 - \int \mathrm{d}^2x \, g_i A_i(\mathbf{x}) \\ &+ \frac{1}{2} g_i g_j \int \mathrm{d}^2x \, \mathrm{d}^2x' \, A_i(\mathbf{x}) A_j(\mathbf{x}') + \mathcal{O}(\mathcal{L}_{int}^3) \Big] \, \mathrm{e}^{-S_0[\Delta\theta]} \, . \end{aligned} \tag{A.3}$$

To obtain an action for the new field $\hat{\theta}$, take the expectation value for the short-distance field $\Delta\theta$. Since the action S_0 separates as $S_0[\theta] = S_0[\hat{\theta}] + S_0[\Delta\theta]$, this does not affect S_0. For now, it is assumed that the expectation value $\hat{A}_i(\hat{\theta}) = \langle A_i(\theta) \rangle_{\Delta\theta}$ with respect to $\Delta\theta$

with weight $\exp(-S_0[\Delta\theta])$ of the perturbations A_i can be brought into the same funtional form as A_i. The first order term is then

$$\int \mathrm{d}^2x\, g_i \hat{A}_i(\hat{\mathbf{x}}) = \int \mathrm{d}^2\hat{x}\, L^2 g_i \hat{A}_i(\hat{\mathbf{x}}) \mapsto g_i L^{2-\Delta_i} \int \mathrm{d}^2\hat{x}\, \hat{A}_i(\hat{\mathbf{x}})\,, \tag{A.4}$$

where in the last step, the coordinate $\hat{x}$ is rescaled by $\hat{x} \mapsto \frac{1}{L}\hat{x}$ to regain the original scale. Therefore, the scaling properties of $\hat{A}_i$, which are the same as those of A_i, are employed. The second order term is treated using the operator product expansion (OPE) of the perturbation

$$A_i(\mathbf{x})A_j(\mathbf{x}') = \frac{C_{ijk}}{|\mathbf{x}-\mathbf{x}'|^{\Delta_i+\Delta_j-\Delta_k}} A_k(\mathbf{x}')\,. \tag{A.5}$$

Note that not all operators A_k appearing in the expansion need to have $g_k \neq 0$ in the original action, i.e. compared to first order, there can be additional perturbations in second order. This is precisely the reason for the renormalization of K. Using this short-distance expansion, the second order term can be approximated the same way as the first order term with the additional approximation of the integral over the relative coordinate, leading to the second order term

$$g_i g_j \int \mathrm{d}^2x\;\; A_i(\mathbf{x})A_j(\mathbf{x}') \approx 2\pi\; g_i g_j C_{ijk} L^{2-\Delta_k} V_{ijk}(L) \hat{A}_k(\hat{x}')\,, \tag{A.6}$$

with the approximate relative coordinate integral

$$V_{ijk}(L) = \begin{cases} L^{2-\Delta_i-\Delta_j-\Delta_k}, & 2-\Delta_i-\Delta_j-\Delta_k \neq 0 \\ \ln L, & 2-\Delta_i-\Delta_j-\Delta_k = 0 \end{cases}. \tag{A.7}$$

This motivates the introduction of a renormalized perturbation $\hat{S}_{\mathrm{int}}$ via

$$\mathrm{e}^{-S_0[\hat{\theta}]-\hat{S}_{\mathrm{int}}[\hat{\theta}]} \approx \mathrm{e}^{-S_0}\left[1 - \int \mathrm{d}^2\hat{x}\left(g_k L^{2-\Delta_k}\hat{A}_k(\hat{\mathbf{x}}) - \pi g_i g_j C_{ijk} L^{2-\Delta_k} V_{ijk}(L)\hat{A}_k(\hat{\mathbf{x}})\right)\right]. \tag{A.8}$$

Here, new coupling constants can be introduced to regain the form of $S = S_0 + S_{\mathrm{int}}$. To obtain the flow equations, consider $L \approx 1$ and expand the constants in $l = \ln L$. For $\Delta_k \neq 2$ this yields in leading order

$$\hat{g}_k = g_k L^{2-\Delta_k} \approx g_k\,(1 + (2-\Delta_k)l) \tag{A.9}$$

$$\Rightarrow \frac{\mathrm{d}g_k}{\mathrm{d}l} = (2-\Delta_i)g_k\,. \tag{A.10}$$

In the case of marginal perturbations, the behaviour depends on the second order and thereby on the operator product expansion of its coefficients. In the case of a set of marginal perturbations closed under operator product expansion the resulting flow equations are then given by

$$\hat{g}_k = g_k - \pi C_{ijk} g_i g_j l \tag{A.11}$$

$$\Rightarrow \frac{\mathrm{d}g_k}{\mathrm{d}l} = -\pi C_{ijk} g_i g_j\,. \tag{A.12}$$

In the case of a mixing of relevant and marginal perturbations, the flow equations for the marginal ones have to be derived using an expansion of V_{ijk} in terms of l.

Recall the action S_0 from equation (A.1) and consider a perturbation of the form

$$S_{\text{int}} = g \int \mathrm{d}^2x \, A(\mathbf{x}) \tag{A.13}$$

$$A(\mathbf{x}) =: \cos\left(\sqrt{8\pi}\theta(\mathbf{x})\right) : \, . \tag{A.14}$$

This is the well-studied sine-Gordon model [56] for which the RG analysis leads to the Kosterlitz-Thouless equations [67]. To check that A meets the assumption about the expectation value previously met, employ the remarkable identity (2.25) which is derived from the cumulant expansion of the expectation value of the exponential and leads to

$$\begin{aligned}
&\left\langle \cos\left(\sqrt{8\pi}(\hat{\theta} + \Delta\theta)\right)\right\rangle_{\Delta\theta} = \frac{1}{2}\cos(\sqrt{8\pi}\hat{\theta})\left\langle \mathrm{e}^{i\sqrt{8\pi}\Delta\theta} + \mathrm{e}^{-i\sqrt{8\pi}\Delta\theta}\right\rangle - \frac{1}{2i}\sin(\sqrt{8\pi}\hat{\theta})\left\langle \mathrm{e}^{i\sqrt{8\pi}\Delta\theta} - \mathrm{e}^{-i\sqrt{8\pi}\Delta\theta}\right\rangle \\
&= \frac{1}{2}\cos(\sqrt{8\pi}\hat{\theta})\left(\mathrm{e}^{-4\pi\left\langle\Delta\theta^2\right\rangle} + \mathrm{e}^{-4\pi\left\langle\Delta\theta^2\right\rangle}\right) - \frac{1}{2i}\cos(\sqrt{8\pi}\hat{\theta})\left(\mathrm{e}^{-4\pi\left\langle\Delta\theta^2\right\rangle} - \mathrm{e}^{-\frac{1}{2}\sqrt{8\pi}^2\left\langle\Delta\theta^2\right\rangle}\right) \\
&= \mathrm{e}^{-4\pi\left\langle\Delta\theta^2\right\rangle}\cos(\sqrt{8\pi}\hat{\theta})\,.
\end{aligned} \tag{A.15}$$

The necessary condition for this is basically the invariance of the expectation value under transformation $\Delta\theta \mapsto -\Delta\theta$ which is present due to S_0 being quadratic. As mentioned in section 3.1, this perturbation has scaling dimension $\Delta = \frac{2}{K}$, leading to the conjecture that it is relevant for $K > 1$ and irrelevant for $K < 1$. The flow equation is according to previous considerations

$$\frac{\mathrm{d}g}{\mathrm{d}l} = 2(1 - K^{-1})g\,, \tag{A.16}$$

for $K \neq 1$ .In the marginal case $K = 1$ it is indeed $\frac{\mathrm{d}g}{\mathrm{d}l} = 0$, but this case will not be considered for now. This is already one of the well-known Kosterlitz-Thouless equations [67]. However, the Luttinger parameter K is also subject to RG flow in this case since the perturbation A generates a term of the form S_0 in the operator product expansion in the second order of the expansion of $\mathrm{e}^{-S_{\text{int}}}$, following from the OPE of $A(\mathbf{x})A(\mathbf{x}')$. To obtain it, use equation (2.29) keeping only the terms singular at $\mathbf{x} = \mathbf{x}'$

$$\begin{aligned}
A(\mathbf{x})A(\mathbf{x}') &= \frac{1}{4} : \left(\mathrm{e}^{i\sqrt{8\pi}\theta(\mathbf{x})} + \mathrm{e}^{-i\sqrt{8\pi}\theta(\mathbf{x})}\right) :: \left(\mathrm{e}^{i\sqrt{8\pi}\theta(\mathbf{x}')} + \mathrm{e}^{-i\sqrt{8\pi}\theta(\mathbf{x}')}\right) : \\
&\approx \frac{1}{4}\mathrm{e}^{8\pi\langle\theta(\mathbf{x})\theta(\mathbf{x}')\rangle} : \left(\mathrm{e}^{i\sqrt{8\pi}(\theta(\mathbf{x})-\theta(\mathbf{x}'))} + \mathrm{e}^{-i\sqrt{8\pi}(\theta(\mathbf{x})-\theta(\mathbf{x}'))}\right) : \\
&= \frac{1}{2}|\mathbf{x} - \mathbf{x}'|^{-4} : \cos\left(\sqrt{8\pi}(\theta(\mathbf{x}) - \theta(\mathbf{x}')\right) : \, .
\end{aligned} \tag{A.17}$$

Now expand the cosine around $\mathbf{x} = \mathbf{x}'$. It is convenient to do so in the complex space-time coordinates $z = \nu\tau - ix$ and $\bar{z} = \nu\tau + ix$. It is even common to express all fields in terms of these coordinates instead of the real space-time coordinates. This leads to

$$\begin{aligned}
\cos\left(\sqrt{8\pi}(\theta(\mathbf{x}) - \theta(\mathbf{x}'))\right) =& 1 - 4\pi(\mathbf{x} - \mathbf{x}')^2(\partial_z\theta)(\partial_{\bar{z}}\theta) - 4\pi\left((z - z')^2(\partial_z\theta)^2 + (\bar{z} - \bar{z}')(\partial_{\bar{z}}\theta)^2\right) \\
&+ \mathcal{O}\left((\mathbf{x} - \mathbf{x}')^4\right)\,,
\end{aligned} \tag{A.18}$$

Where the higher terms only contribute regular terms to the OPE and are therefore neglected. The terms only depending on z respectively $\bar{z}$ do not appear in the RG equations [34]. This gives as the most divergent terms of the OPE

$$A(\mathbf{x})A(\mathbf{x}') = \frac{1}{2}|\mathbf{x}-\mathbf{x}'|^{-4} + 2\pi|\mathbf{x}-\mathbf{x}'|^{-2}\left[\frac{1}{\nu^2}(\partial_\tau\theta)^2 + (\partial_x\theta)^2\right]. \tag{A.19}$$

Thus, a term of the form S_0 appears in second order, leading to a necessary redefinition of the Luttinger parameter via

$$\hat{K} = K + \pi g^2 \ln L\,, \tag{A.20}$$

whereas the constant contribution is not physically relevant due to normalization of the partition function. Therefore, the RG equation for K is given by the well known [67] identity

$$\frac{\mathrm{d}K}{\mathrm{d}l} = \pi g^2\,. \tag{A.21}$$

Appendix B

Dynamical basis adaption and subspace expansion

In section 2.2.1, the necessity of a normalization of the matrices of the variational state is introduced. The existence of a mixed canonical version of some state $|\psi\rangle$ given in MPS form by matrices A^{σ_i} is an inherent property of the MPS [52]. Such a state can iteratively be brought into the desired mixed canonical shape by repeated application of thin $QR-/RQ-$ decompositions [55] of the concatenated matrices $A^{[i]}_{l/r}$ [45]. For example, for left-normalization, take $A^{[i]}_l$ and apply a thin decomposition

$$A^{[i]}_l = \begin{pmatrix} Q_1 & Q_2 \end{pmatrix} \cdot \begin{pmatrix} R \\ 0 \end{pmatrix} = Q_1 R \,. \tag{B.1}$$

Now, it is $Q_1^\dagger Q_1 = 1$ and Q_1 is of the same dimension as $A^{[i]}_l$. Now, the ambiguity of matrices A^{σ_i} is employed: Whether the matrix R is multiplied into all matrices A^{σ_i}, which corresponds to the decomposition (B.1), or into all matrices $A^{\sigma_{i+1}}$ does not matter as only the product $A^{\sigma_i}A^{\sigma_{i+1}}$ appears in the state. It is hence safe to define new matrices $\tilde{A}^{\sigma_i}$ via $\tilde{A}^{[i]}_l = Q_1$. This does not change the state if at the same time the matrices of the next site are redefined as $\tilde{A}^{\sigma_{i+1}} = RA^{\sigma_{i+1}}$. Now, the state is left-normalized at site i, while the possible normalization at the next site is lost. This step can be repeated however, leaving a scalar R at the last site corresponding to the norm of the state as the norm is given as in figure 2.8. Analogously, the matrices can be right-normalized using a QR-decomposition of the adjoint matrix, which is an RQ-decomposition. When performing these steps from site 1 to $i-1$ from the left and from site L to $i+1$ from the right, the desired mixed-canonical form is obtained. This description of the normalization procedure is based on [45].

Now, turn towards the problem of fixing good quantum numbers in an MPS. The main difficulty is here the definition of the labeling functions q_i as introduced in section 2.2.2. First, a set of labeling functions has to be defined initially such that the initial state can be constructed, normalized and the initial contractions can be computed. This is non-trivial as the initial functions also highly restrict the initial state. In particular they have to be chosen such that there is a nonzero state satisfying the constraint (2.51) and it has to be possible to bring this state into left-canonical form without violating (2.51), which is another non-trivial constraint. The key idea here is to construct the functions q_i both from left to right and from right to left and then combining the results. In principle, there is no need for an initial definition of the quantum number labels if they are updated

dynamically, but omitting it will not only slow down the initialization but will also lead to pretty bad initial states.

The more subtle difficulty is however not the initialization but the dynamic updating of the labeling functions during runtime. If the initial choice is not optimal, which it is probably only at the exact point within this thesis as the optimal choice is known there, the labeling functions have to be adapted dynamically to reach an optimal state [47]. However, it is not possible to do so in a meaningful way in the standard single-site algorithm [45].

To achieve a dynamic choice of the q_i, the subspace expansion method as presented in [47] is employed. The main aspect of this extension of the algorithm is a modification of the normalization scheme described above. In the following, the procedure and results from [47] are sketched, for a thorough analysis of the method also in comparison to other enrichment methods, see [47]. For demonstration, the left-enrichment at some site i will be described, which replaces the left-normalization as described above.

Instead of just using a thin QR-decomposition, the matrices A^{σ_i} are expanded by additional matrices P^{σ_i} of size $D_{i-1} \times D_P$, where D_{i-1} is the virtual bond dimension at bond $i-1$ and D_P is at this point arbitrary. Now, replace

$$A^{\sigma_i} \mapsto A'^{\sigma_i} = \begin{pmatrix} A^{\sigma_i} & P^{\sigma_i} \end{pmatrix} . \tag{B.2}$$

If the matrices $A^{\sigma_{i+1}}$ are at the same time replaced by

$$A^{\sigma_{i+1}} \mapsto A'^{\sigma_{i+1}} = \begin{pmatrix} A^{\sigma_{i+1}} \\ 0 \end{pmatrix} , \tag{B.3}$$

where the 0-block is of size $D_P \times D_{i+1}$, this does not change the state.

Next, the new matrix $A_l'^{[i]}$ has to be normalized and at the same time truncated to dimension $dD_{i-1} \times D_i$. Therefore, apply an SVD to $A_l'^{[i]}$, resulting in a matrix U of size $dD_{i-1} \times dD_{i-1}$, a matrix $V^\dagger$ of size $(D_i + D_P) \times (D_i + D_P)$ and $\min(dD_{i-1},\, D_i + D_P)$ singular values λ_j, in form of a diagonal matrix S of size $dD_{i-1} \times (D_i + D_P)$. Truncation is then executed by keeping only the D_i largest singular values and setting the other singular values to 0. If the dimensions D_i are build correctly, it is always $D_i \leq dD_{i-1}$, such that this truncation is always possible. Keeping only the first D_i singular values means that only the first D_i columns of U and the first D_i rows of $V^\dagger$ contribute, therefore, the matrix U is now of effective size $dD_{i-1} \times D_i$ and the matrix $V^\dagger$ is of effective size $D_i \times (D_i + D_P)$.

Now, the labeling functions q_i are redefined based on the kept singular values. Each singular value λ_j can be assigned two indices $a_{i-1} \in \{1, \ldots, D_{i-1}\}$ and $\sigma_i \in \{1, \ldots, d\}$ as the singular values are initially just entries in a matrix of size $dD_{i-1} \times (D_i + D_P)$. After truncation, there are D_i singular values, each of those gets assigned an index a_i. This can be done arbitrarily, but the columns of U have to be labeled in the same way. The new q_i is now just defined via

$$q_i(a_i) = q_{i-1}(a_{i-1}) + q(\sigma_i) , \tag{B.4}$$

using the indices a_i, a_{i-1} and σ_i just assigned to the singular values. As mentioned below, the SVD has to be implemented blockwise such that the truncated matrix U now fullfills

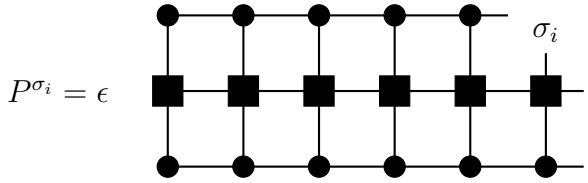

Figure B.1: Heuristic expansion term [47] for the left-sided subspace expansion in the graphical notation introduced in figures 2.1 and 2.2. It can be computed easily as the left side of the expression is anyway available as $T^{[i]}$ in the main algorithm. With this term, it is $D_P = D_i D_w$. The scalar parameter ϵ is used to control the impact of the expansion.

the constraint (2.51) with the new labels. Then, the truncated matrix U of size $dD_{i-1} \times D_i$ is the new matrix $A_l^{[i]}$ and is left-normalized by construction.

The truncated matrix $SV^\dagger$ of size $D_i \times (D_i + D_P)$ on the other hand encodes the transformation from the old labeling functions to the new ones for the tensor of site $i+1$. As in the standard normalization procedure, it is multiplied into the matrices of the next site. Since these were also expanded, this can be done as

$$A'^{\sigma_{i+1}} \mapsto SV^\dagger A'^{\sigma_{i+1}} \,, \tag{B.5}$$

which works analogously to the standard normalization procedure as described above.

For the expansion term P^{σ_i}, the heuristic term from figure B.1 is used, a discussion thereof can also be found in [47].

The right-sided subspace expansion works analogously with the right-sided expansion term, see [47].

In the end, a few comments shall be made about the implementation. In the description of the algorithm so far, the operations are not guaranteed to conserve the block structure given by equation (2.51). Both the normalization, or subspace expansion respectively, and the optimization step have to be implemented such that the constraint (2.51) is retained. Using a standard SVD for the subspace expansion will in general break the constraint for example. Also, there is little gain in computational costs if the constraint (2.51) is just imposed without making use of the highly diminished number of variational parameters.

To both make operations more efficient and conserve the structure given by (2.51), it is useful to identify the blocks of the tenors $A^{[i]}$ for which $q_i(a_i) = M$ for some constant block quantum number M. Then, the operations like SVD or contractions of the tensors $A^{[i]}$ with other tensors are performed blockwise on all those blocks. For the subspace expansion, the implementation is a bit more subtle as only the expansion and the SVD are performed blockwise, but not the truncation, since it is the role of that step to adapt the functions q_i and therefore also update the block structure.

Appendix C

Construction of the projector for excited state search

In section 2.2.3 the idea behind the computation of excited states was sketched. The main expansion to the algorithm is there the addition of an additional constraint on the state, implemented as a modified eigenvalue problem for the variation of the single matrices. To perform this step, a projection operator onto the space orthogonal to all previously obtained states $|\phi_k\rangle$ has to be constructed. This can be done efficiently such that both the construction of the projector and its application scale as $\mathcal{O}(D^2)$ [46]. This section closely follows [46] for introducing the projection operator.

To be efficient, the projection has to be evaluated locally, like any other operation in the MPS language. Since the scalar product of two states $|\psi_{1,2}\rangle$ is just the matrix element of identity, it can be computed iteratively analogously to the procedure for calculating matrix elements of operators. Of course, the contractions with the identity MPO are not carried out but the MPO is just omitted in the contractions. The local orthogonality constraint can then be easily expressed using the partial contractions of the scalar product as

$$F_k^{[i]} A^{[i]} = 0\,, \tag{C.1}$$

with $F_k^{[i]}$ being defined like in figure C.1 as $F_k^{[i]} = \frac{\partial}{\partial A^{[i]}} \langle \psi \,|\, \phi_k \rangle$ [46]. The product is to be understood as a contraction over all indices and the equation has to hold for all $|\phi_k\rangle$ to which orthogonalization is required.

The projector can then be constructed in terms of the matrices $F_k^{[i]}$ as derived in [46] as

$$P^{[i]} = 1 - \sum_{kk'} F_k^{[i]} F_{k'}^{[i]\dagger} (\mathcal{N}^+)_{kk'}\,. \tag{C.2}$$

$F_{k\ a_{i-1}\ a_i}^{[i]\ \sigma_i} =$

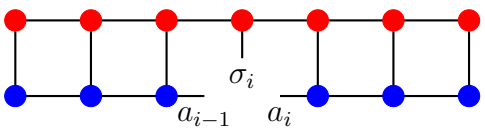

Figure C.1: Definition of the matrix $F_k^{[i]}$. The blue dots represent the matrices of the variational state $|\psi\rangle$ and the red dots to those of the state $\langle\phi_k|$ to which orthogonalization is desired. In this notation, equation (C.1) follows straigtforward as a necessary and sufficient condition for orthogonality since $F_k^{[i]} A^{[i]} = \langle \phi_k \,|\, \psi \rangle$.

For the projector to be idempotent, the inverse of the Gram matrix $\mathcal{N}_{kk'} = \mathrm{Tr}\left(F_k^{[i]\dagger} F_{k'}^{[i]}\right)$ has to be included [46]. For increased numerical stability [46], the Moore-Penrose pseudoinverse $\mathcal{N}^+$ [55] is used instead.

As the projector is required in each step of a sweep, it has to be construced anew for each i. However, the matrices $F_k^{[i]}$ can be computed iteratively analogously to T and R from the computation of matrix elements. Then, after optimizing the matrices at site i, the new matrices have to be used to compute $F_k^{[i\pm1]}$ from $F_k^{[i]}$, which can be done in $\mathcal{O}(D^3)$ operations.

The matrices $F_k^{[i]}$ have dimension dD^2 and therefore, using the form (C.2) of the projector would scale as $\mathcal{O}(D^4)$. To reduce the operational cost, it is convenient to rewrite the projector by introducing a auxiliary matrices $G_\mu^{[i]}$ as discussed in [46]. Let V_μ be the eigenvectors of the Gram matrix and λ_μ the corresponding eigenvalues which are greater than some threshold. Then, define

$$G_\mu^{[i]} = \frac{1}{\sqrt{\lambda_\mu}} \sum_k V_{k\mu} F_k^{[i]} \,. \tag{C.3}$$

These can obviously be be constructed with $\mathcal{O}(D^2)$ operations. The projection can now be executed directly in $\mathcal{O}(D^2)$ operations [46] as

$$P^{[i]} A^{[i]} = A^{[i]} - \sum_\mu \mathrm{Tr}\left(G_\mu^{[i]\dagger} A^{[i]}\right) G_\mu^{[i]} \,. \tag{C.4}$$

A generalization to two-site or many-site algorithms is straightforward and can be found in [46].

Appendix D

Performance of the DMRG implementation

To profile the performance of the implementation of the variational MPS algorithm used here and to allow for efficient optimization, runtime and convergence are profiled for some systems, where the focus is put on the ladder system (1.2). Here, some exemplary results are listed. As a reference, the same calculations are done using the *mps_optim* function of ALPS [49]. The measurements are done using the performance profiler Intel® Vtune™ Amplifier XE 2016, which allows for function-resolved runtime analysis of parallel programms, and run on an Intel® Xeon® E5-2630 v3 processor.

The implementation used within this thesis is compiled using the Intel® C++ compiler 16.0 with optimization option -O3 and linked against OpenMP for parallelization.

Several systems are considered, which are the ladder system with Hamiltonian (1.2), the spin-$\frac{1}{2}$ antiferromagnetic Heisenberg chain and the Bose Hubbard model. Runtimes for computing the ground state of these models are depicted in figure D.1a. Some explicit values together with reference values from the ALPS library are given in table D.1.

The runtimes from figure D.1a qualitatively agree with the expectations for the cost of the dominant step of computing $\frac{\partial}{\partial A^{*\sigma_i}_{a_{i-1}\,a_i}} \langle \psi \,|\, H \,|\, \psi \rangle$ of $\mathcal{O}(dD_W D^3)$ in case $D_W \ll D$, showing an algebraic increase in runtime with D. Also, the Bose Hubbard model and the spin-$\frac{1}{2}$ Heisenberg model both have a bond dimension of the Hamiltonian of $D_W = 5$ and differ only in the local Hilbert space dimension which is $d = 2$ for the Heisenberg model. Since bosonic systems have an infinite dimensional local Hilbert space, a truncation has to be made, and the number of bosons is limited to 3 per site. This is somewhat justified by the repulsive interaction in the model that prevent the bosons from clustering at one site. Therefore, the calculations referred in D.1a are done using $d = 4$ for the Hubbard model, explaining the larger runtime. The ladder system (1.2) also has a local Hilbert space dimension of $d = 4$ but a much larger bond dimension of the Hamiltonian of $D_W = 12$. However, optimizations for the computation of contractions using the sparse structure of the Hamiltonian and the higher symmetry keep the additional cost at bay.

The convergence of the ground state energy shown in figure D.1b indicates that the bond dimension required to obtain results with a comparable accuracy is much higher in the topological phase away from the exact point than at the exact point, where $D = 200$ is enough to obtain a variance of energy in the order of magnitude of 10^{-9} for a chain length of $L = 100$. Therefore, most of the calculations whose results are used in this thesis use $D \geq 300$ for $L = 50$.

Model	Runtime [s]	Energy
Heisenberg	188.9	-21.9721
Bose Hubbard	383.7	-25.5983
Double ladder	774.4	-2.5759

(a)

Model	Runtime [s]	Energy
Heisenberg AFM	86.9	-21.9721
Bose Hubbard	132.4	-24.8611
Double ladder	437.2	-2.3973

(b)

Table D.1: Exemplary runtimes and obtained energies (a) for my implementation of the variational MPS algorithm and (b) reference values obtained using the *mps_optim* function of ALPS. All values are for system sizes of $L = 50$ with bond dimension $D = 200$ and 14 sweeps. For the Heisenberg model, the total spin in z-direction is set to $S_Z = 0$. For the Bose Hubbard model, the total particle number is fixed to $N = 50$ and the number of bosons per site is limited to 3. The parameters $U = 2$, $t = 1$ are taken. The ladder system is considered with $W = 1$, $J = g = 0.9$, a total particle number of $N = 14$. Note that the results depend on the further parameters like tolerance of the iterative eigensolver, coefficient for the density matrix perturbation or the details of the algorithm.

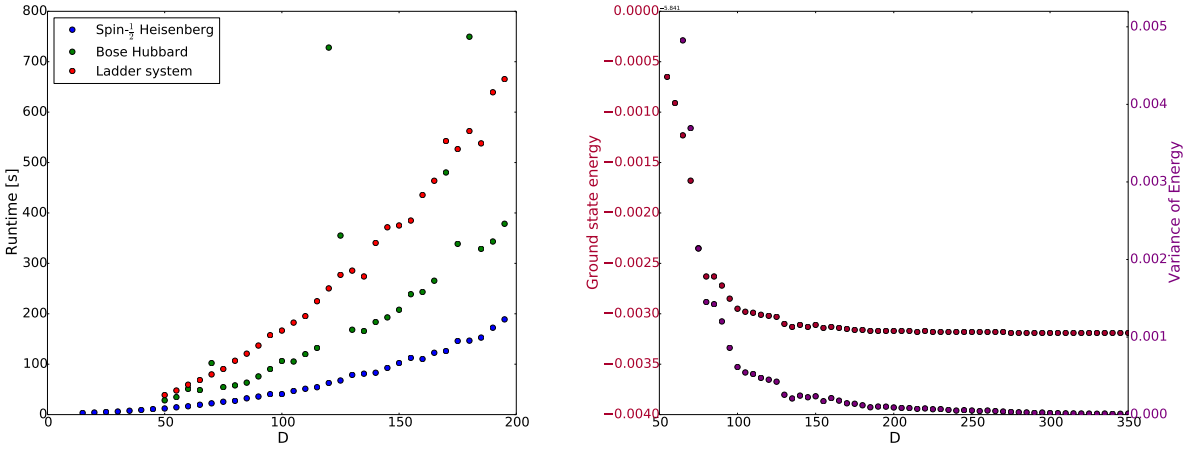

(a) (b)

Figure D.1: (a) Runtime of the program over bond dimension for the Bose Hubbard model, the Heisenberg Spin-$\frac{1}{2}$ chain and the ladder system described by (1.2). Here, the scaling of the algorithm as $\mathcal{O}(D^3)$ can be observed. All systems are taken with a size of $L = 50$ and sweeping is proceeded until either 14 sweeps have been executed or the variance of energy is below 10^{-7}. For the Heisenberg model, the total spin in z-direction is set to $S_z = 0$. The parameters of the Hubbard model are $U = 2$, $t = 1$ and those of the ladder system $W = 1$, $J = g = 0.9$ at half filling with subchain parity of the lower chain $\alpha = 1$. (b) Computed ground state energy and variance of energy for the ladder system with parameters $W = 1$, $J = g = 0.9$ at half filling with $\alpha = 1$ after 14 sweeps.

Note that the data given are exemplary and still dependent on internal parameters like tolerance of the eigensolver, the rate at which the tolerance is adapted or the coefficient of subspace expansion, or on the utilized library versions or on hardware specifications.

List of Figures

2.1 Graphical notation for a tensors of an MPS 18
2.2 Graphical notation for a tensors of an MPO 18
2.3 Coefficients of an MPS 18
2.4 Graphical notation for a matrix element of an operator 19
2.5 Iterative evaluation of matrix elements from left to right 19
2.6 Iterative evaluation of matrix elements from right to left 20
2.7 Application of $H_{\text{eff}}^{[i]}$ to an MPS 21
2.8 Scalar product of two MPS 22
2.9 Left-/right-normalization of MPS matrices 23

3.1 Numerical results at the exact point 43
3.2 Degeneracy of entanglement spectrum 44
3.3 Effect of perturbations around the exact point 46
3.4 Characteristic correlations for the topological phase 47
3.5 Topological phase and exact point 47
3.6 Entanglement spectrum and entropy for the topological phase 48
3.7 Gap scaling for the topological phase 48
3.8 Density and pair correlations at half filling 50
3.9 Scaling of energy gap for the charge density wave 51
3.10 Characteristics of the charge density wave 51
3.11 Symmetric charge density wave 52
3.12 Antisymmetric charge density wave 52
3.13 $J - g$ phase diagram for $W = 1$ at half filling 53
3.14 Properties away from half filling and algebraic correlation 54
3.15 Entanglement entropy and superconducting correlations 54
3.16 Effect of a global symmetry breaking term 56
3.17 Effect of a local symmetry breaking term 56
3.18 Effect of a local symmetry breaking term at the edge 57
3.19 Dependence of gap of the position of a symmetry breaking term 57
3.20 Energy splitting due to disorder 58
3.21 $J - g$ phase diagram for $W = 0.1$ 59

B.1 Expansion term for the subspace expansion 67

C.1 Derivative of the scalar product 68

D.1 Benchmarks of the variational MPS program 71

Acknowledgments

In the end, I would like to thank Hans Peter Büchler most sincerely for giving me the opportunity to work in such a great environment and who managed to enthuse me for topological states of matter in general and even more so for the methods he suggested to use. His guidance proved to be essential more than once, but he also gave me the free space to pursue my own ideas. Also, thank you for the opportunities to visit interesting workshops and conferences which allowed me to broaden my horizon.

I would also like to express my gratitude towards Nicolai Lang for the countless discussions and for always taking the time when I asked him for advise. Also, his excellent administration of the Institute's cluster enabled me to use the available computational resources without difficulty and granted me large flexibility in the numerical part, making effortive calculations possible.

Further I would like to thank Maria Daghofer for discussing my results with me and for her great lectures on strongly correlated electron systems and modern topics of solid state theory.

For helpful and stimulating discussions about topological phases, DMRG and numerics in general, C++ and phyiscs at large I thank Michael Schmid, Sebastian Weber, Jan Kumlin and David Peter. In particular, thanks to Michael Schmid for proofreading early concepts of the thesis and Jan Kumlin for his helpful proofreading of large parts of the thesis.

A special thanks goes to my family for their support and for always encouraging me to pursue my plans.

Bibliography

[1] N. Lang and H. Büchler, "Topological states in a microscopic model of interacting fermions," *Phys. Rev. B*, vol. 92, p. 041118, Jul 2015.

[2] D. J. Thouless, M. Kohmoto, M. P. Nightingale, and M. den Nijs, "Quantized hall conductance in a two-dimensional periodic potential," *Phys. Rev. Lett.*, vol. 49, pp. 405–408, Aug 1982.

[3] X. Wen, "Topological orders and edge excitations in fractional quantum hall states," *Advances in Physics*, vol. 44, no. 5, pp. 405–473, 1995.

[4] K. v. Klitzing, G. Dorda, and M. Pepper, "New method for high-accuracy determination of the fine-structure constant based on quantized hall resistance," *Phys. Rev. Lett.*, vol. 45, pp. 494–497, Aug 1980.

[5] V. J. Goldman and B. Su, "Resonant tunneling in the quantum hall regime: Measurement of fractional charge," *Science*, vol. 267, no. 5200, pp. 1010–1012, 1995.

[6] D. Arovas, J. R. Schrieffer, and F. Wilczek, "Fractional statistics and the quantum hall effect," *Phys. Rev. Lett.*, vol. 53, pp. 722–723, Aug 1984.

[7] M. Levin and X.-G. Wen, "Fermions, strings, and gauge fields in lattice spin models," *Phys. Rev. B*, vol. 67, p. 245316, Jun 2003.

[8] G. Moore and N. Read, "Nonabelions in the fractional quantum Hall effect," *Nucl. Phys.*, vol. B360, 362, 1991.

[9] M. Z. Hasan and C. L. Kane, "*Colloquium* : Topological insulators," *Rev. Mod. Phys.*, vol. 82, pp. 3045–3067, Nov 2010.

[10] P. Hauke, O. Tieleman, A. Celi, C. Ölschläger, J. Simonet, J. Struck, M. Weinberg, P. Windpassinger, K. Sengstock, M. Lewenstein, and A. Eckardt, "Non-abelian gauge fields and topological insulators in shaken optical lattices," *Phys. Rev. Lett.*, vol. 109, p. 145301, Oct 2012.

[11] H. Miyake, G. A. Siviloglou, C. J. Kennedy, W. C. Burton, and W. Ketterle, "Realizing the harper hamiltonian with laser-assisted tunneling in optical lattices," *Phys. Rev. Lett.*, vol. 111, p. 185302, Oct 2013.

[12] A. Bühler, N. Lang, C. Kraus, G. Möller, S. Huber, and H. Büchler, "Majorana modes and p-wave superfluids for fermionic atoms in optical lattices," *Nature Communications*, vol. 5, 2014.

[13] A. Kitaev, "Fault-tolerant quantum computation by anyons," *Annals of Physics*, vol. 303, no. 1, pp. 2 – 30, 2003.

[14] C. Nayak, S. H. Simon, A. Stern, M. Freedman, and S. Das Sarma, "Non-abelian anyons and topological quantum computation," *Rev. Mod. Phys.*, vol. 80, pp. 1083–1159, Sep 2008.

[15] D. Ivanov, "Non-Abelian statistics of half-quantum vortices in p-wave superconductors," *Physcial Review Letters*, vol. 86, 268, 2001.

[16] A. Kitaev, "Unpaired Majorana fermions in quantum wires," *Physics-Uspekhi*, vol. 44, 131, 2001.

[17] D. Asashi and N. Nagaoso, "Topological indices, defects and Majorana fermions in chiral superconductors," *Physical Review B*, vol. 86, 100504, 2012.

[18] D. G. N. Read, "Paired states of fermions in two dimensions with breaking of parity and time-reversal symmetries and the fractional quantum Hall effect," *Physical Review B*, vol. 61, 10267, 1999.

[19] Y. Rang, Y. Zhang, and A. Vishwanath, "One-dimensional topologically protected modes in topological insulators with lattice dislocations," *Nature Physics*, vol. 5, 298, 2009.

[20] V. Mourik, K. Zuo, S. M. Frolov, S. R. Plissard, E. P. A. M. Bakkers, and L. P. Kouwenhoven, "Signatures of majorana fermions in hybrid superconductor-semiconductor nanowire devices," *Science*, vol. 336, no. 6084, pp. 1003–1007, 2012.

[21] S. Nadj-Perge, I. K. Drozdov, J. Li, H. Chen, S. Jeon, J. Seo, A. H. MacDonald, B. A. Bernevig, and A. Yazdani, "Observation of majorana fermions in ferromagnetic atomic chains on a superconductor," *Science*, vol. 346, no. 6209, pp. 602–607, 2014.

[22] A. Kitaev, "Anyons in an exactly solved model and beyond," *Annals of Physics*, vol. 321, 2, 2006.

[23] F. Iemini, L. Mazza, D. Rossini, R. Fazio, and S. Diehl, "Localized majorana-like modes in a number-conserving setting: An exactly solvable model," *Phys. Rev. Lett.*, vol. 115, p. 156402, Oct 2015.

[24] C. V. Kraus, M. Dalmonte, M. A. Baranov, A. M. Läuchli, and P. Zoller, "Majorana edge states in atomic wires coupled by pair hopping," *Phys. Rev. Lett.*, vol. 111, p. 173004, 2013.

[25] M. Sato, Y. Takahashi, and S. Fujimoto, "Non-abelian topological order in s-wave superfluids of ultracold fermionic atoms," *Phys. Rev. Lett.*, vol. 103, p. 020401, Jul 2009.

[26] D. Matthis and E. Lieb, "Exact solution of a many-fermion system and its associated boson field," *Journal of Mathematical Physics*, vol. 6, 1965.

[27] J. von Delft and H. Schoeller, "Bosonization for beginners - refermionization for experts," *Annalen der Physik*, vol. 7, no. 4, 1998.

[28] S. R. White, "Density matrix formulation for quantum renormalization groups," *Phys. Rev. Lett.*, vol. 69, pp. 2863–2866, Nov 1992.

[29] S. R. White and D. A. Huse, "Numerical renormalization-group study of low-lying eigenstates of the antiferromagnetic S =1 heisenberg chain," *Phys. Rev. B*, vol. 48, pp. 3844–3852, Aug 1993.

[30] L. Fidkowski, R. M. Lutchyn, C. Nayak, and M. P. A. Fisher, "Majorana zero modes in one-dimensional quantum wires without long-ranged superconducting order," *Phys. Rev. B*, vol. 84, p. 195436, Nov 2011.

[31] J. D. Sau, B. I. Halperin, K. Flensberg, and S. Das Sarma, "Number conserving theory for topologically protected degeneracy in one-dimensional fermions," *Phys. Rev. B*, vol. 84, p. 144509, Oct 2011.

[32] M. Cheng and H.-H. Tu, "Majorana edge states in interacting two-chain ladders of fermions," *Phys. Rev. B*, vol. 84, p. 094503, 2011.

[33] A. Keselman and E. Berg, "Gapless symmetry-protected topological phase of fermions in one dimension," *Phys. Rev. B*, vol. 91, p. 235309, Jun 2015.

[34] D. Sénéchal, "An introduction to bosonization," *eprint arXiv:cond-mat/9908262*, Aug. 1999.

[35] R. Heidenreich, R. Seiler, and D. A. Uhlenbrock, "The luttinger model," *Journal of Statistical Physics*, vol. 22, no. 1, pp. 27–57, 1980.

[36] F. D. M. Haldane, "General relation of correlation exponents and spectral properties of one-dimensional fermi systems: Application to the anisotropic $s = \frac{1}{2}$ heisenberg chain," *Phys. Rev. Lett.*, vol. 45, pp. 1358–1362, Oct 1980.

[37] A. Luther and I. Peschel, "Single-particle states, kohn anomaly, and pairing fluctuations in one dimension," *Phys. Rev. B*, vol. 9, pp. 2911–2919, Apr 1974.

[38] P. D. Francesco, P. Mathieu, and D. Sénéchal, *Conformal Field Theory*. Springer-Verlag, 1997.

[39] A. O. Gogolin, A. A. Nersesyan, and A. M. Tsvelik, *Bosonization and strongly correlated systems*. Cambridge [u.a.]: Cambridge University Press, 1998.

[40] K. G. Wilson, "The renormalization group: Critical phenomena and the kondo problem," *Rev. Mod. Phys.*, vol. 47, pp. 773–840, Oct 1975.

[41] K. G. Wilson and J. Kogut, "The renormalization group and the ϵ expansion," *Physics Reports*, vol. 12, no. 2, pp. 75 – 199, 1974.

[42] A. Tsvelik, *Quantum Field Theory in Condensed Matter Physics*. Cambridge University Press, 2007.

[43] S. Östlund and S. Rommer, "Thermodynamic limit of density matrix renormalization," *Phys. Rev. Lett.*, vol. 75, pp. 3537–3540, Nov 1995.

[44] J. Dukelsky, M. A. Martín-Delgado, T. Nishino, and G. Sierra, "Equivalence of the variational matrix product method and the density matrix renormalization group applied to spin chains," *EPL (Europhysics Letters)*, vol. 43, no. 4, p. 457, 1998.

[45] U. Schollwöck, "The density-matrix renormalization group in the age of matrix product states," *Annals of Physics*, vol. 326, 2011.

[46] M. L. Wall and L. Carr, "Out-of-equilibrium dynamics with matrix product states," *New Journal of Physics*, vol. 14, no. 12, p. 125015, 2012.

[47] C. Hubig, I. P. McCulloch, U. Schollwöck, and F. A. Wolf, "Strictly single-site dmrg algorithm with subspace expansion," *Phys. Rev. B*, vol. 91, p. 155115, Apr 2015.

[48] S. Sharma and A. Alavi, "Multireference linearized coupled cluster theory for strongly correlated systems using matrix product states," *The Journal of Chemical Physics*, vol. 143, no. 10, 2015.

[49] M. Dolfi, B. Bauer, S. Keller, A. Kosenkov, T. Ewart, A. Kantian, T. Giamarchi, and M. Troyer, "Matrix product state applications for the ALPS project," *Computer Physics Communications*, vol. 185, no. 12, pp. 3430 – 3440, 2014.

[50] F. Pollmann, A. M. Turner, E. Berg, and M. Oshikawa, "Entanglement spectrum of a topological phase in one dimension," *Phys. Rev. B*, vol. 81, p. 064439, Feb 2010.

[51] J. Eisert, M. Cramer, and M. B. Plenio, "*Colloquium* : Area laws for the entanglement entropy," *Rev. Mod. Phys.*, vol. 82, pp. 277–306, Feb 2010.

[52] I. P. McCulloch, "From density-matrix renormalization group to matrix product states," *Journal of Statistical Mechanics: Theory and Experiment*, vol. 2007, no. 10, p. P10014, 2007.

[53] F. Verstraete, D. Porras, and J. I. Cirac, "Density matrix renormalization group and periodic boundary conditions: A quantum information perspective," *Phys. Rev. Lett.*, vol. 93, p. 227205, Nov 2004.

[54] P. Pippan, S. R. White, and H. G. Evertz, "Efficient matrix-product state method for periodic boundary conditions," *Phys. Rev. B*, vol. 81, p. 081103, Feb 2010.

[55] G. Golub and C. V. Loan, *Matrix Computations (3rd Ed.)*. Baltimore, MD, USA: Johns Hopkins University Press, 1996.

[56] S. Coleman, "Quantum sine-gordon equation as the massive thirring model," *Phys. Rev. D*, vol. 11, pp. 2088–2097, Apr 1975.

[57] B. Bauer, P. Corboz, R. Orús, and M. Troyer, "Implementing global abelian symmetries in projected entangled-pair state algorithms," *Phys. Rev. B*, vol. 83, p. 125106, Mar 2011.

[58] S. R. White, "Density matrix renormalization group algorithms with a single center site," *Phys. Rev. B*, vol. 72, p. 180403, Nov 2005.

[59] C. L. Lawson, R. J. Hanson, D. R. Kincaid, and F. T. Krogh, "Basic linear algebra subprograms for fortran usage," *ACM Trans. Math. Softw.*, vol. 5, no. 3, pp. 308–323, 1979.

[60] E. Anderson, Z. Bai, C. Bischof, S. Blackford, J. Demmel, J. Dongarra, J. D. Croz, A. Greenbaum, S. Hammarling, A. McKenney, and D. Sorensen, *LAPACK Users' Guide*. Philadelphia, PA: Society for Industrial and Applied Mathematics, third ed., 1999.

[61] R. Lehoucq, D. Sorensen, and C. Yang, "Arpack users' guide," 1997.

[62] *Intel Math Kernel Library Developer Reference*. Intel Corporation, 2014.

[63] F. Gomes and D. Sorensen, "Arpack++ documentation," 2000.

[64] J. Hunter, "Matplotlib: A 2d graphics environment," *Computing In Science & Engineering*, vol. 9, no. 3, pp. 90–95, 2007.

[65] D. Cabra and P. Pujol, *Field-theoretical methods in quantum magnetism*, pp. 253–305. Berlin, Heidelberg: Springer Berlin Heidelberg, 2004.

[66] J. M. Kosterlitz and D. J. Thouless, "Ordering, metastability and phase transitions in two-dimensional systems," *Journal of Physics C: Solid State Physics*, vol. 6, no. 7, p. 1181, 1973.

[67] J. V. José, L. P. Kadanoff, S. Kirkpatrick, and D. R. Nelson, "Renormalization, vortices, and symmetry-breaking perturbations in the two-dimensional planar model," *Phys. Rev. B*, vol. 16, pp. 1217–1241, Aug 1977.

[68] C. Itzykson and J.-M. Drouffe, *Statistical Field Theory*, vol. 1. Cambridge University Press, 1989. Cambridge Books Online.

[69] E. Rebhan, *Theoretische Physik: Relativistische Quantenmechanik, Quantenfeldtheorie und Elementarteilchentheorie*. Springer-Verlag, 2010.

[70] N. Lang. PhD thesis, University of Stuttgart, In preparation.

[71] H. Li and F. D. M. Haldane, "Entanglement spectrum as a generalization of entanglement entropy: Identification of topological order in non-abelian fractional quantum hall effect states," *Phys. Rev. Lett.*, vol. 101, p. 010504, Jul 2008.

[72] C. L. Kane and E. J. Mele, "Z_2 topological order and the quantum spin hall effect," *Phys. Rev. Lett.*, vol. 95, p. 146802, Sep 2005.